uOttawa

L'Université canadienne
Canada's university

FACULTÉ DES ÉTUDES SUPÉRIEURES ET POSTOCTORALES

uOttawa

L'Université canadienne
Canada's university

FACULTY OF GRADUATE AND POSDOCTORAL STUDIES

Mohamed Hashi
AUTEUR DE LA THÈSE / AUTHOR OF THESIS

M.A.Sc. (Chemical Engineering)
GRADE / DEGREE

Department of Chemical Engineering
FACULTÉ, ÉCOLE, DÉPARTEMENT / FACULTY, SCHOOL, DEPARTMENT

Ethanol Recovery from Carbon Dioxide Stripped Ethanol-Water Vapor Mixture Using Absorption

TITRE DE LA THÈSE / TITLE OF THESIS

Handan Tezel
DIRECTEUR (DIRECTRICE) DE LA THÈSE / THESIS SUPERVISOR

Jules Thibault
CO-DIRECTEUR (CO-DIRECTRICE) DE LA THÈSE / THESIS CO-SUPERVISOR

André Tremblay

Boguslaw Kruczek

Tong Xu

Gary W. Slater
Le Doyen de la Faculté des études supérieures et postdoctorales / Dean of the Faculty of Graduate and Postdoctoral Studies

Ethanol Recovery from Carbon Dioxide Stripped Ethanol-Water Vapor Mixture Using Adsorption

Mohamed Hashi

Thesis submitted to the
Faculty of Graduate and Postdoctoral Studies
In partial fulfillment of the requirements
For the M.A.Sc. degree in Chemical Engineering

Department of Chemical and Biological Engineering
Faculty of Engineering
University of Ottawa

Your file Votre référence
ISBN: 978-0-494-65966-3
Our file Notre référence
ISBN: 978-0-494-65966-3

Abstract

In this research project, adsorption is used in conjunction with carbon dioxide stripping to increase the efficiency of ethanol production by decreasing the effect of the product inhibition. The reduction in product inhibition is particularly important when ethanol is produced from the lignocellulosic biomass because genetically-modified microorganisms able to use all fermentable sugars are less tolerant to ethanol. Carbon dioxide removes some ethanol from the fermentation broth and reduces the level of ethanol toxicity, while adsorption is used to recover the entrained ethanol from the vapour phase.

A series of adsorption screening experiments were performed to compare four activated carbon adsorbents and two hydrophobic ZSM-5 type zeolites. One activated carbon (WV-B 1500) exhibited the highest ethanol capacity. Adsorption isotherms for ethanol and water in the presence of carbon dioxide at different temperatures were determined. The temperature-dependent Toth isotherm model provided satisfactory fits for these isotherms. Ethanol adsorption experiments with and without the presence of water were conducted and showed similar ethanol adsorption capacities indicating that the presence of water has negligible effect for ethanol adsorption.

A mathematical model was developed to predict the adsorption performance of activated carbon WV-B 1500 for ethanol vapour adsorption in the presence of carbon dioxide and water. The model takes into account changes in velocity due to adsorption, heat effects during adsorption, and heat losses to the surroundings. The model was validated with experimental data. Finally the model was used to predict the adsorption working capacities to assess the performance of the adsorption process in an industrial process.

An economic analysis was performed by comparing a simulated base case ethanol production plant with a similar process coupled with carbon dioxide stripping and adsorption technology. The process was modeled using Aspen HYSYS to perform material and energy balances. The packed bed adsorption system, operating as a temperature-swing adsorption (TSA) or a vacuum-swing adsorption (VSA) system, was simulated to evaluate the performance of the adsorption system and to size and cost the associated equipment. Preliminary results showed that the grass roots cost for the ethanol production process coupled with carbon dioxide stripping and adsorption technology for three different TSA (purge gas at 80, 100, and 120°C) and VSA (adsorption pressure at 0.5, 0.2, and 0.1 atm) systems were more cost effective than the base case ethanol plant.

Résumé

Dans ce projet de recherche, un procédé d'absorption de l'éthanol extrait du milieu de fermentation par le dioxyde de carbone suivi de son adsorption est utilisé pour diminuer l'inhibition par le produit et ainsi accroître l'efficacité de la production d'éthanol. La diminution de l'inhibition par le produit est particulièrement importante lorsque l'éthanol est produit à partir de la biomasse lignocellulosique, car les micro-organismes génétiquement modifiés capables d'utiliser tous les sucres fermentescibles sont moins tolérants à l'éthanol. Le dioxyde de carbone retire une partie de l'éthanol du bouillon de fermentation et réduit le niveau de toxicité de l'éthanol, tandis que l'adsorption est utilisée pour récupérer l'éthanol entraîné dans la phase vapeur.

Une série d'expériences ont été effectuées pour comparer quatre adsorbants au charbon activé et deux zéolites ZSM-5 hydrophobes. Le meilleur adsorbant pour sa capacité d'adsorption en éthanol est le charbon activé WV-B 1500. Les isothermes d'adsorption de l'éthanol et de l'eau en présence du dioxyde de carbone ont été déterminées à différentes températures et modélisées par le modèle de Toth à température variable. La capacité d'adsorption de l'éthanol n'est pas affectée par la présence d'eau. Un modèle mathématique a été développé pour prédire l'adsorption de l'éthanol, du dioxyde de carbone et de l'eau pour un cycle d'adsorption. Le modèle prend en compte les changements de débit dus à l'adsorption, la chaleur dégagée lors de l'adsorption, et les pertes de chaleur à l'environnement. Le modèle a été validé avec des données expérimentales. Enfin, le modèle a été utilisé pour prédire la capacité effective d'adsorption afin d'évaluer les performances du procédé d'adsorption à l'échelle industrielle.

Une analyse économique a été réalisée en comparant la simulation d'une usine de production d'éthanol conventionnelle avec une usine similaire mais couplée au système d'absorption au dioxyde de carbone et d'adsorption. Le procédé a été modélisé en utilisant Aspen HYSYS pour effectuer les bilans de matières et d'énergie. Le système d'adsorption, fonctionnant par modulation de température (TSA) ou par modulation de la pression sous vide (VSA), a été simulé pour en évaluer sa performance et déterminer la taille et le coût des équipements. Les résultats préliminaires ont montré que le procédé de production d'éthanol couplé au système d'absorption au dioxyde de carbone suivi par

l'adsorption de l'éthanol pour trois systèmes différents de TSA (gaz de purge à 80, 100 et 120°C) et de VSA (pression de 0.5, 0.2, et 0.1 atm) est plus rentable que l'usine de base de production.

Acknowledgements

I would like to first thank my supervisors Dr. F. Handan Tezel and Dr. Jules Thibault for giving me the opportunity to work on this research project and their guidance and faith in my ability to complete this thesis. Without their help this would not have been possible and I cannot thank them enough for everything.

I would also like to thank the other members of the research group, Dan Dicaire, Rudy Jones, Muhammad Tawalbeh, Chris Bestfather, Vinay Mulgundmath for the help and ideas they have given me throughout my graduate studies.

Many thanks to the technical support staff, namely Mr. Louis Tremblay, Mr. Franco Ziroldo and Mr. Gerard Nina, who have help me greatly with the experimental set-up and Labview programming.

Finally, I would like to thank my family and friends for all the support and encouragement they have given me, I could not have done it without the support of everyone.

Statement of Contributions of Collaborators

I hereby declare that I am the first author of this thesis which was completed under the guidance of my two supervisors: F. Handan Tezel and Jules Thibault. The experimental set-up was designed and constructed individually with some help from the technical support staff of Louis Tremblay, Franco Ziroldo and Gérard Nina. Gérard and I programmed the thermocouple readings using Labview used to monitor the temperature profile of the adsorption bed. I performed all experiments, data analysis, HYSYS simulations, adsorption/desorption simulations, and the economic analysis. The FORTRAN program for modeling the packed bed adsorber was developed in partial collaboration with Rudy Jones.

Table of Contents

List of Tables

List of Figures

Chapter I: Introduction

Introduction

The world landscape is on the brink of a fundamental change on how human beings integrate their relationship with nature in all their activities. A major emphasis has been placed on greenhouse gas emissions and lowering the demand for fossil fuels. The reasons for this inevitable paradigm shift are numerous but two of the most important trends that will shape future thinking are the increasing world population and the scarcity of fossil fuels.

World population has increased from 1.65 billion in 1900 to 6.68 billion in 2008. At the present growth rate, it has been estimated that the world population could approach 9 billion by 2050 (United Nations, 2004). The impact of world population is major since there is a strong correlation between population and energy consumption. As technology has advanced over the years since the industrial revolution, worldwide energy consumption has steadily increased and currently continues to increase. In the *IEO2009* reference case, world energy consumption will increase from 498 quadrillion kJ in 2006 to 582 quadrillion kJ in 2015 and 715 quadrillion kJ in 2030 - a total increase of 44% over the projection period (U.S. Energy Information Administration, 2009). These two trends have a combined adverse effect on the world ecosystem.

The other major issue is the world's reliance on fossil fuels, namely natural gas, coal and oil. It was estimated by the Energy Information Administration that in 2005, 86% of primary energy production in the world came from burning fossil fuels, with the remaining non-fossil fuel sources being hydroelectric (6.3%), nuclear (6.0%), and other (including geothermal, solar, wind, and wood) at 0.9% (Grillot, 2007). Current levels in 2009 are not that much different with a large portion of energy resources still dependent on fossil fuels. Fossil fuels produce carbon dioxide during combustion with the great majority being released to the atmosphere. Carbon dioxide accumulates in the atmosphere while prohibiting a higher fraction of solar radiation from escaping the Earth's atmosphere. This higher carbon dioxide accumulation theoretically increases the temperature of the Earth and could cause problems such as increasing sea levels, extreme weather patterns, etc. There is some dissent with scientists that greenhouse gas emissions are the cause for global warming but the increased levels of carbon dioxide in the

atmosphere is not something that can be ignored. It has been reported that carbon dioxide levels in the atmosphere have risen 35% faster than expected since 2000 (BBC News, 2007).

With all the publicity surrounding the global warming and the depleting fossil fuel, government and the public in general are demanding newer and greener technology to alleviate the dependence on fossil fuels and to develop alternative fuels that are renewable and more environmentally friendly. Biodiesel and bioethanol are currently the two alternative fuels that can more readily partly solve this problem with the advantage that they be more easily integrated with the current infrastructure. This thesis focuses on the production of bioethanol.

Bioethanol is a renewable source of fuel that could potentially ease the reliance on fossil fuels and eventually partly replace fossil fuels as the fuel of choice for industry and transportation. Ethanol is produced by fermentation of sugars obtained via the hydrolysis of biomass. The most promising source of fermentable sugars is the lignocellulosic biomass because it can use agricultural and forest residues with the advantage of limiting the dependence on corn based ethanol where land usage and fuel versus food debate become an issue. However, obtaining fermentable sugars from the lignocellulosic biomass compared to sugar cane and corn is much more complicated because of the structure and chemical composition of lignocellulosic biomass (cellulose, hemicelluloses and lignin). In addition, genetically-modified microorganisms normally required converting the resulting sugar mixture of pentoses and hexoses into bioethanol have a much lower tolerance to ethanol than native microorganisms. This lower tolerance significantly limits the final ethanol concentration that can be obtained through fermentation. For example, the resulting ethanol concentration using the genetically-modified yeast *Saccharomyces cerevisiae* developed at Purdue University is between 4 to 6% by weight compared to common yeasts that can reach 10 to 12% (Caputo et al., 2007). Therefore, developing a technology to lower the ethanol inhibition within the fermentation broth is of paramount importance to improve the efficiency of the process and make ethanol via fermentation a more economically viable venture.

The scope of the research project is mainly focused on two aspects. The first aspect considers the use of carbon dioxide stripping to remove a portion of the ethanol

during fermentation in order to lower the ethanol concentration and, as a result, to lower the product inhibition thereby increasing ethanol productivity. The product stream of the carbon dioxide stripping is a vapour mixture containing ethanol and water. The second aspect of the project is to devise an efficient separation system to recover the entrained ethanol from the vapour phase. In this investigation, an adsorption system is used to selectively adsorb ethanol from the ethanol-water-carbon dioxide mixture.

Research Objectives

The main objectives for the proposed thesis are:

1. Conduct a thorough literature search to determine the desired adsorbent characteristics needed to selectively adsorb ethanol in the presence of water and carbon dioxide.
2. Run a series of adsorption screening experiments under the same conditions for a vapour mixture including ethanol, water and carbon dioxide.
3. From the results of the adsorption screening, identify the best adsorbent on the basis of ethanol adsorption capacity and selectivity.
4. Obtain complete isotherms over the range of stripped gas ethanol concentration that would be encountered in practice for the selected adsorbent and for pure carbon dioxide, water-carbon dioxide mixtures, ethanol-carbon dioxide mixtures, and ethanol-water-carbon dioxide ternary mixtures.
5. Develop a mathematical model to predict adsorption breakthroughs and validate the model with experimental data.
6. Conduct a preliminary economic analysis based on experimental data and adsorption models to compare a base case ethanol production plant with a plant coupled with carbon dioxide stripping and adsorption technology.

Thesis Structure

The current thesis structure is a paper-based thesis. The first chapter presents a general introduction and list the research objectives to be undertaken. Chapters II-IV are scientific journals that were submitted or will be submitted to refereed journals. Chapter II presents the adsorption screening experiments that were performed to identify the best

adsorbent on the basis of ethanol adsorption capacity and selectivity. Chapter III looks into predictive modeling using a mathematical model followed by a series of validations using experimental data. Chapter IV analyzes the economic feasibility and quantify the benefits of using carbon dioxide stripping and adsorption technology for ethanol production. Chapter V gives the general conclusions that can be drawn from the work done in this investigation, and presents some recommendations for future work to further develop the concepts proposed in this research. Chapters VI-VIII contains the appendices associated to the Chapters II - IV, respectively. Chapter IX introduces some fundamentals about adsorption.

References

BBC, "Unexpected growth in CO_2 found," BBC News, 2008, http://news.bbc.co.uk/2/hi/7058074.stm (Retrieved April 8, 2008)

Caputo, D., Iucolano, F., Pepe, F., Colella, C., "Modeling of water and ethanol adsorption data on a commercial zeolite-rich tuff and prediction of the relevant binary isotherms," Microporous and Mesoporous Materials, 105 (3), 260-267 (2007)

Grillot, M. J., "International Energy Annual 2005: World Energy Overview: 1995-2005," Energy Information Administration, Official Energy Statistics from the U.S. Government, 2007 www.eia.doe.gov/iea/overview.html (Retrieved March 18, 2008)

United Nations, "The world at six billion," UN Report 2004, 2004, 1-11, www.un.org/esa/population/publications/sixbillion/sixbilpart1.pdf (Retrieved November 1, 2009)

U.S. Energy Information Administration., "International energy outlook 2009," 2009, www.eia.doe.gov/oiaf/ieo/world.html (Retrieved October 21, 2009)

Chapter II: Ethanol recovery from fermentation broth via carbon dioxide stripping and adsorption

Mohamed Hashi, F. Handan Tezel, and Jules Thibault

Department of Chemical and Biological Engineering

University of Ottawa, Ottawa, Ontario, Canada K1N 6N5

To whom correspondence should be addressed. Telephone: +1-613-562-5800 x6099.

Email: handan.tezel@uottawa.ca

Abstract

With the depletion of fossil fuels, research in alternative energy sources that can provide the world's energy demand has increased significantly during the past decade. One alternative energy source in particular that has gained worldwide recognition as a potential replacement to oil is bio-ethanol. It is renewable and environmentally friendlier than fossil fuels. In this study, adsorption is used to increase the efficiency of ethanol production by decreasing the effect of product inhibition using carbon dioxide stripping technology. The reduction in product inhibition is particularly important when ethanol is produced from lignocellulosic biomass because microorganisms that are able to use all fermentable sugars are less tolerant to ethanol. Carbon dioxide removes ethanol from the fermentation broth and reduces the level of ethanol toxicity, while adsorption is used to recover the entrained ethanol from the vapour phase. Literature review showed that activated carbon and hydrophobic zeolites would be the most appropriate adsorbents for ethanol recovery in the vapour phase. A series of adsorption screening experiments were performed to compare four activated carbon adsorbents (Filtrasorb 200, Nuchar RGC 40, Sorbonorit B4, and WV-B 1500) and two hydrophobic ZSM-5 type zeolites (HiSiv 3000, CBV 8014). The vapour composition used was controlled to resemble the fermenter outlet vapour concentration after stripping with carbon dioxide. Activated WV-B 1500 exhibited the highest ethanol capacity among activated carbons having higher ethanol adsorption capacities than the two zeolites.

Adsorption isotherms for ethanol and water in the presence of carbon dioxide at different temperatures were determined using WV-B 1500 as the adsorbent with temperature dependent Toth isotherm model providing satisfactory fits for these isotherms. Ethanol adsorption experiments with and without the presence of water were conducted and showed similar ethanol adsorption capacities indicating that the presence of water has negligible effect for ethanol adsorption.

Introduction

North America and much of the world are faced with complex economic and environmental issues associated with energy use that must be addressed if lifestyles that are currently enjoyed are to be maintained and improved (Wyman, 1996). The most predominant source of fuel presently consumed comes from fossil fuels in the form of coal, oil and natural gas. It was estimated by the Energy Information Administration that in 2005, 86% of primary energy production in the world came from burning fossil fuels, with the remaining non-fossil fuel sources being hydroelectric (6.3%), nuclear (6.0%), and others (including geothermal, solar, wind, and wood) at 0.9% (Grillot, 2005). The reliance on fossil fuels has led to a rapid depletion of this source of energy since coal, oil and natural gas are essentially non-renewable. One study predicted the depletion times for oil, coal and natural gas at approximately 35, 107, and 37 years, respectively (Shafiee and Topal, 2009). Some assumptions made, including an assumed growth in world energy consumption of approximately 2% per annum, may not be as accurate due to the decreased growth worldwide because of the current global economic crisis, but nevertheless show the imminent energy crisis facing the world.

The need for an alternative energy fuel source has led to extensive research in bio-ethanol production. Bio-ethanol is a renewable source of fuel that could potentially ease the reliance on fossil fuels and eventually partly replace fossil fuels as the fuel of choice for industry and transportation. Ethanol is produced via fermentation of sugars obtained via the hydrolysis of biomass. Three sources of biomass are commonly used: sugar canes, corn and lignocellulosic materials. The most promising source is the lignocellulosic biomass because it can use agricultural and forest residues and prevent the heated debate on food vs. fuel. However, due to its rigid structure and composition (cellulose, hemicellulose and lignin), lignocellulosic biomass is the most difficult source for the extraction of fermentable sugars and, in addition, gives a mixture of pentose and hexose sugars. The most abundant sugars from lignocellulosic biomass are glucose and xylose. However, most ethanologenic microorganisms are only able to metabolize glucose and one must resort to genetically-modified microorganisms to make use of all available sugars. These microorganisms usually have a lower tolerance to ethanol. For example, the resulting ethanol concentration using the yeast *Saccharomyces cerevisiae* developed

at Purdue University (Ho et al., 1998) is between 4 to 6% by weight compared to common yeasts that can reach 10 to 12% (Caputo et al., 2007).

The economic viability of the ethanol production process is strongly affected by the low ethanol concentration obtained in the fermenter, as well as the need to break the azeotrope between ethanol and water which occurs at an ethanol concentration of 95.57 wt%. A lot of research has been directed towards using adsorption to break the azeotrope at high ethanol concentration including the use of zeolites (Carmo and Gubulin, 1997; Guan and Hu, 2003; Kupiec et al., 2008) and cellulosic adsorbents (Al-Asheh et al., 2004; Chang et al., 2006a; Chang et al., 2006b; Chang et al., 2006c; Crawshaw and Hill, 1990).

One alternative to decrease the cost of production of ethanol is to increase the productivity by reducing ethanol inhibition within the fermentation broth. Research has been conducted to determine the best method for ethanol removal from the fermentation broth as ethanol is produced. As ethanol is produced and removed, the concentration within the broth decreases allowing a greater conversion of sugars to ethanol. A series of papers by Taylor et al. (Taylor et al., 1995; Taylor et al., 1996; Taylor et al., 1997; Taylor et al., 1998; Taylor et al., 2000) have shown the merits for using carbon dioxide to strip the ethanol from the fermenter. The productivity of today's fuel ethanol fermenter will vary, depending on factors such as the amount of yeast added and the final ethanol concentration, but in most plants it is no more than approximately 2 g l^{-1} h^{-1}, even in continuous-cascade fermenters. Using gas stripping, the productivity of ethanol has been experimentally shown to increase to as much as 15.8 g/l h (Taylor et al., 1997).

In an industrial carbon dioxide stripping fermentation process, a large amount of ethanol would be present within the stripped carbon dioxide and a cost effective way to recover this ethanol is needed for the process to be economically viable. Very little research has been done on this topic. In 1983, Walsh et al. used one type of activated carbon (Filtrasorb F-200) and showed its ability to preferentially adsorb ethanol from the ethanol-water mixture at concentrations of 6 mol% ethanol. These authors did not discuss the effect carbon dioxide has on the separation nor conducted an adsorption screening indicating the best performing adsorbents for ethanol recovery.

Motivated by the reported benefits of carbon dioxide stripping and the need for an efficient ethanol recovery method, this paper presents an in-depth study on the use of adsorption for ethanol recovery. The aim of this investigation is two-fold: an adsorbent screening to determine the best performing adsorbent followed by a series of adsorption characterization experiments using the best performed adsorbent. The characterization experiments analyze carbon dioxide adsorption as well as binary and ternary combinations between carbon dioxide, ethanol and water.

Experimental Methods and Materials

Adsorbent Characteristics

Past literature has shown that for ethanol adsorption, the best performing adsorbents are activated carbons (Saha et al., 2007; Walsh et al., 1983) and hydrophobic zeolites (Milestone and Bibby, 1981; Oumi et al., 2002). The adsorption sites in activated carbons and hydrophobic zeolites are highly non-polar and hydrophobic and, as a result, they repel the more polar water molecules compared to ethanol molecules. The main focus of the present study was to determine the adsorbent having the best characteristics for the preferential adsorption of ethanol. Table II.1 lists the main physical properties of the six adsorbents used in this investigation.

Table II.1 - Adsorbent characteristics and properties.

Adsorbent Name	Supplier	BET Surface Area (m^2/g)	Particle size (mm)	Mesh Size	Hydrophobicity (SiO_2/Al_2O_3 ratio)
SORBONORIT B4	Norit America, Marshall, TX, USA	1250	>3.35	< 6	-
Nuchar RGC 40	MeadWestvaco, Glen Allen, VA, USA	1600	1.68 - 0.42	12 x 40	-
WV-B 1500	MeadWestvaco, Glen Allen, VA, USA	2200	2.00 - 0.707	10 x 25	-
Filtrasorb 200	Calgon, Pittsburgh, PA, USA	835	0.6 - 0.7	12 x 40	-
HiSiv 3000	UOP, Des Plaines, IL, USA	-	1.59	-	> 1000
CBV 8014	Zeolyst, Conshohocken, PA, USA	-	-	-	80

Adsorbents studied were chosen for their hydrophobic characteristics and their higher capacity for ethanol adsorption reported in the literature (Milestone and Bibby, 1981; Oumi et al., 2002). Four activated carbons (SORBONORIT B4, Nuchar RGC 40, WV-B 1500, and Filtrasorb 200) were studied due to their wide range of BET surface areas while the two zeolites (HiSiv 3000 and CBV 8014) were studied to determine the effect of hydrophobicity (SiO_2/Al_2O_3 ratio) on ethanol adsorption.

Apparatus

Figure II.1 shows the schematic diagram of the adsorption system used for testing the adsorbents. Downstream of the carbon dioxide gas cylinder are two gas mass flow controllers (MKS, Ottawa, Ontario, Canada) used to control the flow of carbon dioxide through the two 1-L Erlenmeyer flasks (used as bubblers) containing pure ethanol and water, respectively. The two vapour streams combine just before entering an adsorption column (0.78 cm I.D. and 36 cm in length) wrapped in a heating tape. The inlet vapour composition fed into the column was controlled by adjusting the flows through the two

mass flow controllers. A bypass around the column was added to allow for the determination of the inlet vapour composition. The inlet and outlet vapour streams of the adsorption column were analyzed using a GOW-MAC (Bethlehem, Pennsylvania, USA) Series 580 TCD (Thermal Conductivity Detector) isothermal Gas Chromatograph (GC) using a Porapak Q column. The flow of the gas mixture through GC's sample loop was controlled using a Thermo Scientific (Ottawa, Ontario, Canada) vacuum pump. All connections and piping were purchased from Swagelok except for the ball valves which were bought from Parker Hannifin Corp (Montreal, Quebec, Canada). The GC's operating column, the detector and the injection port were kept at a temperature of 135°C, 165°C, and 160°C, respectively.

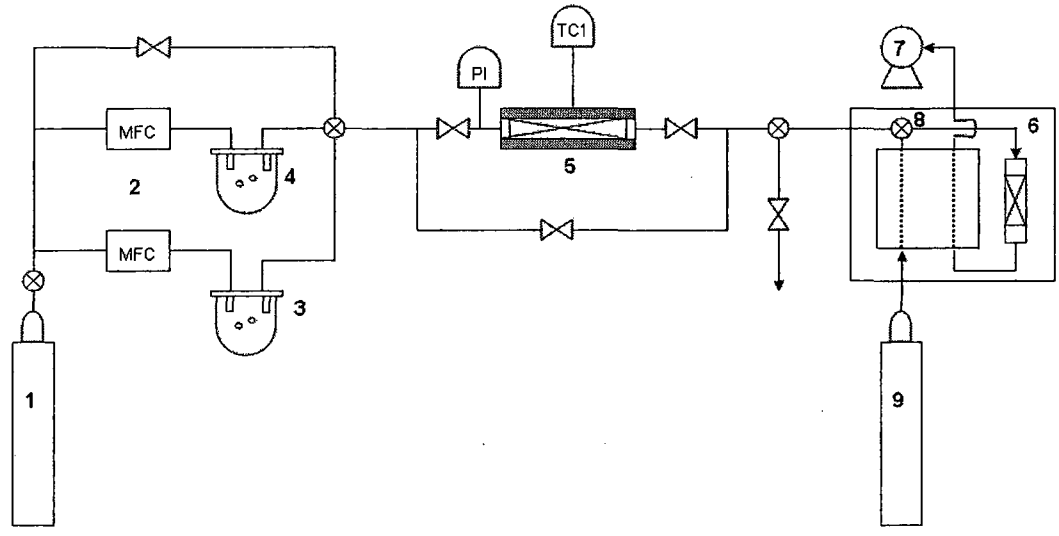

Figure II.1 - Schematic diagram of the experimental adsorption system: 1 – carbon dioxide gas cylinder; 2 – MKS mass flow controllers 3 – ethanol bath; 4 – water bath; 5 – adsorption column wrapped with a heating tape; 6 – GOW MAC Gas Chromatograph; 7 – vacuum pump; 8 - sample injection valve; 9 - helium carrier gas cylinder; TC1 – Thermocouple; PI – pressure gauge.

Experimental Procedure and Theory

Before each adsorption experiment, the adsorbent was degassed at 250°C overnight (minimum of 8 h) using air as the purge gas. The next day, the gas chromatograph was heated until all set temperatures reached equilibrium. Once the gas

chromatograph was ready, the carbon dioxide stream from the gas cylinder was split using the two mass flow controllers and bubbled through the ethanol and water flasks, respectively. The ethanol and water vapour streams, together with carbon dioxide were combined before entering the adsorption column where they came into contact with the adsorbent packed into the column. The composition of the stream entering the adsorption column was controlled by adjusting the flow rate of carbon dioxide going into the ethanol and water baths, separately. The vapour mixture not adsorbed onto the adsorbent passed through the packed column. Using a vacuum pump, a sample is drawn from the outlet stream exiting the adsorption column every five minutes and injected into the gas chromatograph. The determination of outlet gas composition as a function of time allowed determining the breakthrough curve and experimentally calculating the adsorption capacity of the packed column for each experiment performed.

The experimental set-up was constructed so carbon dioxide flows through two flasks containing pure water and pure ethanol, respectively. This was done for two main reasons. The first reason was to more easily set the ethanol and water composition by controlling the flow of carbon dioxide through the water and ethanol flasks. The second reason deals with the consistency of the inlet composition to the adsorption column. It would be possible to bubble carbon dioxide through a flask containing a mixture of ethanol and water to obtain a representative gas stream that would mimic more realistically the one that would exit a fermenter. However, since ethanol is more volatile than water, the relative concentration of ethanol in the mixture would decrease, resulting in a composition change with time of the inlet stream entering the adsorption column. Using two distinct carbon dioxide flow rates through the ethanol and water baths allows for a consistent vapour concentration entering the adsorption column.

The adsorption capacities were determined using a series of breakthrough curves with a stream of carbon dioxide containing water and ethanol over a wide range of inlet concentrations up to their respective saturation concentration. The area above the breakthrough curve is proportional to the total amount adsorbed in the column. Equation 1 gives the relationship between the adsorption capacity and the area above the breakthrough curve where AC_i, $m_{flow,i}$, and $m_{adsorbent}$ represent the adsorption capacity for

component i (g/g adsorbent), the mass flow rate for component i (g/s), and the mass of the adsorbent (g), respectively.

$$AC_i = \frac{t_i \cdot m_{flow,i}}{m_{adsorbent}} \tag{1}$$

The variable t_i, defined in Equation (2), corresponds to the calculation of the area above the normalized breakthrough curve in seconds. c_i, and c_{io} represent the outlet and inlet concentrations for component i (g/l), respectively.

$$t_i = \int_0^\infty \left(1 - \frac{c_i}{c_{io}}\right) dt \tag{2}$$

Another useful performance parameter is the separation factor, λ. This parameter can be used when different concentrations are compared to determine how well the adsorption process performed. Equation 3 gives the definition of the separation factor. X_w and X_e represent the mass fraction of water and ethanol in the adsorbed phase whereas Y_w and Y_e represent the mass fraction of water and ethanol in the vapour phase.

$$\lambda = \frac{X_w / X_e}{Y_w / Y_e} \tag{3}$$

With the multi-temperature isotherms, it is possible to predict the adsorption capacity not only at different concentrations but also at different temperatures using the temperature dependent Toth isotherm model. The benefit of using the Toth isotherm model is its ability to predict the adsorption capacity at any temperature and concentration provided that experimental isotherms at different temperatures are available to determine the fitting parameters of the model. Since the Toth isotherm possesses this additional flexibility, the isotherm model is necessarily more complex when compared to other isotherm models such as Langmuir and Freundlich. Equation 4 represents the Toth adsorption isotherm model with q_m, b and t representing the model parameters (Toth, 1962).

$$q_i = \frac{q_m bC}{\left[1 + (bC)^t\right]^{1/t}} \tag{4}$$

Each of these parameters can be written as a function of temperature as follows:

$$b = b_\infty \exp\left[\frac{Q}{RT_O}\left(\frac{T_O}{T} - 1\right)\right] \tag{5}$$

$$t = t_o + \alpha\left(1 - \frac{T_O}{T}\right) \tag{6}$$

$$q_m = q_{mo} \exp\left[\chi\left(1 - \frac{T}{T_O}\right)\right] \tag{7}$$

When equations 5-7 are substituted into equation 4, a total of six fitting parameters (b_∞, q_{mo}, t_o, $\frac{Q}{RT_O}$, χ, and α) can be determined for the Toth isotherm model based on experimental isotherms obtained at different temperatures. This allows the prediction of adsorption capacities at other temperatures and pressures for which experimental data are not available.

Results and Discussion

Adsorbent Screening

An adsorbent screening process was conducted to determine the capacity of each adsorbent for the ethanol, water, and carbon dioxide ternary vapour mixture. Before the selection of adsorbents, a thorough literature review was conducted to determine the types of adsorbents that were considered to be more appropriate for this separation (see Table II.2).

Four activated carbon adsorbents and two zeolites were selected and screened to determine the best performing adsorbent and the adsorbent characteristics. Activated carbons were selected due to their hydrophobic characteristics, as well as to cover a wide range of BET surface areas (between 800 and 2200 m^2/g) for this study. This was done to determine if there is a direct correlation between ethanol adsorption capacity and the surface area of the adsorbent. Zeolite samples were used for two reasons. The first reason was to compare zeolites with activated carbon to see which type adsorbs the most ethanol and is more selective towards ethanol. The second reason was to study the effect of hydrophobicity on ethanol adsorption in the vapour phase. Both zeolites studied have ZSM-5 type structures with the only difference being their SiO_2/Al_2O_3 ratios. This ratio

indicates hydrophobicity with a higher SiO_2/Al_2O_3 ratio suggesting a more hydrophobic surface.

Figure II.2 shows the amount of ethanol and water adsorbed by the six adsorbents at an inlet vapour mixture partial pressure of 1.9 kPa for ethanol and water with the balance being carbon dioxide. These experiments were performed under atmospheric pressure and at room temperature (24°C).

Table II.2 – Literature review summary of desired adsorbents.

Reference	Adsorbents Used	Type of Adsorbent	Feed Components*	Adsorbed Component*	Adsorption Phase
Milestone and Bibby, 1981	Silicalite - 1	Hydrophobic Zeolite	W, E	E	Liquid
Walsh et al., 1983	Calgon Filtrasorb F-200	Activated Carbon	W, E	E	Vapour
Pitt et al., 1983	XAD-2, XAD-4	Ion-exchange Resins	W, E	E	Liquid
Oumi et al., 2002	Silicalite	Hydrophobic Zeolite	W, E	E	Vapour
Saha et al., 2007	ACF (A-20)	Activated Carbon	E	E	Vapour
Naono et al., 1996	AC-1, AC-2	Activated Carbon	W, E	W, E	Vapour
Pletcher et al., 2006	BAX 950	Activated Carbon	W, M	M	Vapour
Weitkamp et al., 1991	NaX, NaY	Hydrophilic Zeolite	W, E	W, E	Vapour
Lee et al., 1991	A. C. S reagent grade	Starchy Material	W, E	W, E	Vapour
Vareli et al., 1997	Various	Cellulosic Materials	W, E	W, E	Vapour
Bowen and Vane, 2006	ZSM-5	High Silica ZSM-5 Zeolite	W, E, A	W, E, A	Liquid

* W stands for water, E for ethanol, M for methanol and A for acetic acid

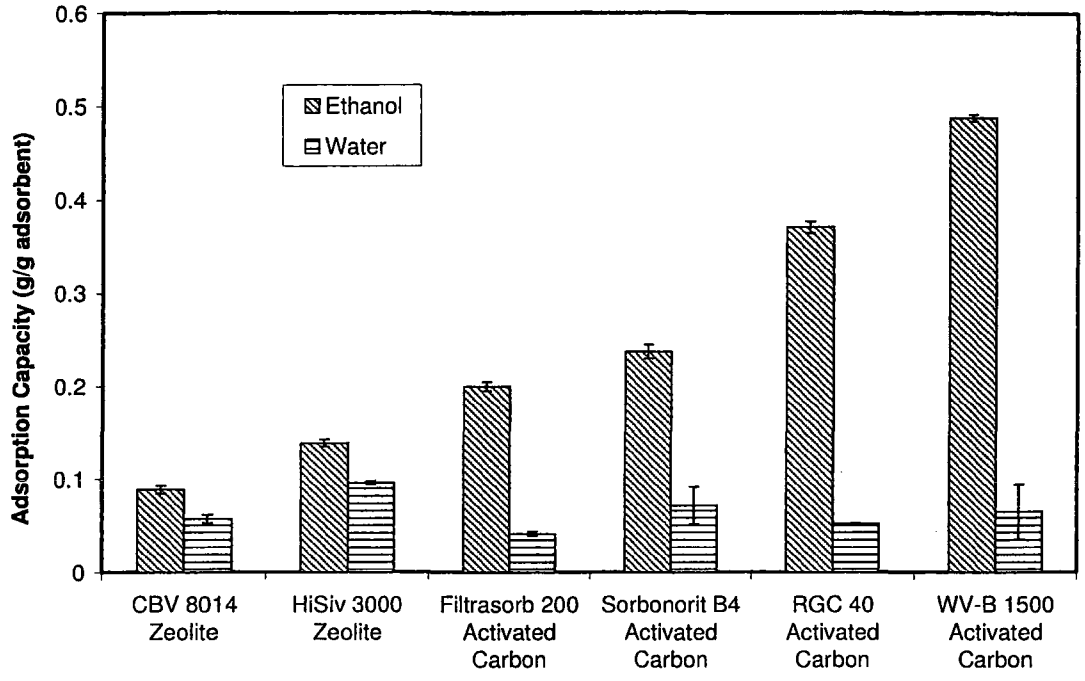

Figure II.2 - Amount of ethanol and water adsorbed for the six different adsorbents studied under atmospheric total pressure at 24°C and at ethanol and water partial pressures of approximately 1.9 kPa each.

Adsorbent WV-B 1500 showed the highest amount of ethanol adsorbed followed by RGC - 40, SORBONORIT B4, Filtrasorb 200, and HiSiv 3000 and lastly CBV 8014. One key observation is that the activated carbons adsorbed much more ethanol on average compared to the two zeolite samples. On average, the capacity of activated carbon adsorbents for ethanol was threefold compared to the hydrophobic zeolites. Comparing the two zeolite samples, the increase in hydrophobicity for the HiSiv 3000 enabled higher adsorption for both ethanol and water compared to CBV 8014. One explanation is that although both adsorbents have the same ZSM-5 pore structure, CBV 8014 has a much higher number of cations due to the much lower SiO_2/Al_2O_3 ratio. The additional cations lead to a smaller pore size and therefore inhibit the ethanol and water molecules from entering the adsorption sites. Also, another explanation for increased ethanol adsorption for HiSiv 3000 zeolite is the fact that the absence of cations in its structure makes it more organophilic.

Another interesting observation is the linear relationship between the BET surface area for the activated carbons and the amount of ethanol adsorbed. Figure II.3 shows a positive linear correlation with a correlation coefficient of 0.961. As the BET surface area increases, more adsorption sites become available and therefore more ethanol is adsorbed onto the surface. This observation can also be made for water adsorption although the linear relationship is less pronounced with a correlation coefficient of 0.256 as shown in Figure II.3.

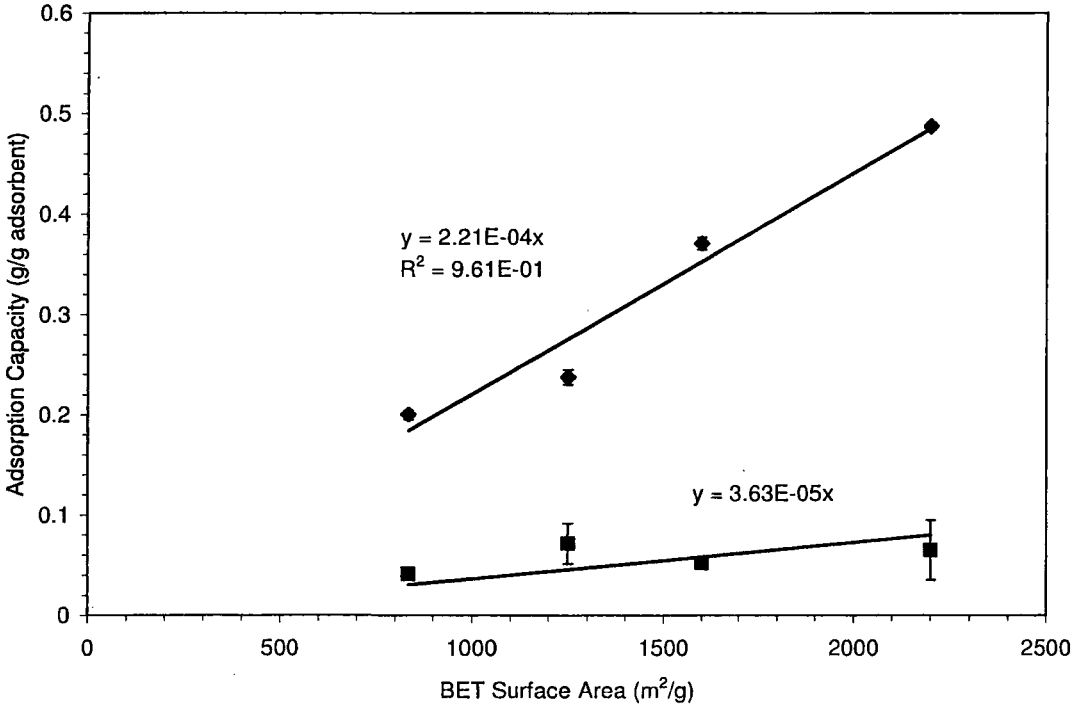

Figure II.3 - Change in the amount of ethanol (♦) and water (■) adsorbed with BET surface area for activated carbons studied under atmospheric total pressure at 24°C.

Adsorption Process Validation

When carrying out an adsorption experiment through a packed column, the flow rate determines the contact time between the adsorbent and the adsorbate, and the adsorption capacity should theoretically be independent of flow rate. Using breakthrough curves to produce isotherms introduces possible errors mainly due to the fluctuating concentration readings once equilibrium is reached. Two measures can be taken into account to ensure equilibrium has been reached. The first one is to prolong the

adsorption process beyond the time steady state is reached to ensure equilibrium prevails. The second one is to lower the flow rate to make sure the vapour has sufficient time to be adsorbed within the adsorption column.

A series of experiments at different flow rates were conducted to determine the best flow regime to complete the isotherms. It was found that above a given flow rate, the calculated adsorption capacity decreased as the flow rate increased. It is believed that the reason for this discrepancy in adsorption capacity is due to the lack of accuracy in calculating of the adsorption capacity because of the tailing in the breakthrough curve as the column approaches saturation. This, combined with possible channelling in the column at higher flow rates and the inherent variability of the composition measurements with the gas chromatograph, limits the accuracy of the determination of the adsorption capacity which is proportional to the area above the breakthrough curve. As well, condensation within the adsorption column at higher flowrates could affect adsorption capacity calculations.

Figure II.4 shows two adsorption breakthrough curves obtained at different flow rates. It depicts the tailing in the breakthrough curves as well as the variability in the measured ethanol column outlet concentration. The two experiments in Figure II.4 were done at the same inlet ethanol partial pressure of 2.3 kPa with the total flow rate being the only difference: 0.4875 l/min and 1.104 l/min, respectively. The adsorption at the higher flow rate experienced a faster breakthrough since more ethanol is passing through the column per unit time. For the two breakthrough curves shown in Figure II.4, the calculated adsorption capacities for the adsorption runs at 0.488 l/min and 1.104 l/min experiments are 0.552 and 0.503 g ethanol/g adsorbent, respectively. The difference in adsorption capacity represents a 9.2 % decrease in the measured adsorption capacity obtained at the higher flow rate.

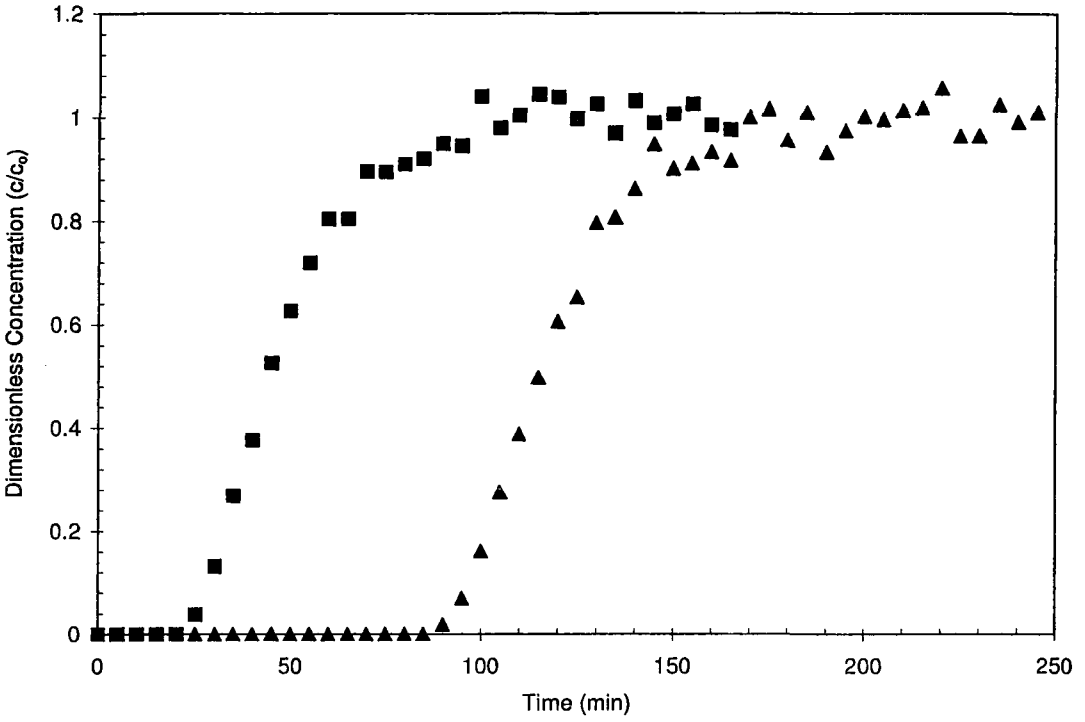

Figure II.4 - Breakthrough curves of ethanol - carbon dioxide vapour mixture under atmospheric total pressure at ethanol partial pressure of 2.3 kPa and 24°C for flow rates of 0.488 (▲) and 1.104 l/min (■).

A series of experiments were performed to determine the range of flow rates for which the accuracy in the determination of the adsorption capacity becomes independent on the gas flow rate. Three different flow rates at essentially the same ethanol partial pressure of 2.63 kPa were used. Figure II.5 shows the breakthrough curves as a function of time at flow rates of 0.512, 0.702 and 0.898 l/min.

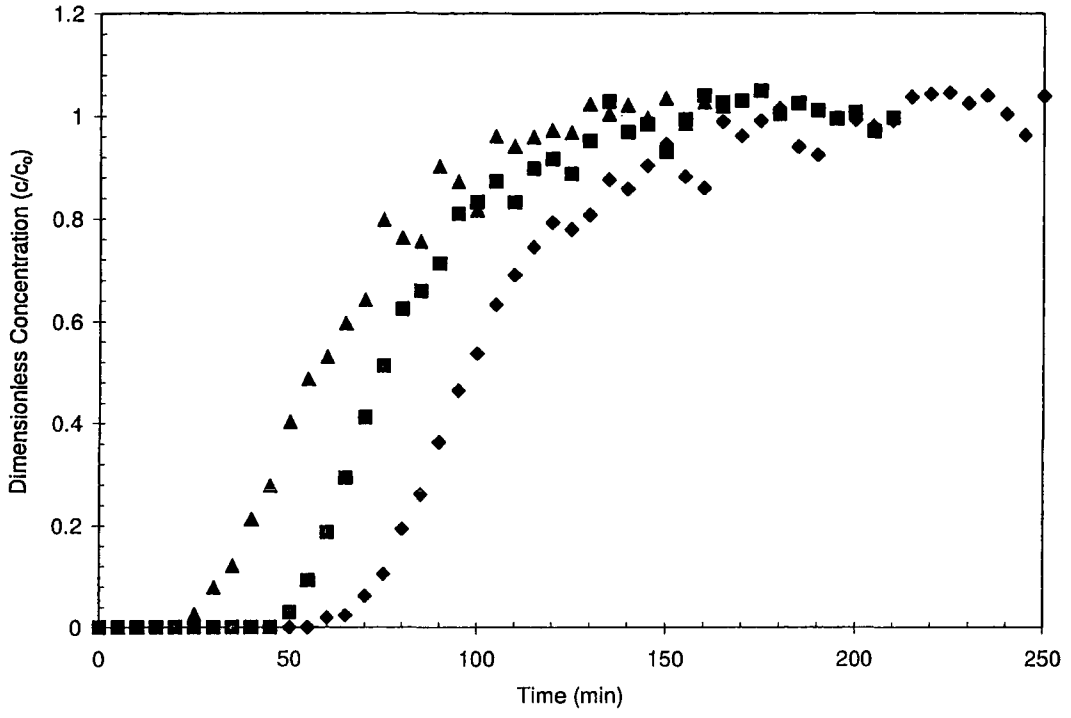

Figure II.5 - Breakthrough curves at 2.6 kPa ethanol - carbon dioxide vapour mixture under atmospheric total pressure and 24°C for flow rates of 0.512 (♦), 0.702 (■) and 0.898 l/min (▲).

The adsorption capacities for all three breakthrough curves converge to approximately 0.6 g ethanol/g adsorbent with a difference in adsorption capacity between the three experimental runs under 4 %. The adsorption capacities for these experiments are slightly higher than the two adsorption runs shown in Figure II.4 due to the slightly higher ethanol partial pressure. All the other experiments for this investigation were therefore performed at flow rates between 0.5 - 0.7 l/min, in order for the adsorption capacities to be considered independent of the flow rate and provide a better means for comparison.

Adsorbent Characterization

Since the best performing adsorbent was determined to be WV-B 1500 from MeadWestvaco due to higher ethanol adsorption capacity under the conditions considered for fermentation application, the adsorption characteristics of this adsorbent were examined in closer detail than the other adsorbents. Ethanol and water adsorption

isotherm experiments were conducted in the vicinity of atmospheric total pressure for vapour mixtures with carbon dioxide as the carrying gas. These experimental conditions resemble the conditions that would prevail in the envisaged gas stripping process where water and ethanol would be present in concentrations up to saturation in a stream of carbon dioxide. Figure II.6 and Figure II.7 show ethanol and water adsorption isotherms in the presence of carbon dioxide under atmospheric total pressure at 24°C, 35°C, and 50°C using WV-B 1500 activated carbon adsorbent.

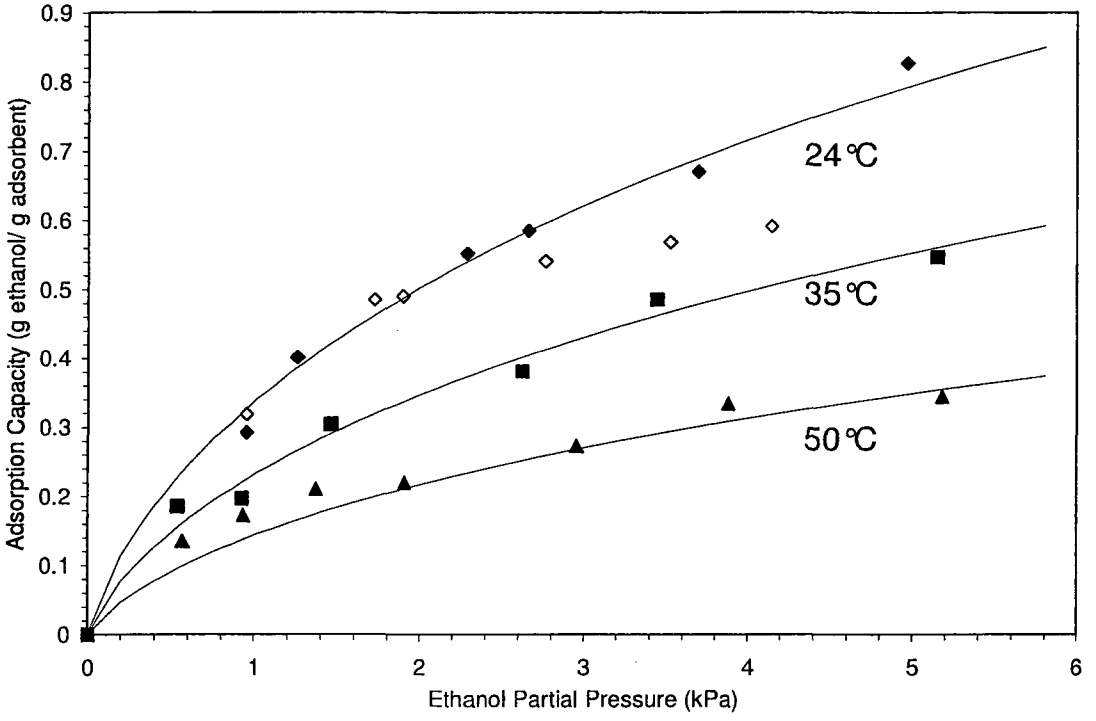

Figure II.6 - Multi-temperature isotherms for ethanol in the presence of carbon dioxide with WV-B 1500 activated carbon under atmospheric total pressure, together with temperature dependent Toth isotherm model fits at 24°C (♦), 35°C (■) and 50°C (▲). For 24°C data, isotherms were repeated in the presence of water and carbon dioxide (◊) using adsorbent WV-B 1500.

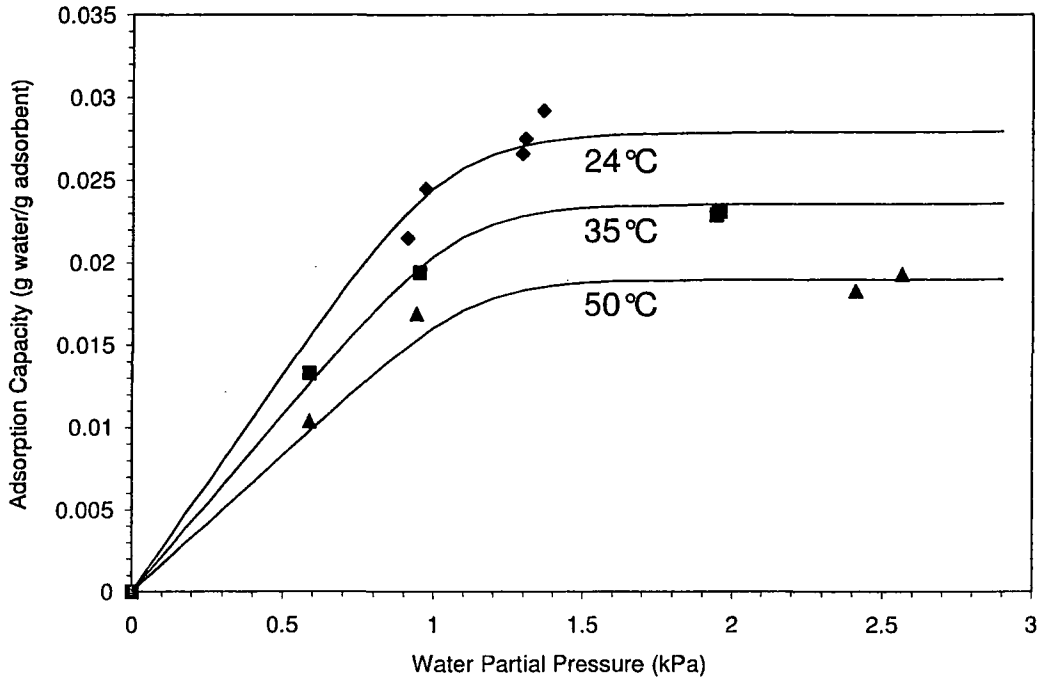

Figure II.7 - Multi-temperature isotherms for water in the presence of carbon dioxide with WV-B 1500 activated carbon under atmospheric conditions together with temperature dependent Toth isotherm model fits using adsorbent WV-B 1500 at 24°C (♦), 35°C (■) and 50°C (▲).

Ethanol adsorption capacity at higher ethanol concentrations of 5 kPa ethanol is approximately 0.8 g/g at 24°C. At a higher temperature (50°C), the ethanol adsorption capacity decreases to a value slightly below 0.35 g/g. At 35°C and a partial pressure of 2.5 kPa, the ethanol and water adsorption capacities were 0.41 and 0.024 g/g adsorbent, respectively. This result clearly shows that the WV-B 1500 activated carbon preferentially adsorbs ethanol over water by at least an order of magnitude under the conditions that would prevail for the exit stripping gas concentration of the fermentation broth.

Most of the data given in Figure II.6 and Figure II.7 were obtained separately for water and ethanol in a stream of carbon dioxide. However, in actual fermentation processes both species will form a ternary system. Therefore, isotherms for ternary ethanol/water/carbon dioxide mixtures needed to be obtained in order to determine the ethanol uptake in the presence of both water and carbon dioxide. The results of these

ternary mixture experiments are also shown in Figure II.6, which compares the adsorption capacity of ethanol with and without the presence of water at 24°C to determine if water affects the adsorption uptake of ethanol. Ethanol in the presence of water isotherm is shown for 24°C (◊) and compared to ethanol without the presence of water (♦) at the same temperature. The adsorption isotherms show that for an ethanol partial pressure of 2 kPa, the effect of water is minimal in terms of ethanol adsorption capacity. This makes sense when analyzing the water isotherms compared to the ethanol isotherms both in the presence of carbon dioxide with ethanol being adsorbed ten times as much as water in all cases and sometimes approaching 20 - 30 times. As ethanol concentration exceeds a partial pressure of 2 kPa, a noticeable decrease in its adsorption capacity is observed in the presence of water. Above a partial pressure of 4 kPa, the ethanol adsorption capacity in the presence of water decreases by approximately 20 %.

Table II.3 presents the separation factors for ethanol adsorption compared to water adsorption based on the data that were obtained from the ternary adsorption experiments performed.

Table II.3 – Separation factors for ternary adsorption runs.

Inlet Ethanol Concentration (kPa)	Inlet Water Concentration (kPa)	Separation Factor (Eq. 3) (-)
0.94	1.9	4.43
1.7	1.82	4.61
1.87	1.88	2.24
2.73	1.68	1.55
3.48	1.25	1.57
4.09	0.92	1.55

Since activated carbon can also adsorb some carbon dioxide, it is important to calculate the amount of carbon dioxide that could be adsorbed under experimental conditions prevailing in this investigation. Figure II. shows the isotherms for carbon dioxide adsorption by the adsorbent WV-B 1500 activated carbon. These experiments were done at atmospheric total pressure using helium as the carrier gas through the

column to obtain a range of carbon dioxide partial pressures, assuming that helium is not adsorbed on activated carbon.

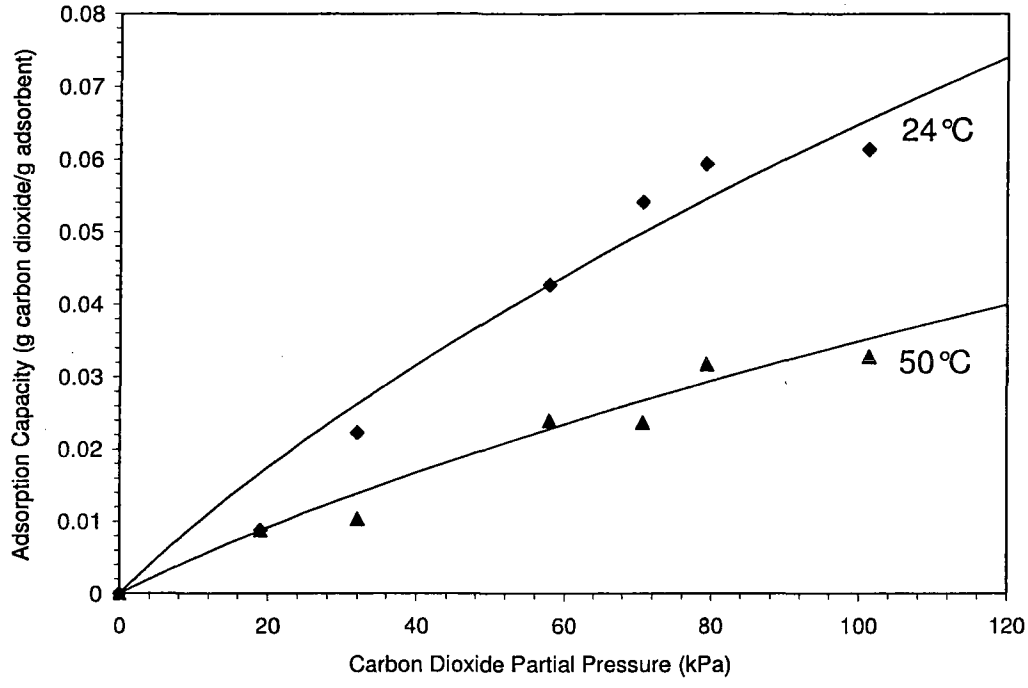

Figure II.8 - Multi-temperature isotherms at 24°C (♦) and 50°C (▲) for carbon dioxide adsorption by WV-B 1500 activated carbon with temperature dependent Toth isotherm model fits shown as curves.

In order to test the performance of activated carbon WV-B 1500 under conditions similar to an actual fermentation process, an experiment using a liquid ethanol - water mixture was conducted. Figure II.9 shows the breakthrough curves for ethanol and water under atmospheric conditions and 24°C.

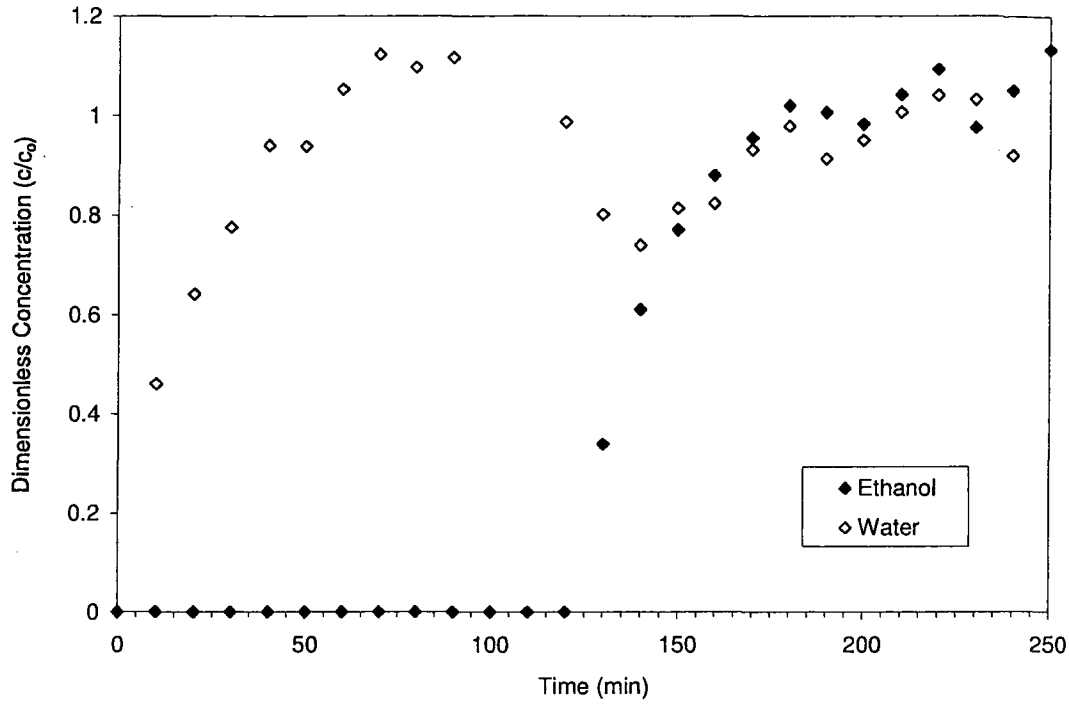

Figure II.9 - Breakthrough curves of ethanol - water - carbon dioxide vapour mixture under atmospheric total pressure at 24°C and ethanol (♦) and water (◊) partial pressures of 1.3 kPa and 1.85 kPa respectively.

The adsorption capacities for ethanol and water were determined to be 0.44 and 0.04 g/g adsorbent, respectively. The isotherm predictions for ethanol and water were 0.4 and 0.03 g/g adsorbent, respectively. This shows that the isotherm model accurately predicts the adsorption performance and ethanol adsorption does not vary to a large degree in the presence of carbon dioxide under fermentation conditions.

Another experiment was conducted where a water adsorption breakthrough was conducted followed by an ethanol adsorption breakthrough. The goal was to determine the effect of ethanol adsorption after water has already passed through the column to saturation. Water - carbon dioxide vapour mixture with a water partial pressure of 1.95 kPa ran through the adsorption column for a period of two hours to ensure saturation. After saturation was reached, an ethanol - carbon dioxide vapour mixture with an ethanol partial pressure of 4.2 kPa passed through the column. The adsorption capacity for ethanol calculated from the breakthrough curve was determined to be 0.73 g ethanol/g

adsorbent which fell very closely with the isotherm predicted value of 0.74 g ethanol/g adsorbent. Again, this shows ethanol adsorption is not strongly affected by moisture for adsorption.

Comparison of Figure II.6 and Figure II. clearly shows that the WV-B 1500 activated carbon adsorbs significantly more ethanol than carbon dioxide. For pure carbon dioxide under atmospheric pressure (101.3 kPa), the adsorbent has an experimental adsorption capacity of approximately 0.061 g/g. The carbon dioxide adsorption capacity corresponds well to literature values (Berlier and Frere, 1996; Goetz et al., 2006; Van der Vaart et al., 2000). At an ethanol-carbon dioxide mixture of 4.88 mol % ethanol (4.94 kPa ethanol partial pressure), the corresponding experimental adsorption capacities of ethanol and carbon dioxide adsorbed are 0.83 and 0.061 g/g, respectively under atmospheric total pressure at 24°C. This represents an order of magnitude difference in the total amount adsorbed. To better illustrate the difference in adsorption capacities between ethanol, water and carbon dioxide, Figure II.10 shows the water and carbon dioxide adsorption capacities relative to the ethanol adsorption capacities at 24°C. In Figure II.10b, in order to better visualize and compare individual isotherms, the partial pressures were normalized by dividing the partial pressure measurements with its maximum attained experimentally. In these series of experiments, the maximum partial pressures attained for ethanol, water and carbon dioxide were 4.96 kPa, 1.37 kPa, and 101.3 kPa, respectively. These values were therefore used to normalize the three isotherms as shown in Figure II.10b.

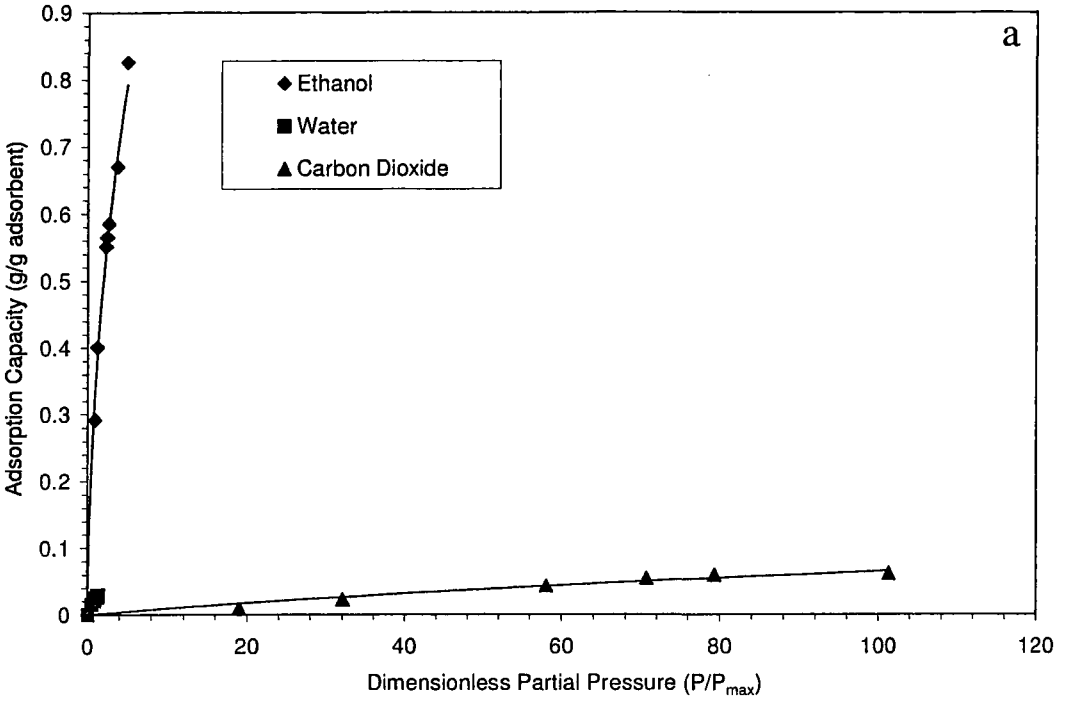

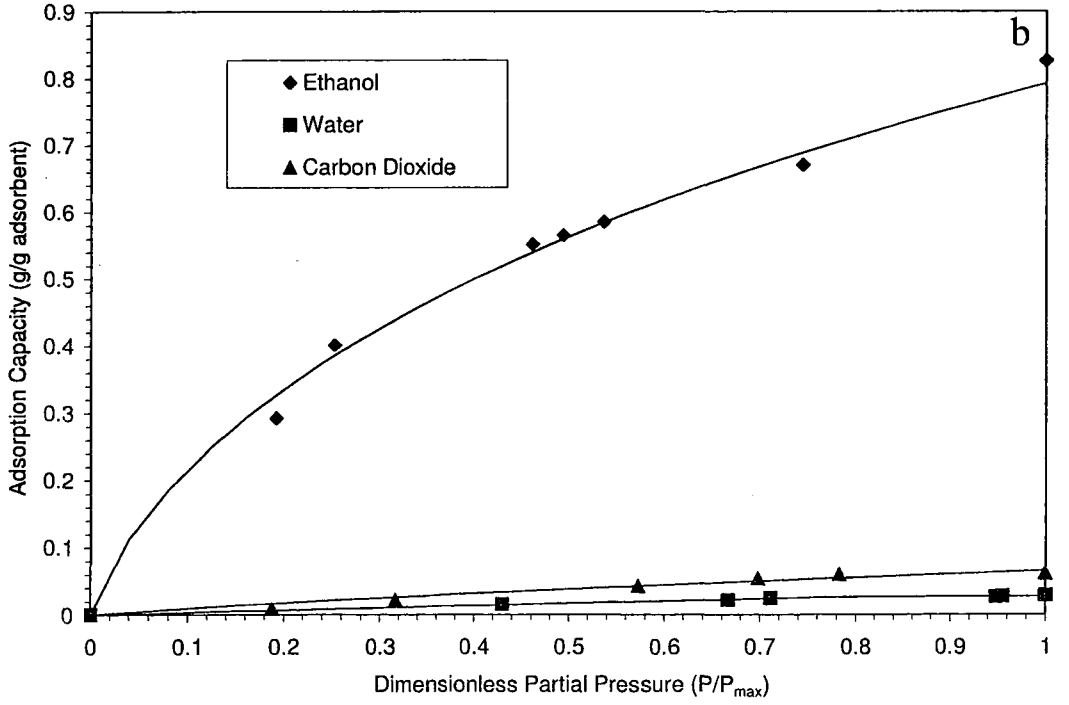

Figure II.10 - Multi-component adsorption isotherms for ethanol (♦), water (■) and carbon dioxide (▲) under atmospheric total pressure at 24°C using (a) the component partial pressure in kPa and (b) the dimensionless partial pressure.

For the operation of an adsorption process, an important adsorption characteristic is the adsorption working capacity. The working capacity is defined as the difference between adsorption capacities at the adsorption and the desorption conditions. This capacity determines how much of the desired adsorbate would be recovered after one adsorption - desorption cycle.

The Toth isotherm fits allow the prediction of adsorption capacities at varying concentrations and temperatures. This helps when calculating the adsorption working capacity since the adsorption capacity for the adsorption and desorption conditions can be predicted. The Toth isotherm fits obtained from the experimental ethanol isotherm data obtained at three different temperatures (parameters given in Table II.4) were used to predict the ethanol adsorption capacities at 125°C to illustrate the expected decrease in the ethanol adsorption capacity at a higher temperature. Note that the TOTH isotherm model parameters for ethanol and water are in the presence of carbon dioxide since carbon dioxide was used as the carrier gas.

Table II.4 – TOTH Isotherm fitting parameters for ethanol, water and carbon dioxide isotherms

TOTH Isotherm Parameters	Component		
	Ethanol	Water	Carbon Dioxide
n_{so} (mol/kg)	4.15	1.55	33.30
b_o (atm^{-1})	0.31	0.95	0.002
Q/RT_{ref} (unitless)	2.50	1.00	0.50
t_o (unitless)	0.37	6.92	0.60
α (unitless)	0.12	18.34	0.50
χ (unitless)	9.25	4.58	7.70

The ethanol content when running a carbon dioxide stripping fermentation process has an ethanol partial pressure of approximately 1.6 kPa. Assuming the adsorption and desorption steps are done at 30°C and 125°C respectively, the adsorption working capacity was determined to be approximately 0.349 g/g adsorbent. Note that the accuracy of the Toth isotherm is most accurate within the range of experimental temperatures. Therefore the prediction at 125°C is less accurate than the 30°C prediction.

Conclusions

Research in ethanol production is gaining steam with new discoveries coming out at a rapid pace. This study focused on utilizing the benefits of adsorption for the fermentation process using carbon dioxide stripping for the production of bio-ethanol from agricultural residues. Carbon dioxide stripping has been found to increase ethanol productivity and lower the effect of ethanol inhibition while picking up a portion of ethanol within the vapour phase.

An adsorption screening process was conducted showing that activated carbon WV-B 1500 adsorbed the most ethanol compared to the other adsorbents. For the different adsorbents studied, the order in performance was WV-B 1500 followed by RGC - 40, SORBONORIT B4, Filtrasorb 200, and HiSiv 3000 and lastly CBV 8014. All activated carbon samples showed higher ethanol adsorption capacities compared to the zeolite samples as well as a linear relationship between BET surface area and ethanol adsorption capacity. Analyzing the WV-B 1500 adsorbent, it was determined that ethanol adsorption was an order of magnitude higher than water and carbon dioxide adsorption which is a favourable result. The temperature-dependent Toth isotherm model represented the ethanol adsorption isotherms well for WV-B 1500 activated carbon. These results show that utilizing adsorption to effectively adsorb ethanol from the vapour mixture is a viable option for ethanol recovery.

References

Al-Asheh, S., Banat, F., Al-Lagtah, N., *Chemical Engineering Research and Design, 82 (A7)*, 855-864, 2004

Berlier, K., Frere, M., Journal of Chemical & Engineering Data, *41*, 1144-1148, 1996

Bowen, T.C., Vane, L.M., Langmuir, *22 (8)*, 3721-3727, 2006

Caputo, D., Iucolano, F., Pepe, F., Colella, C., *Microporous and Mesoporous Materials, 105*, 260-267, 2007

Carmo, M.J., Gubulin, J. C., *Brazilian Journal of Chemical Engineering, 14 (3)*, 1-9, 1997

Chang, H., Yuan, X-G., Tian, H., Zeng, A-W., *Chemical Engineering and Processing, 45*, 747-754, 2006a

Chang, H., Yuan, X-G., Tian, H., Zeng, A-W., *Chemical Engineering and Technology, 29 (4)*, 454-461, 2006b

Chang, H., Yuan, X-G., Tian, H., Zeng, A-W., *Industrial and Engineering Chemistry Research, 45*, 3916-3921, 2006c

Crawshaw, J. P., Hills, J. H., *Ind. Eng. Chem. Res., 29,* 307-309, 1990

Fletcher, A. J., Yuzak, Y., Thomas, K. M. "Adsorption and desorption kinetics for hydrophilic and hydrophobic vapours on activated carbon," Carbon, *44*, 989-1004, 2006

Goetz, V., Pupier, O., Guillot, A., Adsorption, *12*, 55-63, 2006

Grillot, M. J., *International Energy Annual 2005: World Energy Overview: 1995-2000*, Energy Information Administration, Official Energy Statistics from the U.S. Government, 2007; http://www.eia.doe.gov/iea/overview.html

Guan, J., Hu, X., *Separation and Purification Technology, 31*, 31-35, 2003

Ho, N. W. Y., Chen, Z., Brainard, A. P., *Applied and Environmental Microbiology, 64 (5)*, 1852-1859, 1998

Kupiec, K., Rakoczy, J., Zielinski, L., Georgiou, A., *Adsorption Science & Technology, 26 (3)*, 209-224, 2008

Lee, J.Y., Westgate, P.J., Ladisch, M.R., American Institute of Chemical Engineering Journal, *37 (8)*, 1187-1195, 1991

Milestone, N. B., Bibby, D. B., Journal of Chemical Technology and Biotechnology, *31 (1)*, 732-736, 1981

Naono, H., Hakuman, M., Shimoda, M., Nakai, K., Kondo, S., Journal of Colloid and Interface Science, *182*, 230-238, 1996

Oumi, Y., Miyajima, A., Miyamoto, J., Sano, T., Studies in Surface Science and Catalysis, *142*, 1595-1602, 2002

Pitt Jr., W. W., Haag, G. L., Lee, D.D., Biotechnology and Bioengineering, *25*, 123-131, 1983

Saha, B. B., El-Sharkawy, I. I., Chakraborty, A., Koyama, S., International Journal of Refrigeration, *30*, 86-95, 2007

Shafiee, S., Topal, E., Energy Policy, *37*, 181-189, 2009

Taylor F., Kurantz, M. J., Goldberg, N., Craig Jr., J. C., Biotechnology Progress, *11*, 693-696, 1995

Taylor F., Kurantz, M. J., Goldberg, N., Craig Jr., J. C., Biotechnology and Bioengineering, *51*, 33-39, 1996

Taylor F., Kurantz, M. J., Goldberg, N., Craig Jr., J. C., Applied Microbiology and Biotechnology, *48*, 311-316, 1997

Taylor F., Kurantz, M. J., Goldberg, N., Craig Jr., J. C., Biotechnology Letters, *20 (1)*, 67-72, 1998

Taylor F., Kurantz, M. J., Goldberg, N., McAloon, A. J., Craig Jr., J. C., Biotechnology Progress, *16*, 541-547, 2000

Toth, J., Acta Chimica Academiae Scientiarum Hungaricae, *15*, 415-424,1962

Van der Vaart, R., Huiskes, C., Bosch, H., Reith, T., Adsorption, *6*, 311-323, 2000

Vareli, G.D., Demertzis, P.G., Akrida-Demertzi, K., Z Lebensm Unters Forsch A, *205*, 204-208, 1997

Walsh, P. K., Liu, C. P., Findley, M. E., Liapis, A. I., Siehr, D. J., Biotechnology and Bioengineering Symposium, *No. 13*, 629-647, 1983

Weitkamp, J., Ernst, S., Gunzel, B., Deckwer, W. D., Zeolites, *11*, 314-317, 1991

Wyman, C. E., *Handbook of Bioethanol: Production and Utilization* Applied Energy Technology Series: Washington, DC, 1996; pp. 2-10

Chapter III: Recovery of ethanol from carbon dioxide stripped vapour mixture: Adsorption prediction and modeling

Mohamed Hashi, Jules Thibault, and F. Handan Tezel

Department of Chemical and Biological Engineering

University of Ottawa, Ottawa, Ontario, Canada K1N 6N5

To whom correspondence should be addressed. Telephone: +1-613-562-5800 x6094.

Email: jules.thibault@uottawa.ca

Abstract

A mathematical model was used to predict the adsorption performance of activated carbon WV-B 1500 for ethanol vapour adsorption in the presence of carbon dioxide and water. Adsorption and recovery of ethanol is important for the production of bio-ethanol produced from agricultural residue. The model takes into account changes in velocity due to adsorption, heat effects during adsorption, and heat losses to the surroundings. The model, developed without resorting to fitting parameters, was validated successfully by comparing the model predictions with experimental adsorption data. Finally, the model was used to predict the adsorption working capacities to assess the performance of the adsorption process in an industrial process.

Introduction

Bio-ethanol has become a hot topic of discussion within the public and industrial communities as a source of renewable energy. Due to the fluctuating economic climate and changing oil prices, the need for an alternative, sustainable energy source becomes more apparent every day. Bio-ethanol has many advantages such as reduced net greenhouse gas emissions and being renewable. A particular emphasis is now being placed on bio-ethanol derived from lignocellulosic materials because feed stocks to produce fermentable sugars can be obtained from agricultural waste as opposed to sugar cane, corn or wheat. The benefits include better utilization of waste biomass as well as an alleviation of the food versus fuel debate. On the other hand, there are disadvantages using lignocellulosic feed stocks: (1) greater difficulty accessing fermentable sugars, (2) the need to use genetically-modified yeast or bacteria, yet less tolerant to ethanol, to metabolize pentose and hexose sugars resulting from the hydrolysis of cellulose and hemicellulose, and (3) the higher cost for separating ethanol from water due to the lower final ethanol concentration (2-6% by weight) of the fermentation broth. In addition, the challenge of overcoming the azeotrope at 95.6 wt% is a problem common to all types of feed stocks.

To make the production of bio-ethanol an economically viable alternative, it is imperative to seek ways of lowering the energy demand at both ends of the ethanol concentration spectrum. Since a large amount of energy is needed to overcome the ethanol-water azeotrope, various separation techniques have been examined to replace the more energy-intensive methods such as the azeotropic distillation. One of these techniques is adsorption where water is preferentially removed from the final distillate to bring its concentration to above 99% purity (Chang et al., 2006; Lalik et al., 2006; Lu et al., 2007; Carmo and Gubulin, 2002; Guan and Hu, 2003). Another section of the process that could greatly enhance the economic viability of ethanol is to find a way to increase the ethanol yield in the fermenter. By partially removing ethanol from the fermentation broth, it would be possible to reduce the toxicity of the fermentation broth and therefore allow microorganisms to convert an increase quantity of sugars. A stripping gas can be used to remove ethanol during fermentation, thereby prolonging the production of ethanol. The stripped ethanol can also be recovered using adsorption except that, instead

of a water specific adsorbent used for ethanol dehydration to break the azeotrope, an ethanol specific adsorbent is required (Bobok and Besedova, 2004; Bradley et al., 1987; Taylor at al., 2000; Walsh et al., 1983).

There have been multiple papers published on the modeling of activated carbon adsorption (Manjare and Ghoshal, 2006; Cheng et al., 2004), temperature swing adsorption (Kim et al., 2004) and pressure swing adsorption processes (Ruthven, et al., 1994; Warmunzinski and Tanczyk, 1997). Some authors have modeled adsorption packed beds for the dehydration of ethanol to break the azeotrope (Caputo et al., 2007; Simo at al., 2008). A large percentage of these papers assumed isothermal conditions. In this investigation, it is desired to consider simultaneous changes in concentration and temperature along the packed bed.

The objective of this study is to enhance the ethanol production yield within the fermentation broth using a combination of in-situ ethanol removal using carbon dioxide as a stripping gas and an adsorption process. In addition, the modeling of the adsorption process for the uptake of ethanol from a carbon dioxide stripped vapour mixture is performed and validated using experimental data. The model was then used to predict an industrial adsorption column's performance.

Materials and Methods

Equipment Set-up

Figure III.1 shows the schematic diagram of the adsorption system used for screening and selecting the most appropriate adsorbents as well as studying the performance of a packed bed adsorber for its efficiency for preferentially adsorbing ethanol. Downstream of the carbon dioxide gas cylinder, two gas mass flow controllers (MKS, Ottawa, Ontario, Canada) are used to control the flow of carbon dioxide through the two 1-L Erlenmeyer flasks (used as bubblers) containing pure ethanol and water, respectively. The two vapour streams combine just before entering an adsorption column (0.78 cm I.D. and 36 cm long) wrapped in a heating tape. The inlet vapour composition fed to the column was set by controlling the flows through the two mass flow controllers. A by-pass around the column was added to allow for the determination of the inlet vapour composition. The inlet and outlet vapour streams of the adsorption column were

analyzed using a GOW-MAC (Bethlehem, Pennsylvania, USA) Series 580 TCD (Thermal Conductivity Detector) isothermal Gas Chromatograph (GC) using a Porapak Q column. The flow of the gas mixture through GC's sample loop was controlled using a Thermo Scientific (Ottawa, Ontario, Canada) vacuum pump. All connections and piping were purchased from Swagelok except for the ball valves which were obtained from Parker Hannifin Corp (Montreal, Quebec, Canada). The GC's operating column, the detector and the injection port were kept at a temperature of 135°C, 165°C, and 160°C, respectively.

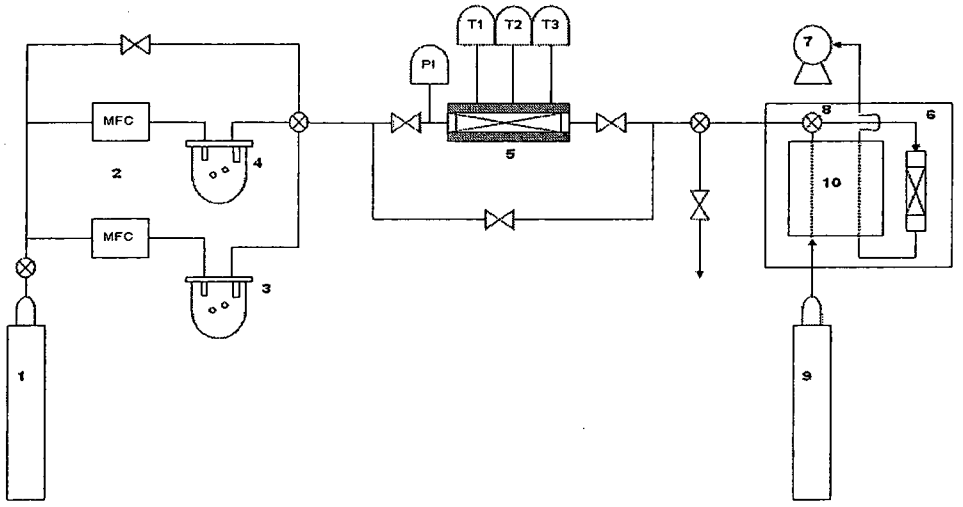

Figure III.1 - Schematic diagram of the experimental adsorption system: 1 – carbon dioxide gas cylinder; 2 – mass flow controllers (MFC) 3 – ethanol bath; 4 – water bath; 5 – adsorption column wrapped with a heating tape; 6 – GOW MAC Gas Chromatograph; 7 – vacuum pump; 8 - sample injection valve; 9 - helium carrier gas cylinder; TC1-3 – Thermocouples 1 through 3; PI – pressure gauge.

The adsorbent selected for this study was MeadWestvaco's (Glen Allen, VA, USA) WV-B 1500 activated carbon. The adsorbent provided the highest ethanol adsorption capacity based on a previous study where an adsorbent screening was conducted to determine the best performing adsorbents (Hashi et al., 2010). The characteristics of the adsorbent and the adsorption bed are listed in
Table **III.1** and Table III.2, respectively.

Table III.1 - Characteristics of the WV-B 1500 activated carbon adsorbent used in this study.

Pellet diameter	0.67	mm
Void fraction in the pellet[1]	0.793	-
BET surface area[2]	2200	$m^2 g^{-1}$
Heat capacity of the solid	1130	$J kg^{-1} K^{-1}$

[1] Calculated from Pushnov, 2006
[2] Literature value from the manufacturer

Table III.2 - Characteristics of the adsorption column used in this study.

Length	0.36	m
Diameter	7.8	mm
Void fraction in the column	0.35	-
Heat capacity of the column wall	500	$J kg^{-1} K^{-1}$
Density of the wall	8238	$kg m^{-3}$
Wall thickness	0.9	mm
Bulk density of the bed	489.6	$kg m^{-3}$

Experimental Procedure

Before each adsorption experiment, the adsorbent was degassed at 250°C overnight (minimum of 8 h) using air as the purge gas. The next day, the gas chromatograph was heated until all set temperatures reached equilibrium. Once the gas chromatograph was ready, carbon dioxide flow was split into two streams using the two mass flow controllers and bubbled through the ethanol and water baths, in parallel. The ethanol-CO_2 and water-CO_2 gas streams were then recombined before entering the adsorption column where they came into contact with the adsorbent packed in the column. The composition of the stream entering the adsorption column was adjusted to the desired value by controlling the flow rate of carbon dioxide going into the ethanol and the water baths, separately. Using a vacuum pump, a sample was taken from the outlet stream of the adsorption column every five minutes and injected into the gas chromatograph to determine the vapour mixture composition leaving the packed column. The determination of the outlet gas composition from the column as a function of time allowed obtaining the complete breakthrough curve and subsequently determining the column adsorption capacity for all the components in the adsorbate gas. Throughout the experiment, the temperature of the packed bed was monitored at three strategic points along the column using Type T thermocouple (OMEGA Engineering, Laval, Quebec,

Canada). The thermocouples were placed in the column at 9, 18 and 27 cm from the entrance. The temperatures provide additional information that was used to further validate the model with respect to the energy balance.

The adsorption capacities were determined using a series of breakthrough curves with a stream of carbon dioxide containing water and ethanol over a wide range of inlet concentrations up to their saturation concentration. The area above the breakthrough curve is proportional to the total amount adsorbed in the column as expressed by Equation (1). AC_i, $m_{flow,i}$ and $m_{adsorbent}$ represent the adsorption capacity for component i (g/g adsorbent), the mass flow rate for component i (g/s), and the mass of the adsorbent (g), respectively.

$$AC_i = \frac{t_i \cdot m_{flow,i}}{m_{adsorbent}} \tag{1}$$

Variable t_i corresponds to the calculation of the area above the normalized breakthrough curve in seconds, as shown in Equation (2), where c_i and c_{io} represent the outlet and inlet concentrations for component i (g/l), respectively.

$$t_i = \int_0^\infty \left(1 - \frac{c_i}{c_{io}}\right) dt \tag{2}$$

Modeling of the Adsorption Process

The adsorption process was modelled using both material and energy balances for the column. Assumptions made to simplify the solution include: constant void fraction throughout the column, no radial change in concentration and temperature in the column, perfectly spherical adsorbent particles, ideal gas law, and physical characteristics of bulk gas are close to those for pure carbon dioxide since a minimum of 95% of the vapour mixture is composed of carbon dioxide.

Material Balances

Material balance for the column has been written for 2 different scenarios and the modeling was done separately for these 2 scenarios.

In the first scenario, instantaneous equilibrium between the fluid phase and the solid adsorbent surface was assumed. For this case, the governing equation representing the component material balance in the bulk phase is given by Equation (3):

$$\varepsilon_c \frac{\partial c_g}{\partial t} = \varepsilon_c D_Z \frac{\partial^2 c_g}{\partial z^2} - \varepsilon_c v_g \frac{\partial c_g}{\partial z} - \varepsilon_c c_g \frac{\partial v_g}{\partial z} - k_f \frac{3}{r_p}\left(c_g - c_P^*\right) \quad (3)$$

Equation (3) describes that the rate of accumulation is a function of the species axial dispersion within the column, convection through the column and mass transfer due to adsorption.

The initial condition and the boundary conditions for the inlet and the outlet species concentration of the adsorption column are given by Equations (4) - (6).

Initial Conditions: at t = 0, for all z, $c_g\big|_{t=0} = 0$ (4)

Boundary Conditions: at z = 0, $c_g\big|_z^t = c_g\big|_{inlet}$ (5)

at z = L, $\frac{\partial c_g}{\partial z} = 0$ (6)

In the second scenario, the assumption of an instantaneous adsorption was relaxed such that the diffusion of species in the particle was taken into account. For this case, Equation (3) is replaced by Equation (7), and the governing differential equation representing the component material balance within the adsorbent pellet is given by Equation (8).

$$\varepsilon_c \frac{\partial c_g}{\partial t} = \varepsilon_c D_Z \frac{\partial^2 c_g}{\partial z^2} - \varepsilon_c v_g \frac{\partial c_g}{\partial z} - \varepsilon_c c_g \frac{\partial v_g}{\partial z} - k_f \frac{3}{r_p}\left(c_g - c_P\big|_{r=R_p}\right) \quad (7)$$

$$\left[\varepsilon_P + (1-\varepsilon_P)\rho_S \frac{\partial c_A}{\partial c_P}\right]\frac{\partial c_P}{\partial t} = D_e \varepsilon_P \left[\frac{2}{r}\frac{\partial c_P}{\partial r} + \frac{\partial^2 c_P}{\partial r^2}\right] \quad (8)$$

The initial and boundary conditions for the column are identical to those of Equations (4)-(6), and those for the pellet are given in Equations (9)-(11), considering the boundaries at the centre of the pellet and at the pellet surface:

Initial Condition: at t = 0, for all r, $c_P\big|_{t=0} = 0$ (9)

Boundary Conditions: at r = 0, $\frac{\partial c_P}{\partial r} = 0$ (10)

$$\text{at r} = R_p,\ -D_e \frac{\partial c_P}{\partial r} = k_f \left(c_g \Big|_z^t - c_P \Big|_{r=R_P}^t \right) \tag{11}$$

Energy Balances

For the first scenario, where instantaneous equilibrium between the fluid phase and the solid adsorbent surface is assumed, the governing equation representing the energy balance in the bulk phase is given by Equation (12).

$$\eta \frac{\partial T_g}{\partial t} = k_g \frac{\partial^2 T_g}{\partial z^2} - v_g \rho_g C_{Pg} \varepsilon_c \frac{\partial T_g}{\partial z} - \rho_b \Delta H_{ads} k_f \frac{3(1-\varepsilon_c)}{\varepsilon_c r_p} \{ c_A^* - \bar{c}_A \} - h_{fD} \frac{2}{r_c} (T_g - T_w) \tag{12}$$

where the average heat thermal capacity (η), taking into account the void fraction of the bulk phase and the pellet, is given by Equation (13).

$$\eta = \rho_g C_{Pg} [(\varepsilon_c + (1-\varepsilon_c)\varepsilon_P)] + (1-\varepsilon_c)(1-\varepsilon_P)\rho_s C_{Ps} \tag{13}$$

Equation (12) states that the accumulation of energy in the column depends on the axial dispersion, convection through the column, heat of adsorption and heat lost to the surroundings. The initial and boundary conditions for energy balance in the bulk phase are shown in Equations (14) – (16) below:

Initial Condition: $\quad \text{at t} = 0, \text{ for all z}, \ T_g \big|_{t=0} = 0 \tag{14}$

Boundary Conditions: $\quad \text{at z} = 0, \ T_g \big|_z^t = T_g \big|_{inlet} \tag{15}$

$$\text{at z} = \text{L}, \ \frac{\partial T_g}{\partial z} = 0 \tag{16}$$

For the second scenario, where heat and mass diffusion within the adsorbent pellet cannot be neglected, Equation (12) is replaced by Equation (17) and the governing equation representing the energy balance within the adsorbent pellet is given by Equation (18).

$$(\rho_g C_{Pg} \varepsilon_c) \frac{\partial T_g}{\partial t} = k_g \frac{\partial^2 T_g}{\partial z^2} - v_g \rho_g C_{Pg} \varepsilon_c \frac{\partial T_g}{\partial z} - h_{fP} \frac{3}{r_p} (1-\varepsilon_c)(T_g - T_P \big|_{r=R_p}) - h_{fD} \frac{2}{r_c} (T_g - T_w) \tag{17}$$

$$\left[(\varepsilon_P)\rho_g C_{Pg} + (1-\varepsilon_P)\rho_S C_{PS}\right]\frac{\partial T_P}{\partial t} = k_{GS}\left[\frac{1}{r^2}\frac{\partial}{\partial r}\left(r^2\frac{\partial T_P}{\partial r}\right)\right] + (\Delta H_{ads})\rho_{bed}\frac{\partial c_a}{\partial c_p}\frac{\partial c_p}{\partial t} \quad (18)$$

The change in temperature at any radial position within the pellet depends on heat diffusion and heat gained through adsorption. The initial and boundary conditions for the column for this scenario are given by Equations (14)-(16) and those for the pellet are given by Equations (19)-(21):

Initial Condition: at t = 0, for all r, $T_P\big|_{t=0} = 0$ (19)

Boundary Conditions: at r = 0, $\frac{\partial T_P}{\partial r} = 0$ (20)

at r = R_p, $-k_{gs}\frac{\partial T_P}{\partial r} = h_f\left(T_g\big|_z^t - T_P\big|_{r=R_P}^t\right)$ (21)

The heat balance for the bulk phase in the column must also consider the heat loss to the surrounding through the column wall. To calculate the wall temperature, an energy balance across the adsorption column wall (Equation (22)) needs to be solved.

$$\left[r_o^2 - r_c^2\right]\rho_w C_{Pw}\frac{\partial T_w}{\partial t} = 2r_c h_{fD}\left(T_g - T_w\right) - 2r_o h_o\left(T_w - T_{sur}\right) \quad (22)$$

Ergun Equation for the Pressure Drop in the Column

Even though the pressure drop across the adsorption column used in this investigation is relatively small, the effect still needs to be considered. The pressure drop across the column was measured to be less than 2 kPa and was predicted very well using the Ergun Equation, given in Equation (23).

$$\frac{\Delta P}{L} = \frac{-150(1-\varepsilon_c)^2 v_g \mu}{\varepsilon_c^3 \Phi^2 D_P^2} + \frac{1.75(1-\varepsilon_c)v_g \rho_g}{\varepsilon_c^3 \Phi D_P} \quad (23)$$

Empirical Equations

The molecular diffusion and Knudsen diffusion through the macropores of the adsorbent were considered for the estimation of the diffusion coefficient in the pellet. For a binary mixture, Equation (24) was used to estimate the molecular diffusivity (Hirschfelder et al., 1949).

$$D_M = \frac{0.001858\,T^{1.5}\left(\frac{1}{M_A}+\frac{1}{M_B}\right)^{0.5}}{P\sigma_{AB}^2\Omega_D} \tag{24}$$

The Knudsen diffusion coefficient in the macropores was estimated using Equation (25).

$$D_K = 9700 r_p \sqrt{T/MW_{AB}} \tag{25}$$

After the calculation of molecular and Knudsen diffusion coefficients, Equation (26) is used to calculate the overall effective diffusivity taking into account both mass transfer mechanisms.

$$D_e = \frac{\left[\frac{1}{D_M}+\frac{1}{D_K}\right]^{-1}}{\tau} \tag{26}$$

The axial dispersion and mass transfer coefficients are calculated using empirical Equations (27) and (28), respectively (Wakao and Funazkri, 1978):

$$D_Z = \frac{D_M}{\varepsilon_c}[20 + 0.5(\mathrm{Re})(Sc)] \tag{27}$$

$$k_f = \frac{D_M}{D_p}\left[2.0 + 1.1(\mathrm{Re})^{0.6}(Sc)^{0.33}\right] \tag{28}$$

Within the energy balance equations, the main parameters that need to be estimated include heat transfer coefficients and thermal conductivities. The outside heat transfer coefficient is estimated using Equations (29)-(31) (Churchill and Chu, 1975; Incropera, at al., 2007).

$$Ra = \frac{\beta \Delta T g L^3 \,\mathrm{Pr}}{\nu^2} \tag{29}$$

$$Nu = \left\{0.60 + \frac{0.387 Ra^{1/4}}{\left[1 + (0.559/\mathrm{Pr})^{9-14}\right]^{8/27}}\right\}^2 \tag{30}$$

$$h_o = \frac{k_g \cdot Nu}{L} \tag{31}$$

With laminar flow, as well as assuming fully developed conditions, the Nusselt number is a constant and is independent of Re_D, Pr, and axial location. The value for the Nusselt number was calculated to be 4.36 (Incropera et al., 2007).

Results and Discussion

Experimental Results and Model Validation

Isotherm Models

When modeling the experimental adsorption and desorption breakthrough curves and temperature profiles, an accurate representation of the adsorption characteristics is needed. The temperature-dependent Langmuir isotherm was chosen for this study to represent adsorption isotherms. The Langmuir isotherm is the most common isotherm model and was derived for monolayer adsorption on homogeneous surfaces (Langmuir, 1918) and is described in Equation (32).

$$q = \frac{q_m bP}{1 + bP} \tag{32}$$

The Langmuir isotherm can also be extended for other conditions with some success. Since adsorption processes are non-isothermal, the temperature increase during the process affects adsorption capacity and needs to be taken into account. The parameters q_m and b of Equation (32) can be extended to become temperature-dependent parameters as described in Equations (33)-(34) (Kikkinides et al., 1993; Zahra at al., 2008).

$$q_m = k_1 - k_2 T \tag{33}$$

$$b = k_3 \exp(k_4 / T) \tag{34}$$

The constants k_1, k_2, k_3, and k_4 were obtained by fitting the model with experimental isotherm data obtained at different temperatures. The comparison of the experimental and predicted temperature-dependent isotherms, and the model parameters are presented in Figure III.2 and Table III.3, respectively.

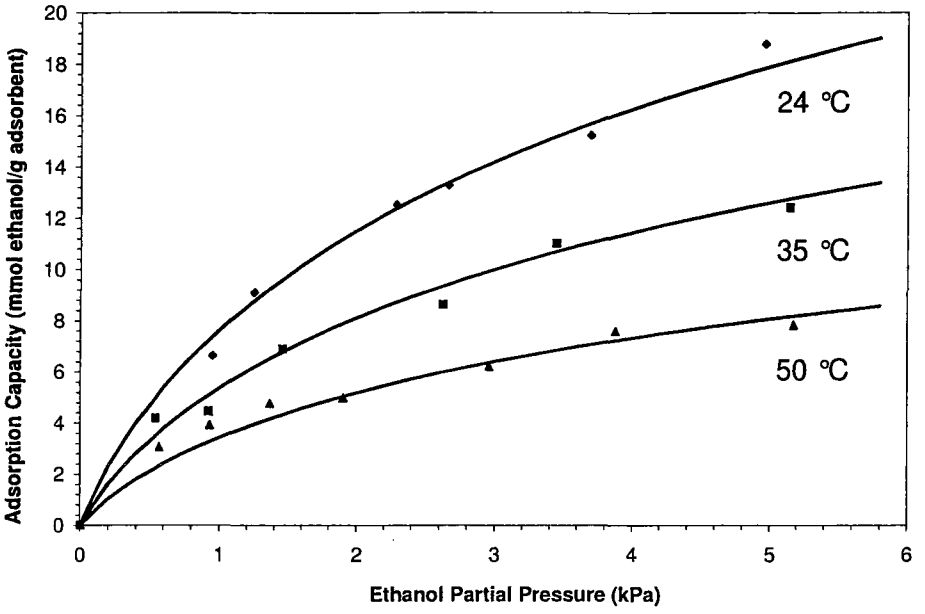

Figure III.2 – Comparison of experimental adsorption isotherms of ethanol at 25 (♦), 35(■), and 50°C (▲) in the presence of carbon dioxide with WV-B 1500 activated carbon under atmospheric total pressure, with temperature-dependent Langmuir isotherm model fits (——). Experimental isotherm data were taken from Hashi et al., 2010.

Table III.3 – Temperature fitted parameters for temperature-dependent Langmuir isotherm model

Parameters	**Components**		
	Ethanol	Carbon Dioxide	Water
k_1 (mmol/g)	188.1	344.8	174.2
k_2 (mmol/g K)	0.545	0.988	0.510
k_3 (atm^{-1})	6.861	0.032	1.375
k_4 (K)	518.2	-4.08	408.2

The temperature-dependent Langmuir isotherm is limited to between 25°C and 50°C due to the assumption that the Langmuir adsorption constant (q_m) changes linearly as a function of temperature. Between these temperatures, the isotherm fits satisfactorily the experimental data as shown in Figure III.2. During the simulations, the change in adsorption capacity with respect to the bulk phase concentration is defined by the derivative of the isotherm. The temperature dependent-Langmuir isotherm was used due to its satisfactory fit and simple differentiation.

Adsorption of CO_2 – ethanol binary system

The ethanol concentration breakthrough curve and bed temperature at three locations along the bed as a function of time are shown in Figure III.3 for an inlet ethanol-carbon dioxide binary vapour for a 2.62 mol% ethanol (partial pressure of 2.65 kPa under atmospheric total pressure) at 24°C. Figure III.3 compares the experimental data for the ethanol concentration and the three temperatures as a function of time with those predicted with the heat and mass transfer models. It is important to stress that, to validate the model, the predicted curves were obtained using estimated model parameters from correlations available in the literature and not using a fitted parameters that would be obtained to minimize the differences between experimental and predicted data. The only experimental data that was used in the model was the isotherm equation that is of course specific for a given adsorbent and cannot be predicted from first principles. Two predicted breakthrough curves are plotted in Figure III.3, one for instantaneous adsorption and one where diffusion within the pellets is included. The prediction of the breakthrough curve is particularly good when the radial diffusion within the pellet (scenario 2) is considered whereas the fit assuming instantaneous adsorption (scenario 2) is also quite good accept possible at the beginning of the breakthrough. These results show that the model represents adequately the dynamic behaviour of the adsorbent packed bed and could be used with confidence to design an adsorption packed bed. A better fit could obviously be obtained by fitting the model to the experimental data but then the model will be more specific for the experimental packed bed.

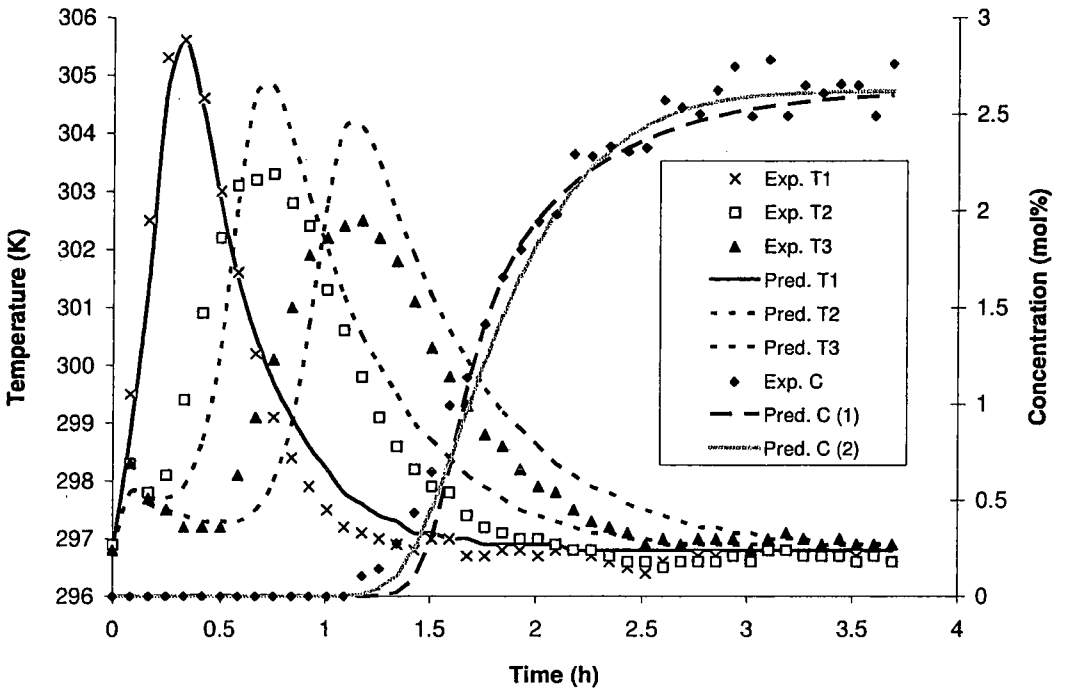

Figure III.3 - Ethanol concentration breakthrough curve and three temperatures along the packed bed for a 2.62 mol % inlet ethanol-carbon dioxide binary vapour mixture (ethanol partial pressure of 2.65 kPa under atmospheric total pressure) at 24°C. Experimental and predicted curves are represented by symbols and lines, respectively. Pred. C(1) represents the model taking into account only the bulk phase while Pred. C(2) takes into account the pore diffusion model.

The scattered tailing in the experimental concentration breakthrough of Figure III.3 represents the limitation of the gas chromatograph used. Nevertheless, the model predicts the tailing end of the curve relatively as it passes through the average ethanol concentration and converges to the inlet concentration.

The initial small hump and dip observed in the temperature variations at three locations along the adsorption column as a function of time is attributed to carbon dioxide adsorption and desorption which are taken into account within the model. This adsorption and desorption behaviour indicates that competitive adsorption occurs on this adsorption whereby a large portion of the CO_2 that was adsorbed was displaced when the ethanol adsorption zone reached a given zone of the packed bed. The prediction of the first temperature peak is predicted very well and much better that the other two temperature

peaks. This poorer prediction for the other two temperatures may be due to an underestimated amount of heat loss to the surroundings. Nevertheless, the model fits the tailing of the temperature curves very well. It is important to stress that the magnitude of the temperature increase in all cases is relatively small. For the experiment reported in Figure III.3, the temperature increase due to adsorption does not exceed 9°C as the maximum temperature is 33°C (306 K) for an inlet temperature of 24°C.

Adsorption and desorption cycles for CO_2 – ethanol binary system

A series of experiments were performed to investigate the adsorption and desorption of ethanol over a complete cycle. Initially, a stream of ethanol and CO_2 is passed through a fresh adsorption column until the column is completely saturated. Then, the inlet feed stream is replaced with a stream of pure carbon dioxide at the same temperature and pressure to desorb ethanol. The experiment proceeds until the column has been completely stripped of ethanol. Figure III.4 presents the results of an experiment performed with an initial inlet ethanol concentration of 4.96 mole % (ethanol partial pressure of 5.03 kPa under atmospheric conditions). This figure presents the exit ethanol concentration and the three temperatures along the adsorption packed bed as a function of time. This figure presents both the experimental and predicted data of these variables. Figure III.4a present the data obtained during the adsorption cycle whereas Figure III.4b presents similar data for the desorption cycle. The long lag time between column saturation and the start of the desorption cycle was to ensure that adsorption saturation was achieved.

The prediction of the concentration profile for both adsorption and desorption cycles is quite satisfactory considering that no optimization was performed to fit the parameters of the model. Performing an integration on both cycles, it was determined that 3.65 g of ethanol were recovered compared to 4.10 g adsorbed, representing a recovery of 89%. This is quite good considering the accuracy of the gas chromatograph at lower ethanol concentration. The results confirm that it is important to consider the diffusive mechanism within the adsorbent pellets since the prediction is significantly better when this phenomenon is taken into account.

The mirror image of the temperature profile is due to the heat of adsorption and desorption. The prediction of the temperature variation at the three locations along the column is quite good. It is important to mention that the temperature changes along the column probably have no impact or only minimal impact on the ethanol breakthrough curve since the column returns to the inlet stream temperature quite rapidly.

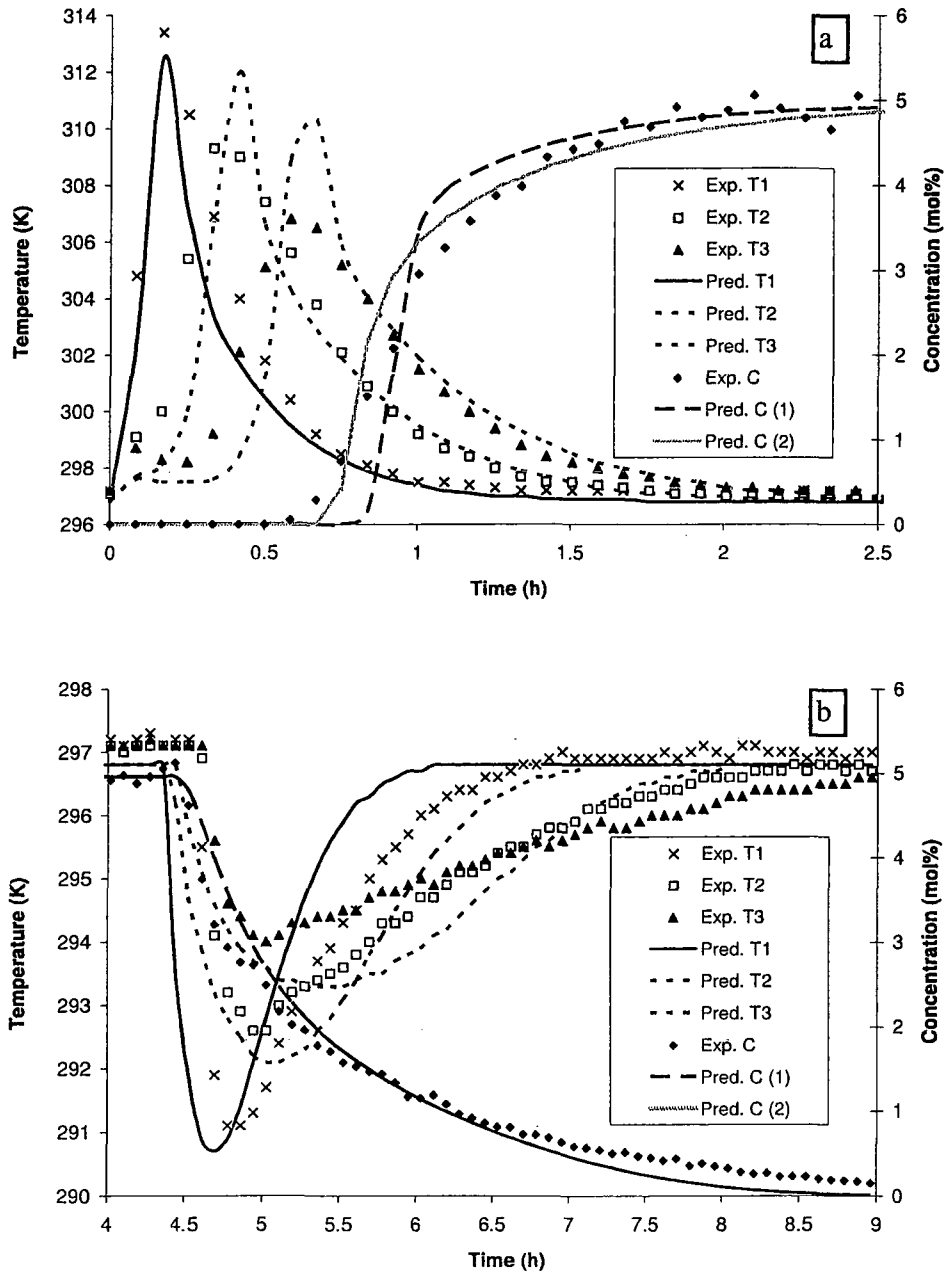

Figure III.4 - Ethanol concentration breakthrough curve and three temperatures along the packed bed for a 4.96 mole % (ethanol partial pressure of 5.03 kPa under atmospheric total pressure) initial binary ethanol-carbon dioxide vapour mixture at an inlet temperature of 24°C. Experimental data are represented by symbols whereas predicted are represented by lines. Pred. C(1) represents the prediction considering instantaneous adsorption while Pred. C(2) represents the predictions with the diffusion model. **a**: adsorption and **b**: desorption.

Ternary adsorption (CO_2 – ethanol – water)

In the envisaged application, the stream leaving the fermenter will be composed mostly of carbon dioxide saturated with ethanol and water. A series of experiments were performed with various concentrations of ethanol and water in the carbon dioxide carrier gas. Figure III.5 presents the experimental and predicted ethanol and water concentration breakthrough curves, at atmospheric total pressure and 24°C, for an inlet gas stream composed of 1.90 inlet water mole % (1.93 kPa), 0.94 mole % ethanol (0.95 kPa) and the balance being carbon dioxide.

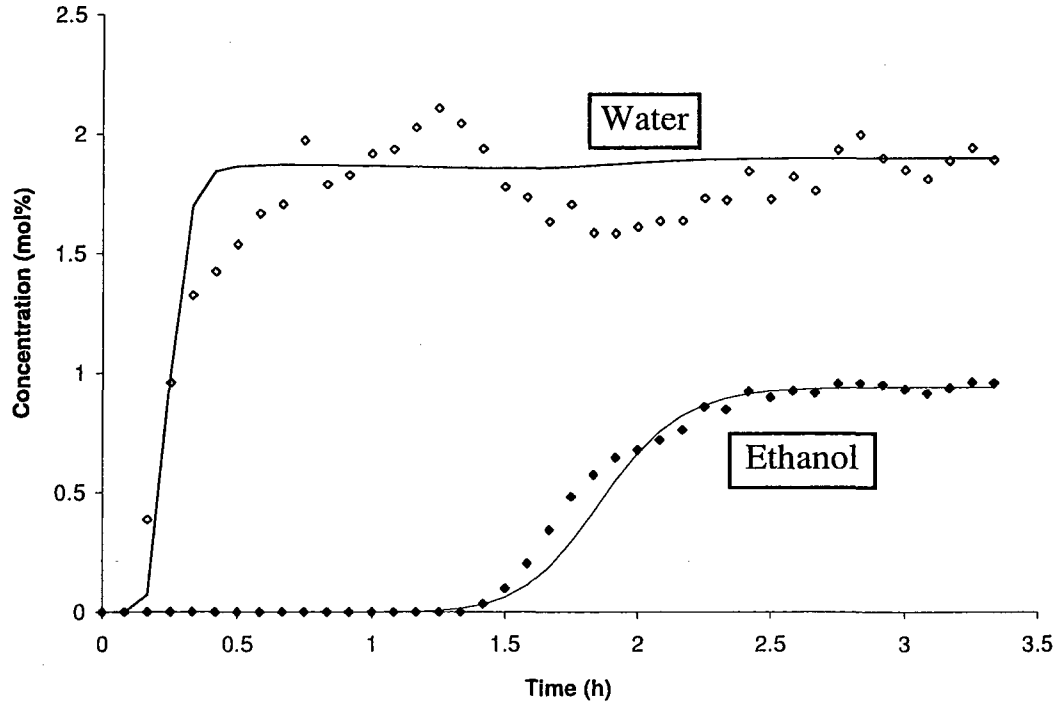

Figure III.5 - Adsorption concentration profile for ethanol-water-carbon dioxide vapour mixture at an inlet water and ethanol mole % of 1.90 and 0.94, respectively under
atmospheric total pressure at 24°C. Experimental and predicted breakthrough curves are represented by symbols and lines, respectively.

The model prediction for the ethanol breakthrough curve is very good. The small deviation is attributed to small differences between the experimental ethanol adsorption

capacity and the predicted adsorption capacity as predicted by the temperature-dependent Langmuir isotherm. The water breakthrough curve displays an early and very sharp increase showing that the water adsorption capacity is relatively low with respect to ethanol. The amount of water adsorption is consistent with previous studies (Hashi et al., 2010). The subsequent behaviour displayed in the water breakthrough curve, where a maximum is observed, is an indication that competitive adsorption exists between water and ethanol. When the ethanol adsorption front reaches a zone of the bed where water was more freely adsorbed, water is partly displaced to free adsorption sites to ethanol which is preferentially adsorbed.

Analysis of a large scale adsorption scenario

In an industrial application, a given adsorption packed bed would be subjected to numerous adsorption and desorption cyles. Depending on the mode of operation, the effective or working capacity of a packed bed adsorber is given by the diffference between the capacity of the column at the end of the adsorption cycle and the capacity at the end of the desorption cycle. Two potential modes of operation of a packed bed adsorber are the temperature swing adsorption (TSA) and the pressure swing adsorption (PSA).

In a TSA, a purge gas at an elevated temperature is used to partly or totally desorb the adsorbed species. For illustrative purposes, gas stripping of a typical fermentation broth at an ethanol concentration of 6 wt% is considered. The carbon dioxide stripped vapour mixture composition, assuming ethanol and water satutation under atmospheric conditions and 30°C, has a composition of 1.62, 4.09, and 94.29 mole %, respectively for ethanol, water and carbon dioxide. These concentrations correspond to partial pressures of 1.64, 4.14 and 95.55 kPa, respectively. Using a purge gas at 80 and 120°C for the desorption cycle, the expected working capacities from the isothermswould be 6.6 and 7.9 mmol/g adsorbent (0.30 and 0.36 g/g adsorbent), respectively. If the purge gas was an inert gas, ethanol would be completely desorbed and the working capacities would be equal to the amount adsorbed. A higher working capacity is obtained at a higher desorption temperature but at the expense of a higher heat load to heat and cool the purge

gas. An economic analysis must be performed to determine the optimal desorption temperature.

A PSA system runs the adsorption cycle at higher pressures and the desorption cycle at either atmospheric pressure or under vacuum. A higher pressure theoretically increases the adsorption uptake potential of the packed bed adsorber and this is applicable to a species that is non condensable under the conditions of operation. However, the concentrations of ethanol and water are thermodynamically limited and their partial pressures are independent of the total pressure such that the adsorption capacity is the same at 1, 3 or 5 atm. A PSA cannot be used for the envisaged application.

Conclusions

In this investigation, a series of adsorption experiments were performed for binary ethanol-CO_2 and ternary ethanol-CO_2 systems to examine the technical viability of carbon dioxide stripping to reduce the ethanol concentration within the fermentation broth in order to increase the ethanol productivity. The experimental data were instrumental to validate a phenomenological mathematical model that was developed to predict the breakthrough curves and temperature variations within a packed bed adsorber. The quality of prediction of the model, which did not resort to fitted parameters except for the isotherms, was very good and could be used with confidence to design and optimize packed bed adsorbers. For the envisaged system, a TSA could be used to operate the packed bed adsorber over numerous cycles whereas a PSA cannot be used for thermodynamic reasons. A complete economic analysis must be completed to properly assess the carbon dioxide stripping plus adsorption process for an ethanol production process.

Nomenclature

ΔH_{ads}	Heat of adsorption	J mol^{-1}
AC_i	Component adsorption capacity	kg/kg adsorbent
c_A	Concentration in the adsorbed phase	mol m^{-3}
c_g	Concentration in the bulk phase	mol m^{-3}
c_i	Outlet component concentration during experiments	mol m^{-3}
c_{io}	Inlet component concentration during experiments	mol m^{-3}
c_p	Concentration within the pellet	mol m^{-3}
C_{Pg}	Heat capacity of vapour mixture	J kg^{-1} K^{-1}
C_{PS}	Heat capacity of solid	J kg^{-1} K^{-1}
D_M	Molecular diffusivity	m s^{-1}
D_Z	Axial dispersion	m s^{-1}
g	Acceleration due to gravity	m s^{-2}
h_{fD}	Heat transfer coefficient in the bulk phase	J s^{-1} $m^{-}2$ K^{-1}
h_{fP}	Heat transfer coefficient at the surface of the pellet	J s^{-1} m^{-2} K^{-1}
h_o	Heat transfer coefficient in the outside	J $^{s-1}$ m^{-2} K^{-1}
k_f	Mass transfer coefficient	m $^{s-1}$
k_g	Thermal conductivity of the vapour mixture	J $^{s-1}$ m^{-1} K^{-1}
k_{GS}	Gas-solid thermal conductivity	J s^{-1} m^{-1} K^{-1}
L	Characteristic length	m
$m_{adsorbent}$	Mass of the adsorbent	kg
$m_{flow,i}$	Component mass flow	kg/s
M_i	Component molar mass	g/mol
Nu	Nusselt number	dimensionless
P	Pressure	atm
Pr	Prandt number	dimensionless
Ra	Rayleigh number	dimensionless
r_b	Inside diameter of column	m
Re	Reynolds number	dimensionless
r_o	Outer diameter of column	m
r_P	Radius of the pellet	m
Sc	Schmidt number	dimensionless
t	Time	s
T_{sur}	Temperature of the surrounding	K
T_g	Temperature in the bulk phase	K
t_i	Breakthrough curve area	s
T_P	Temperature of the pellet	K
T_w	Temperature of the wall	K
τ	Tortuosity	dimensionless
v	Kinematic viscosity	m^2 s^{-1}
v_g	Superficial velocity of the fluid	m s^{-1}
ε_c	Void fraction of the column	dimensionless
ε_p	Void fraction within the pellet	dimensionless
ρ_{bed}	Density of adsorption bed	kg m^{-3}

ρ_g	Density of vapour mixture	kg m^{-3}
ρ_S	Solid density	kg m^{-3}

References

Bobok, D., Besedova, E., "Mechanisms of ethanol vapours diffusion in particles of activated carbons," Chemical Papers, 58 (1), 55-63, 2004

Bradley, K. J., Hamdy, M. K., Toledo, R. T., "Physicochemical factors affecting ethanol adsorption by activated carbon," Biotechnology and Bioengineering, 29, 445-452, 1987

Caputo, D., Iucolano, F., Pepe, F., Colella, C., "Modeling of water and ethanol adsorption data on a commercial zeolite-rich tuff and prediction of the relevant binary isotherms," Microporous and Mesoporous Materials, 105 (3), 260-267, 2007

Carmo, M. J., Gubulin, J. C., "Ethanol-water separation in the PSA process," Adsorption, 8, 235-248, 2002

Chang, H., Yuan, X-G., Tian, H., Zeng, A-W., "Experiment and prediction of breakthrough curved for packed bed adsorption of water vapour on cornmeal," Chemical Engineering and Processing, 45, 747-754, 2006

Cheng, T., Jiang, Y., Zhang, Y., Liu, S., "Prediction of breakthrough curves for adsorption on activated carbon fibers in a fixed bed," Carbon, 42, 3081-3085, 2004

Churchill, S. W., Chu, H.H.S., "Correlating equations for laminar and turbulent free convection from a horizontal cylinder," International Journal of Heat and Mass Transfer, 18, 1049, 1975

Guan, J., Hu, X., "Simulation and analysis of pressure swing adsorption: ethanol drying process by the electrical analogue," Separation and Purification Technology, 31, 31-35, 2003.

Hashi, M., Tezel, F. H., Thibault, J., "Ethanol recovery from fermentation broth via CO_2 stripping and adsorption," Energy & Fuels, submitted. 2010

Hirschfelder J.O, Bird R.B. and Spotz E.L. "The transport properties of gases and gaseous mixtures. II," Chemical Reviews, 44, 205 - 231, 1949.

Incropera, DeWitt, Bergman, Lavine, "Fundamentals of Heat and Mass Transfer - Sixth Edition," John Wiley and Sons, Inc. 2007

Kikkinides, E. S., Yang, R. T., Cho, S. H., "Concentration and recovery of CO_2 from flue gas by pressure swing adsorption," Industrial and Engineering Chemistry Research, 32, 2714-2720, 1993

Kim, M-B., Moon, J-H., Lee, C-H., Ahn, H., Cho, W., "Effect of heat transfer on the transient dynamics of temperature swing adsorption process," Korean Journal of Chemical Engineering, 21 (3), 703-711, 2004

Lalik, E., Mirek, R., Rakoczy, J., Groszek, A., "Microcalorimetric study of sorption of water and ethanol in zeolites 3A and 5A," Catalysis Today, 114, 242-247, 2006

Langmuir, I., "Adsorption of gases on plane surfaces glass mica and platinum," American Chemical Society, 40, 1361-1403, 1918

Lu, L., Shao, Q., Huang, L., Lu, X., "Simulation of adsorption and separation of ethanol-water mixture with zeolite and carbon nanotube," Fluid Phase Equilibria, 261, 191-198, 2007

Manjare, S. D., Ghoshal, A. K., "Studies on adsorption of ethyl acetate vapour on activated carbon," Industrial & Engineering Chemistry Research, 45, 6563-6569, 2006

Pushnov, A.S., "Calculation of average bed porosity," Chemical and Petroleum Engineering, 42 (1-2), 14 - 17, 2006

Ruthven, D.M., Farooq, S., and Knaebel, K.S., "Pressure Swing Adsorption", John Wiley and Sons, Inc., 1994

Taylor F., Kurantz, M. J., Goldberg, N., McAloon, A. J., Craig Jr., J. C., Biotechnology Progress, *16*, 541-547, 2000

Simo, M., Brown, C.J., Hlavacek, V., "Simulation of pressure swing adsorption in fuel ethanol production process," Computers and Chemical Engineering, 32 (7), 1635-1649, 2008

Wakao, N., Funazkri, T., "Effect of fluid dispersion coefficients on particle-to-fluid mass transfer coefficients in packed beds: Correlation of Sherwood numbers," Chemical Engineering Science, 33 (10), 1375 – 1384, 1978

Walsh, P. K., Liu, C. P., Findley, M. E., Liapis, A. I., Siehr, D. J., Biotechnology and Bioengineering Symposium, *No. 13*, 629-647, 1983

Warmunzinski, K., Tanczyk, M., "Multicomponent pressure swing adsorption Part I. Modelling of large-scale PSA installations," Chemical Engineering and Processing, 36, 89-99, 1997

Zahra, M., Jafar, T., Masoud, M., "Study of a four-bed pressure swing adsorption for oxygen separation from air," Industrial & Engineering Chemistry Research, 48, 5439 - 5444, 2009

Chapter IV: Economic analysis of an ethanol production plant couples with carbon dioxide stripping and adsorption

Mohamed Hashi, Jules Thibault(*), and F. Handan Tezel

Department of Chemical and Biological Engineering

University of Ottawa, Ottawa, Ontario, Canada K1N 6N5

(*)To whom correspondence should be addressed. Telephone: +1-613-562-5800 x6094.

Email: jules.thibault@uottawa.ca

Abstract

An economic analysis was completed comparing a simulated base case ethanol production plant with a similar process coupled with carbon dioxide stripping and adsorption technology. The process was modeled using Aspen HYSYS to perform material and energy balances. The packed bed adsorption system, operating as a temperature-swing adsorption (TSA) or a vacuum-swing adsorption (VSA) system, was modeled to evaluate the performance of the adsorption alternative and to size and cost the associated equipment. Preliminary results have shown that the grass roots cost for the ethanol production process coupled with carbon dioxide stripping and adsorption technology for three different TSA (purge gas temperatures of 80°C, 100°C, and 120°C) and VSA (desorption pressures of 0.5, 0.2, and 0.1 atm) systems were more cost effective than the base case ethanol plant except for the VSA case running at a desorption pressure of 0.1 atm. These results show a decrease in operating costs when a carbon dioxide stripping and adsorption technology for ethanol production is implemented even though there is an increase in capital cost.

Introduction

Ethanol production from biomass has increased significantly worldwide for the past few decades due to the impetus from governments to develop greener sources of energy. In Brazil, bioethanol produced from sugar cane occupies an important part of the market for car fuel. An increasing trend in ethanol production in United States, mostly produced from corn, has been observed with the yearly production currently slightly surpassing the one of Brazil. Their ethanol production capacity reached 18.6 billion liters in 2006, compared to 6.2 billion liters in 2000 (Bai et al., 2008). This increased interest for ethanol as an alternative fuel source as well as the requirements of producing ethanol in a cost-effective manner have stimulated research in process design optimization. Research towards developing new valuable co-products and more efficient process technologies is aimed at reducing the overall cost of producing ethanol (Taylor et al., 2000).

To make the production of bioethanol an economically viable alternative, it is imperative to seek ways of lowering the energy demand at both ends of the ethanol concentration spectrum. Much of the research performed so far has been aimed towards breaking the ethanol-water azeotrope. Adsorption beds are often used to selectively adsorb moisture from a high purity ethanol vapour distillate stream (Carmo and Gubulin, 2002; Chang et al., 2006; Guan and Hu, 2003; Lalik et al., 2006; Lu et al., 2007). While most research has been focused on overcoming the azeotrope, adsorption can also be used to increase the efficiency of fermentation by removing ethanol from the broth and thereby leading to a reduction in ethanol toxicity and a higher ethanol production. Ethanol production is limited by the microorganisms' ethanol tolerance. The maximum achievable ethanol concentration that can be reached depends on the type of microorganism used to convert fermentable sugars to bioethanol. For example, a maximum ethanol concentration of 180 g/L can be achieved with a culture of *Saccharomyces cerevisiae* when glucose is used as the sole substrate (Watanabe et al., 2007) while only 12 g/L can be obtained with *Lactobacillus buchneri* with a mixture of glucose and xylose (Liu et al., 2008). These results show a very wide variation in ethanol productivity mainly due to ethanol tolerance but most importantly show that all types of

cultures have a limiting ethanol concentration above which they can no longer produce additional ethanol.

One possible method to partly circumvent the limitation due to ethanol tolerance is to use a stripping gas to continuously remove some ethanol from the fermentation broth. Carbon dioxide is an ideal candidate for the stripping gas since it is a by-product of fermentation. Adsorption can then be used to recover ethanol from the ethanol-water-carbon dioxide vapour mixture. The adsorbent should be highly selective to ethanol (Bobok and Besedova, 2004; Bradley et al., 1987; Taylor et al., 2000; Walsh et al., 1983).

Even if this process has been shown to be technically feasible, it is important to assess its economic viability. The objective of this study was therefore to compare, via modelling of the separation train, a conventional ethanol production plant downstream of the fermenter with a similar production plant coupled with carbon dioxide stripping and adsorption. Only the fermenters and separation train downstream of the fermenters are considered since the operating and capital costs for the process upstream of the fermenters are identical. Some publications discuss the modelling and cost estimation of corn-based ethanol production plants (Kwiatkowski at al., 2006; Perkis et al., 2008; Taylor et al., 2000).

In this paper, the cost of additional equipment and the potential savings are determined for an ethanol production plant where adsorption packed beds are used to recover ethanol stripped from the fermentation broth as well as for breaking the azeotrope. Three ethanol production plant scenarios were considered for this study: a base case ethanol production plant without carbon dioxide stripping, a new ethanol production plant using the carbon dioxide and adsorption technology (Alternative 1), and the base case fermentation model incorporating the carbon dioxide stripping and adsorption technology as an addition to the plant (Alternative 2). Alternative 1 compares the base case plant with a brand new ethanol production plant producing the same amount of ethanol while Alternative 2 quantifies the benefits of introducing the new technology (carbon dioxide stripping plus adsorption) to a pre-existing base case ethanol production plant. For both Alternatives 1 and 2, temperature-swing adsorption (TSA) and vacuum-swing adsorption (VSA) processes are compared. The use of a vapour recompression system as a means to increase the effectiveness of the TSA system is also discussed.

Aspen HYSYS was used to simulate all unit operations of the ethanol production plant except the adsorption packed bed system that was numerically modelled (using a mechanistic model) in a separate FORTRAN computer program in order to size and cost the adsorption units.

Process Model Description

The base case ethanol production model, solved using Aspen HYSYS, contains six major pieces of equipment: a fermenter, two absorbers, a stripping column and a distillation column. For the base case and alternatives using the new technology, the adsorption columns were modelled with a mechanistic model using FORTRAN while the fermentation tank was modeled using an Excel spreadsheet. The feed stream for the HYSYS simulation represents the totality of the fermentation product. The main components of the final fermentation broth are ethanol, water and carbon dioxide with trace amounts of methanol, 1-propanol, 2-propanol, 1-butanol, 2-methyl-1-butanol, 2-pentanol, and acetic acid (Aspen Technology, 2005). Figure IV.1 shows the block flow diagram (BFD) for the base case ethanol production process. The dotted lines in Figure IV.1 indicate that the content of the fermentation vessels and captured ethanol tanks are sent to the separation train at the end of the fermentation. By using a sequence of three fermentation tanks, synchronized in time, it is possible to operate the separation train in continuous mode.

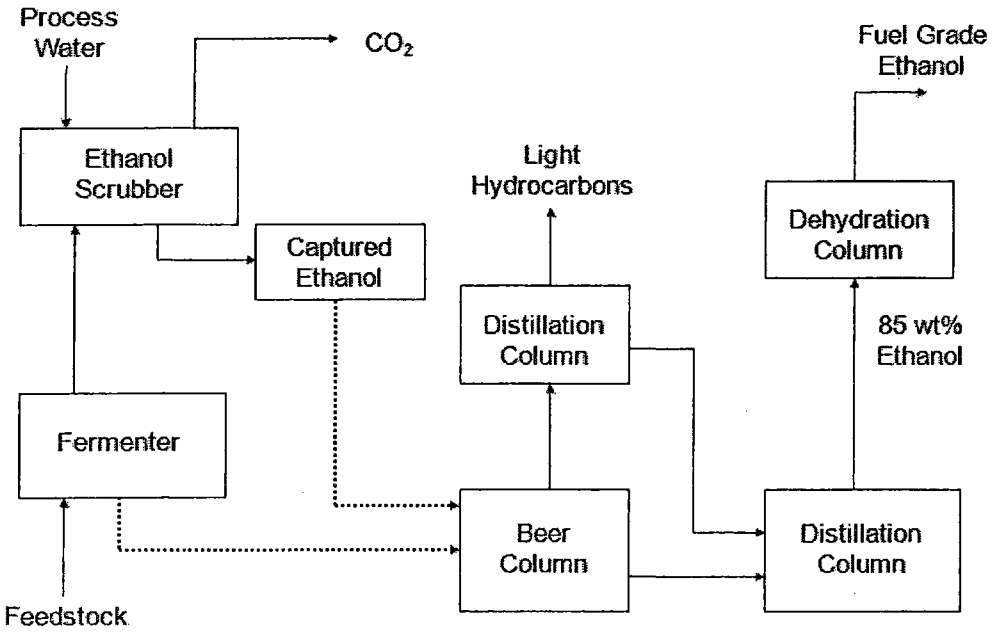

Figure IV.1 – Block flow diagram (BFD) for the base case model for ethanol production.

The fermentation tank was simulated using an Excel macro. The following three equations (Equations (1) - (3)) represent the change in glucose concentration, ethanol concentration and cell activity as a function of time (Martini et al., 2006). The kinetic parameters in these equations were taken from Martini et al. (2006) where G, E_l, C, and E_g represent the glucose concentration, liquid ethanol concentration, cell activity and vapour ethanol concentration, respectively. Symbols V_L and F_{CO2} represent the fermentation volume and carbon dioxide flow rate, respectively.

$$\frac{dG}{dt} = -k_D[G][C] \tag{1}$$

$$\frac{dE_l}{dt} = k_P[G][C] - \frac{F_{CO2}}{V_L}[E_g] \tag{2}$$

$$\frac{dC}{dt} = k_A[G][C] - k_1[E_l][C] \tag{3}$$

The second term of the right-hand side of Equation (2) accounts for the rate of removal of ethanol from the fermenter broth due to carbon dioxide stripping. Figure IV.2 presents the change in glucose and ethanol concentration throughout the fermentation for

both the base case ethanol production plant and the ethanol plant coupled with gas stripping and adsorption. Even in the presence of gas stripping, it is important for economic reason to complete the fermentation with the highest possible ethanol concentration such that the flow of the stripping gas was adjusted as to maintain an ethanol concentration of 46 g/L in the fermenter. Prior to achieving the final ethanol concentration, the carbon dioxide flow rate was 450 m^3/h.

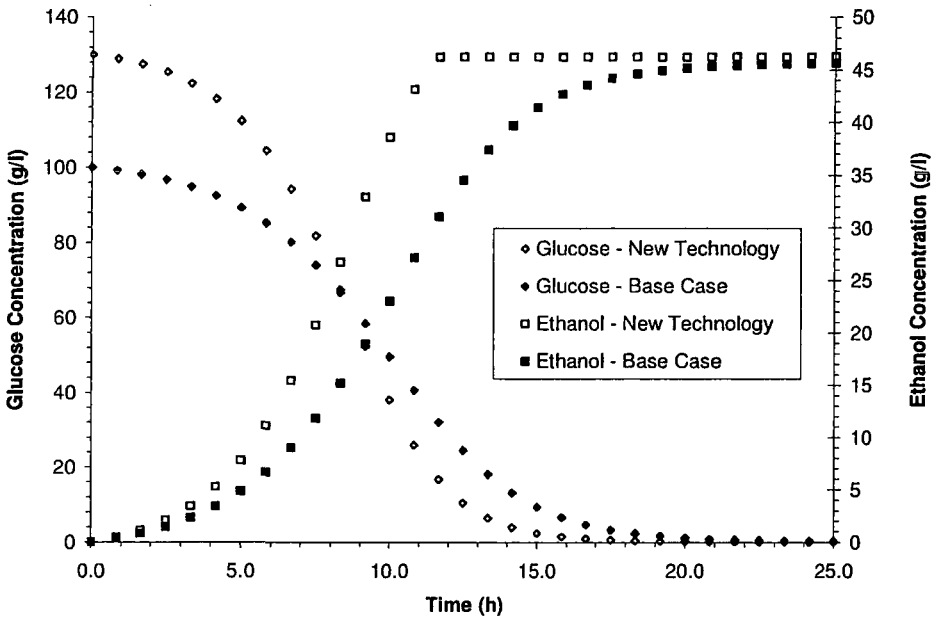

Figure IV.2 - Ethanol and glucose concentration variation during fermentation with (hollow points) and without (solid points) carbon dioxide stripping.

Figure IV.2 shows that when carbon dioxide stripping is implemented, higher glucose concentration can be used since ethanol inhibition is lessened due to ethanol removal. As a result, a smaller fermentation tank is required which in turn implies a reduction in the size of the downstream separation units and energy requirements. The volume of the fermentation broth for the base case was 9 755 L whereas it was 7 504 L the ethanol process with gas stripping and adsorption for the same amount of ethanol produced. Once the fermentation tank has been modeled, the separation units downstream of the fermenter can be simulated using HYSYS. Figure IV.3 shows the HYSYS flow sheet used to model the separation processes for the base case ethanol process.

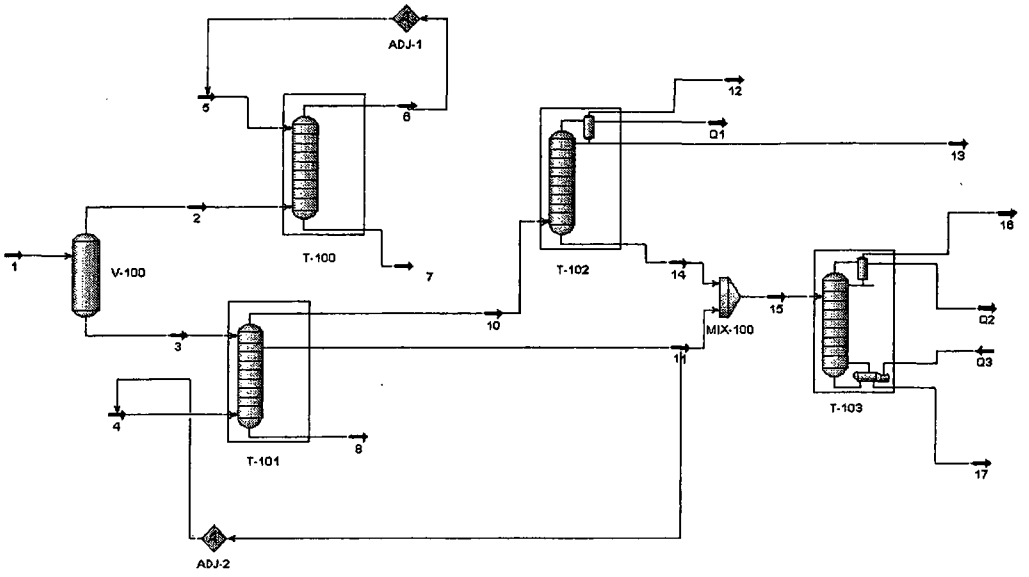

Figure IV.3 – HYSYS process flow sheet used for the base case ethanol production model.

The base case ethanol production process considers a final ethanol concentration of 4.34 wt% (46 g/L). Aspen HYSYS is predominantly a steady-state simulator since the simulation of the ethanol production plant is not straightforward because of the presence of the batch fermentation. To consider a continuous ethanol production rate, the average productivity of the simulated fermentation broth was taken to be1.84 g l^{-1} h^{-1} which is close to 2 g l^{-1} h^{-1}, a typical ethanol productivity value given in the literature (Taylor et al., 1997). To reach an assumed inhibition level of 4.34 wt% ethanol (46 g/l), it requires a total fermentation time of 25 h (Martini et al., 2006).

The base case ethanol production process using HYSYS simulates the separation systems needed to convert the fermentation broth product to fuel grade ethanol, i.e. an ethanol mass fraction of 0.99 (Capiro et al., 2007). Referring to Figures IV.2 and IV.3, Stream 1 represents the fermentation broth with a final concentration of 4.34 wt% (46 g/L) ethanol plus the very small volume of solution for the recovered ethanol from the vapour phase (Figure IV.1). Stream 1 therefore contains the ethanol product along some carbon dioxide by-product, water and trace amounts of light hydrocarbons. The stream is flashed using a two-phase separator (V-100) producing a vapour (Stream 2) and liquid (Stream 3) stream.

Vapour Stream 2 contains predominantly CO_2 with equilibrium ethanol and water with the ethanol of this stream needing to be recovered. A water scrubber has been modeled using an absorption unit (T-100) with Stream 5 representing the process water that needs to absorb ethanol. The amount of water needed was adjusted within HYSYS to ensure an ethanol recovery of 95%. Stream 6 contains mostly carbon dioxide and is either discarded or sent to a CO_2 sequestration system.

Stream 3 exits the phase separator (V-100) and enters the beer column (T-101) which uses steam (Stream 4) to further purify the product. The amount of steam used was adjusted in order to obtain an ethanol purity of 37.5 wt% prior to entering the distillation column. The beer column was represented by a stripping distillation column that has two draws represented by Streams 10 and 11. Stream 10 exits to a reflux absorber (T-102) while Stream 11 mixes with Stream 14 before entering the distillation column (T-103). The beer column also has a liquid phase draw that mainly contains water with some traces of heavy hydrocarbons.

Stream 10 contains ethanol among light hydrocarbons. The lights absorber (T-102) removes the light hydrocarbons as a vapour (Stream 12) with a liquid side draw (Stream 13). The liquid side draw (Stream 13) and liquid bottoms stream (Stream 14) contain the desired ethanol product with Stream 14 mixed with Stream 11 before entering the distillation column for further purification as Stream 15.

Stream 15 enters the distillation column where the ethanol mass fraction is increased from 0.375 to approximately 0.85. A mass fraction of 0.85 was chosen as the final ethanol concentration due to the added energy load that is needed as the azeotrope, which forms at a mass fraction of 0.956, is approached.

Not shown in the HYSYS model is the ethanol dehydration adsorption unit that purifies the ethanol product from an ethanol mass fraction of 0.85 to ethanol fuel grade of 0.99. The adsorption units were modelled using a separate computer program.

Ethanol production process coupled with carbon dioxide stripping

This option is similar to the base scenario except that ethanol is partially stripped from the fermentation broth using carbon dioxide. Carbon dioxide, a by-product of fermentation, can be used as a stripping gas to partly mitigate the ethanol inhibition effect

by removing some ethanol during production. In 1996, Taylor et al. incorporated carbon dioxide stripping within a pilot scale fermentation process and obtained an ethanol productivity as high as 15.8 g l^{-1} h^{-1} at a given carbon dioxide flow rate while typical fermenter plants have productivities no more than 2.0 g l^{-1} h^{-1}. With the current simulation, the productivity was 3.95 g l^{-1} h^{-1} for the process with ethanol stripping (Alternatives 1 and 2) compared to 1.83 g l^{-1} h^{-1} for the base case. A summary for all HYSYS units for the scenarios with and without carbon dioxide stripping are presented in Table IV.1.

Table IV. 1 - Equipment summary for the base case and alternative (1 and 2) ethanol production plant

Simulation	Identification	Unit Name	Description
Base Case	V-100	Phase separator	Flash the carbon dioxide from fermentation broth
	T-100	Absorption Scrubber	Capture the vapour phase ethanol using water to scrub from vapour mixture
	T-101	Beer Column	Addition of steam to further purify fermentation outlet
	T-102	Lights Column	Remove light hydrocarbons from ethanol stream
	T-103	Distillation Column	Ethanol dehydration to remove water up to 85 wt% ethanol levels
	T-104	Adsorption Column	Ethanol dehydration unit to produce fuel grade ethanol
Alternatives using CO_2 stripping and adsorption	V-101	Adsorption Column	Replaces absorption scrubber with an adsorption unit
	E-101	TSA Heat Exchanger	Used to increase temperature of purge gas to desired conditions

Since Aspen HYSYS is mostly a steady-state simulator, the following conditions were used to model the fermenter.

Fermenter Models

1. Fermenters operate in batch mode. To adapt the fermentation data for a separation train that operates under steady-state conditions, an average flow rate of liquid broth was calculated to represent one batch of ethanol production.
2. Each ethanol production plant consists of 3 fermenters and sequenced in a way that for every 25 hour interval: a fermenter is being cleaned and prepared for a new batch, a fermenter converting sugars into ethanol, and a fermenter having the liquid ethanol concentration of 4.32 wt% leaving the fermentation tank and towards the separation units downstream of the fermenter. Having this system produces a continuous process for ethanol production.
3. A fermentation total time of 25 h was considered with gas stripping starting after 4 h until the fermentation is completed. The carbon dioxide flowrate was varied once 46 g/L of ethanol was reached.
4. Initial carbon dioxide stripping flow rate of 450 m^3/h (1 vvm = 1.0 L $min^{-1}L^{-1}$) was considered. As glucose depletes, less ethanol is produced and the amount of carbon dioxide decreased accordingly.
5. An Excel Macro was used to determine the outlet composition of the stripping gas and the resulting composition of the fermentation broth.

Comparative study for the modified ethanol production process

The addition of carbon dioxide stripping and adsorption units to the ethanol production process can be compared with the base case in order to quantify the benefits of this new technology. Two cases incorporating gas stripping/adsorption units were analyzed: a new plant (Alternative 1) and incorporating the new technology to a pre-existing ethanol production plant (Alternative 2). For each alternative, TSA and VSA processes were simulated and compared for their ability to recover ethanol from the stripping gas.

Alternative 1 compares the base case with a new ethanol production plant using the new technology in terms of capital and operating costs assuming both the base case and Alternative 1 produce the same total amount of ethanol. In this study, the amount of ethanol produced was set at a yearly production rate of 1 000 000 L. The main advantages achieved with Alternative 1 include having a smaller fermenter since ethanol is removed as it is produced and a higher sugar concentration can be used in the fermenter while still producing the same final ethanol concentration. Therefore, the liquid stream flow rate entering the separation units is smaller compared to the Base Case due to the lower fermentation broth volume resulting from lower inhibition and higher initial substrate concentration. The lower fermentation broth volume to be processed gives rise to a size reduction of separation units downstream of the fermenter and lower capital and operating costs. The adsorption processes, either TSA or VSA, would bear additional capital and operating costs since the stripped ethanol would need to be recovered from the vapour phase. Figure IV.4 shows the block flow diagram of the ethanol separation units, including the carbon dioxide stripped vapour mixture.

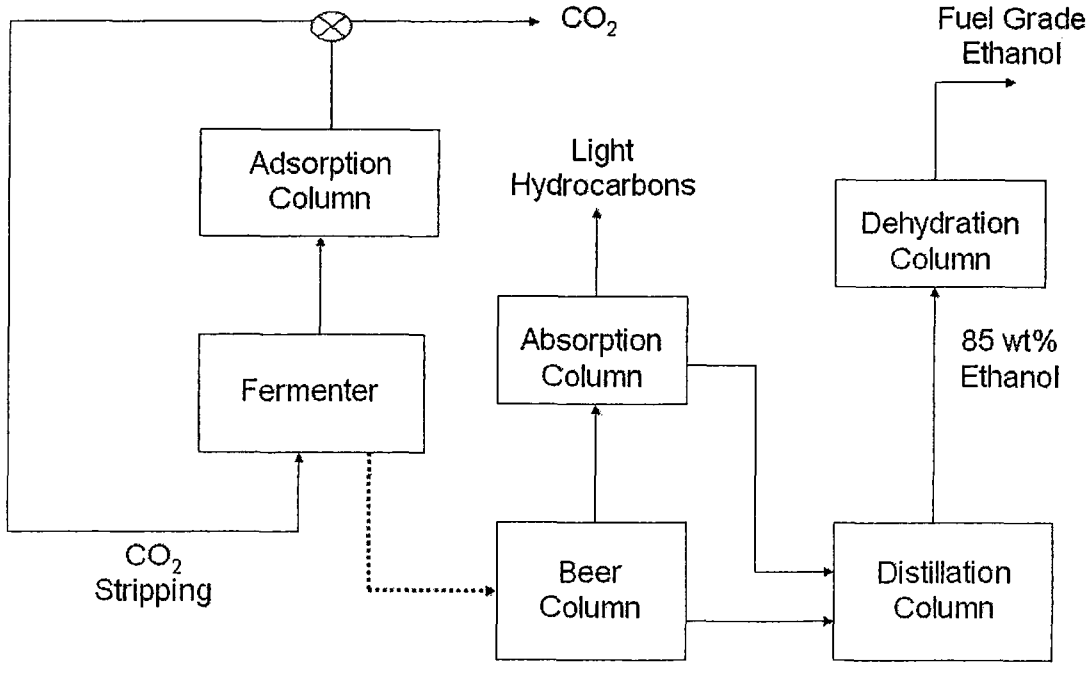

Figure IV.4 - Block flow diagram for the ethanol production process coupled with carbon dioxide stripping and adsorption.

Some additional carbon dioxide is needed to start stripping the ethanol, but after a time the carbon dioxide downstream of the adsorption column can be recycled without any additional carbon dioxide added into the system.

Alternative 2 compares the base case with a pre-existing ethanol fermentation plant incorporating the carbon dioxide stripping and adsorption units afterwards, to evaluate the potential benefits of introducing the new technology. Since the ethanol production plant analyzed was assumed already built, the capital costs would be the same as the base case. Since carbon dioxide stripping lower ethanol inhibition and allows for a higher initial substrate concentration, a higher amount of ethanol for a single batch can be produced for the same fermentation volume. A higher initial sugar concentration can therefore be used to match this increase in production. Therefore, Alternative 2 and the base case were compared using the change in operating cost in terms of the cost per litre of ethanol produced ($/L).

Desorption Techniques

The adsorption process needs an effective desorption system to efficiently recover the ethanol from the adsorbed phase, i.e. a desorption technique that is economically feasible and able to give a high ethanol purity. Two desorption techniques are considered in this study: temperature swing adsorption (TSA) and vacuum swing adsorption (VSA) systems. For each desorption technique, two adsorption columns in parallel are used to ensure a continuous process. When one adsorption column is adsorbing, the other column is desorbing or cooling to prepare for the next adsorption cycle. In a previous study, a mathematical model has been developed and used successfully to predict the adsorption performance of stripped ethanol and therefore provide an accurate means to size and cost the appropriate units (Hashi et al., 2010).

TSA for ethanol recovery will be performed under atmospheric conditions at an adsorption temperature of 30°C, which is the typical temperature of fermentation. The inlet gas stream composition entering the adsorption unit, based on a fermentation broth concentration of 4.34 wt% ethanol, is 1.76, 1.72 and 96.52 wt% (1.64, 4.09, and 94.27 mol%) for ethanol, water and carbon dioxide, respectively. The respective adsorbed

phase concentrations of ethanol, water and carbon dioxide by activated carbon WV-B 1500 were determined experimentally to be 0.383, 0.029, and 0.052 kg/kg adsorbent (Hashi, 2010). In TSA, desorption would be done using an inert gas at an elevated temperature to desorb and purge the adsorbed ethanol. The purge gas inlet temperature is an operating variable. A higher temperature removes the adsorbed ethanol at a faster rate but at the expense of a higher cost due to the higher heat duty. The evaluation was performed for three desorption temperatures: 80°C, 100°C and 120°C. The 80°C and 100°C temperatures were chosen to represent approximately the boiling points for ethanol and water. The 120°C temperature was chosen to quantify the effect of increasing the temperature well above the boiling point. Figure IV.5 shows the concentration of ethanol in terms of mole fractions as a function of time for the three desorption temperatures. It is important to note that a complete adsorption curve was generated to clearly show the breakthrough and the desorption curves. In an actual plant, the adsorption would only proceed to a lower break-point concentration before desorption would be performed.

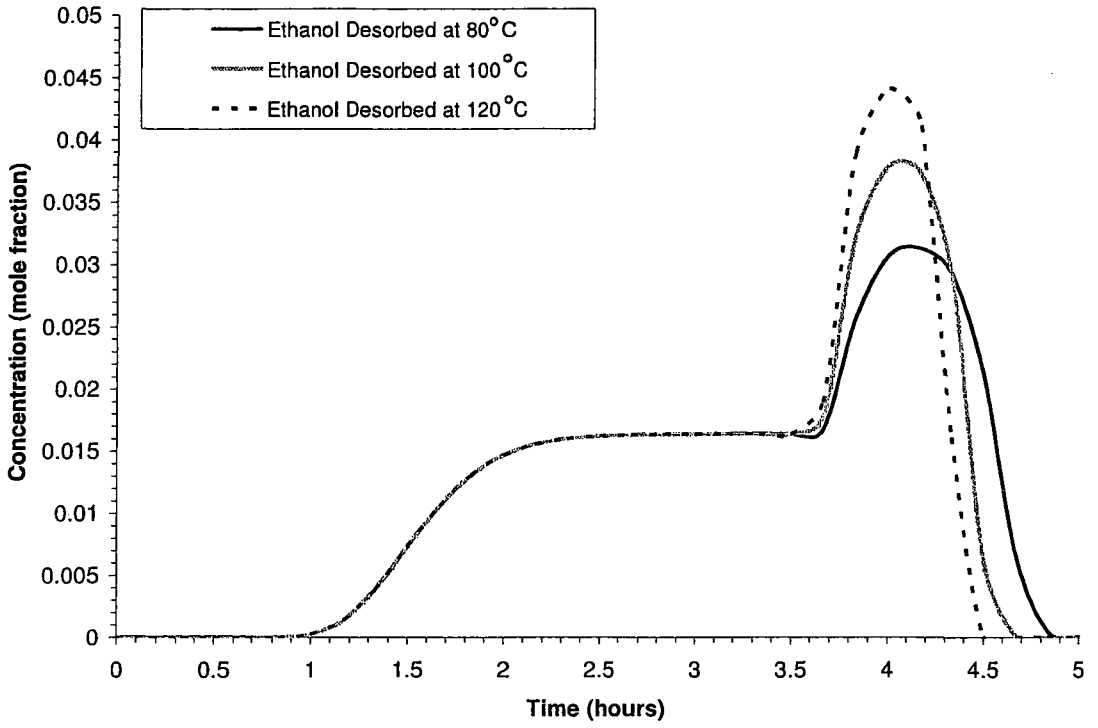

Figure IV.5 – Concentration profile of ethanol in an ethanol-water-carbon dioxide vapor mixture as a function of time using a TSA system under atmospheric pressure at purge gas flow rate of 213 m^3/h for 3 different desorption temperatures.

As the temperature of the inlet purge gas increases, the rate of desorption increases and the time necessary to regenerate the adsorption column decreases. Even though increasing the inlet purge gas temperature decreases the desorption time, it is observed that the adsorption column regeneration is relatively short for all three TSA temperatures at the conditions simulated. It can be concluded that desorption at the lower temperature can be feasible when activated carbon WV-B 1500 is used.

The advantage of a TSA system for this application strongly relies on the important temperature dependence of the ethanol adsorption capacity on activated carbon WV-B 1500. The TSA operates at 30°C during the adsorption cycle and using an inert gas at 80, 100 or 120°C for desorbing ethanol such that the working capacity is only dependent of the adsorption temperature. The working capacity in this case refers to the difference between the amount adsorbed under adsorption operating conditions compared with the amount adsorbed under desorption operating conditions. The adsorption working capacity for the TSA, for an ethanol broth concentration of 4.34 wt% ethanol, is 0.383,

0.029 and 0.052 kg/kg adsorbent for ethanol, water and carbon dioxide, respectively. Using a purge gas to retrieve ethanol from the adsorbent is the main disadvantage of a TSA. An inert gas that is not adsorbed by the adsorbent at the desorption conditions is required. In addition, the inert gas must be easily seperated from ethanol, the desired product. Even for an easily separated purge gas, an additional unit is required to separate ethanol from the purge gas and therefore leading to an increase in capital cost.

In this study, a condenser downstream of the adsorption column was used to separate ethanol from the purge gas. Carbon dioxide was used as the purge gas. When using carbon dioxide as the purge gas as well as a condenser and chilled water to lower the temperature of the vapour mixture to 20°C, the liquid composition was calculated to be 92.8 and 7.1 wt% for ethanol and water, respectively. The ethanol recovery rate was estimated to be approximately 96.6%. Since CO_2 is used both as the stripping gas and the desorption purge gas, the ethanol remaining in the vapour phase can be recycled so that no ethanol is lost within the process.

Once desorption has been completed, an effective means of cooling the adsorption column needs to be addressed. Cooling the adsorption column could be performed by passing carbon dioxide, from an accummulation tank or from the exit of the adsorption bed prior to ethanol breakthrough, through the desorbed column prior to entering the fermenter.

One means to circumvent the need of using a purge gas in a TSA process is to use a vapour recompression system. The vapour recompression system takes advantage of the significant decrease in adsorption capacity with temperature by initially using a high concentration ethanol vapour from the distillation column as the purge gas. Then, when ethanol starts to exit the adsoption column, a portion of that stream would be recompressed and would replace the stream of ethanol that was coming from the distillation column. The high temperature ethanol vapour causes the desorption of ethanol without diluting ethanol and, as a result, there is no need for an additional separation unit downstream of the adsorption column to remove the inert gas required to run a typical TSA process. The advantages of using vapour recompression are numerous: (1) the desorbed mixture is not diluted as is the case with a purge gas or steam desorption, (2) vapour at higher ethanol concentration will already be at a sufficiently high temperature

to effect desorption, (3) the desorption is nearly self-sustained since a portion of the desorbed ethanol exiting the column could then be recompressed to slightly increase its temperature to effect more desorption while the other part would be sent to the distillation column as a vapour. On the other hand, the adsorption capacity should be extremely low at higher temperature because the recompressed vapour will have a higher concentration in ethanol. Since the purge stream is high purity ethanol, even at very high temperatures the possibility of ethanol adsorption on the adsorbent may be a factor. The desorption temperature would have to be sufficienctly high to ensure ethanol adsorption does not significantly occur.

The other desorption process considered was the vacuum-swing adsorption (VSA) system where the adsorption capacity is manipulated by varying the adsorption/desorption pressures. With adsorption done under atmospheric conditions, the desorption steps as the name suggests are conducted under a vacuum. The decrease in pressure liberates the adsorbed molecules and partly desorbs the adsorption column. Unfortunately the same limitations exists with the VSA as the TSA in that a purge gas is necessary to desorb the column. Under vacuum alone, the driving force is not sufficient enough to force the entrained ethanol to leave the solid, therefore a vacuum along side a purge gas is needed. Figure 6 shows the simulated concentration profiles as a function of time for three different desorption pressures and the adsorption step done under atmospheric conditions. In practice, the desorption step would start when ethanol begins to appear at the exit of the column but again it is desired to show the complete adsorption and desorption curve. Figure IV.6 shows the effect of pressure on ethanol desorption for a VSA system operated at 1 atm for adsorption and 0.5, 0.2 and 0.1 atm for desorption.

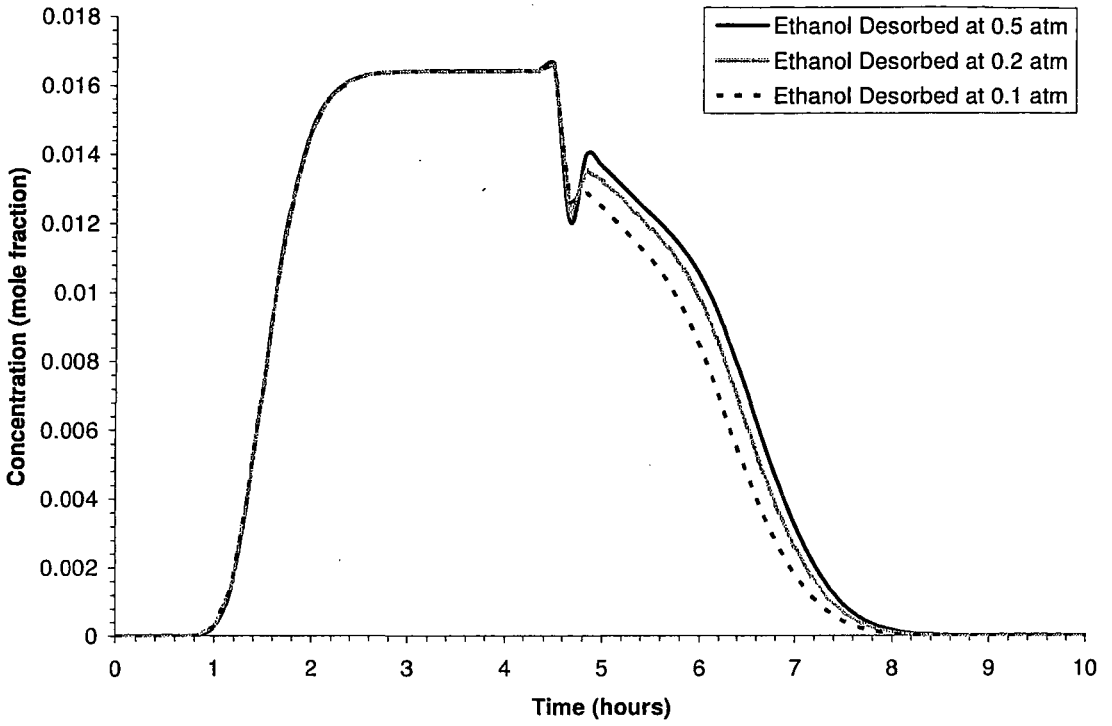

Figure IV.6 – Concentration profiles from an ethanol-water-carbon dioxide vapor mixture as a function of time using a VSA system under atmospheric conditions

At a desorption pressure of 0.5 atm, the liquid composition was calculated to be 92.9 and 7.0 wt% for ethanol and water, respectively. When the desorption pressure was decreased to either 0.2 or 0.1 atm, the liquid composition did not change significantly though the amount of ethanol recovered did vary slightly. These results are very similar compared to compositions obtained in the TSA. The ethanol recoveries were calculated to be 95.1, 92.3, and 90.0 for desorption pressures of 0.5, 0.2 and 0.1 atm, respectively. The ethanol content not found in the liquid product can be recycled and therefore limit the amount of ethanol lost within the process.

One desorption process not mentioned is the pressure-swing adsorption (PSA) system where the adsorption capacity is also manipulated by varying the adsorption/desorption pressures. PSA operates at a higher pressure during adsorption and a lower pressure, often atmospheric pressure, for the desorption cycle. The difference in adsorption capacity between the two pressures defines the working capacity of the PSA process. The main advantage of a PSA process is the absence of a purge gas since the

decrease in pressure liberates the adsorbed components and the problem of dilution is circumvented. With a PSA system, the fermentation would be conducted at the same elevated pressure than the adsorption where ethanol can still be produced provided the pressure is excessive as to lead to carbon dioxide inhibition (Kunkee and Ough, 1966; L'Italien et al., 1989; Thibault et al., 1987). However, the concentrations of ethanol and water are thermodynamically limited and their partial pressures are independent of the total pressure such that the adsorption capacity is the same at 1 or 5 atm. Therefore, a PSA system cannot be used for the envisaged application.

Another consideration is the possibility of fouling within the adsorption column. Taylor et al. (1997) showed in previous studies that fouling became an issue after repeated adsorption runs due to yeast growth. In situ washing allowed for the column to regain its original adsorption performance.

Economic Analysis

An economic analysis was performed to compare a base case ethanol production plant with Alternatives 1 and 2 described earlier utilizing the carbon dioxide stripping and adsorption technology. For each alternative, the cost of using either a TSA or a VSA system was calculated to determine the more suitable adsorption process. The assumed base case ethanol production process has a plant life of 25 years and a yearly production rate of 1 000 000 litres of fuel-grade ethanol. The economic analysis only considers the cost of the fermenter vessels and the separation system downstream of the fermenter. All costs were corrected from 1996 cost values to 2010 values. The economic analysis for the vapour recompression system is not included in the economic analysis because the ethanol adsorption isotherms are not yet available at higher temperatures.

Base Case compared to the two alternative cases

From the model simulations, the capital costs for the base case ethanol production plant and Alternative 1 can be compared using either a TSA (with purge gas temperatures of 80°C, 100°C, and 120°C) or VSA (with a desorption pressure of 0.5, 0.2, and 0.1 atm) system. Table IV.2 shows the breakdown of the equipment capital cost between the base case model and the more cost effective TSA (in this case a TSA operating at a purge gas

temperature of 80°C) and VSA (in this case a VSA operating at a desorption pressure of 0.5 atm) systems although the TSA and VSA did not differentiate much in terms of cost from each other.

Table IV.2 - Base case capital costs compared with the most cost effective TSA and VSA systems using carbon dioxide stripping assuming building brand new facilities.

Identification	Unit Name	Base Case ($)	TSA System* ($)	VSA System** ($)
-	Fermenter Tanks (3 in total)	596 194	500 893	500 893
T-100	Absorption Scrubber	134 744	-	-
T-101	Beer Column	567 967	474 718	474 718
T-102	Lights Column	65 460	70 398	70 398
	Condenser	265 217	265 217	265 217
T-103	Distillation Column	697 021	609 821	609 821
	Condenser	265 217	265 217	265 217
	Reboiler	264 875	246 503	246 503
T-104	Molecular Sieve	216 443	216 443	216 443
V-101	Adsorption Column	-	69 372	100 460
	Adsorbent	-	2 776	4 268
E-101	Heat Exchanger	-	530 434	-
E-102	Heat Exchanger	-	265217	265217
K-101	Blower	-	-	202 871
	Driver	-	-	45 766
	Total Price	3 073 138	3 517 009	3 267 791

* Analyzing the cost for a TSA with a purge gas at 80°C
** Analyzing the cost for a VSA with an adsorption pressure of 0.5 atm

Using the cumulative cost and a predicted plant life of 25 years for comparison, Figure IV.7 compares the base case with a TSA system with a purge gas temperature of 80°C, and a VSA system with desorption pressure of 0.5 atm.

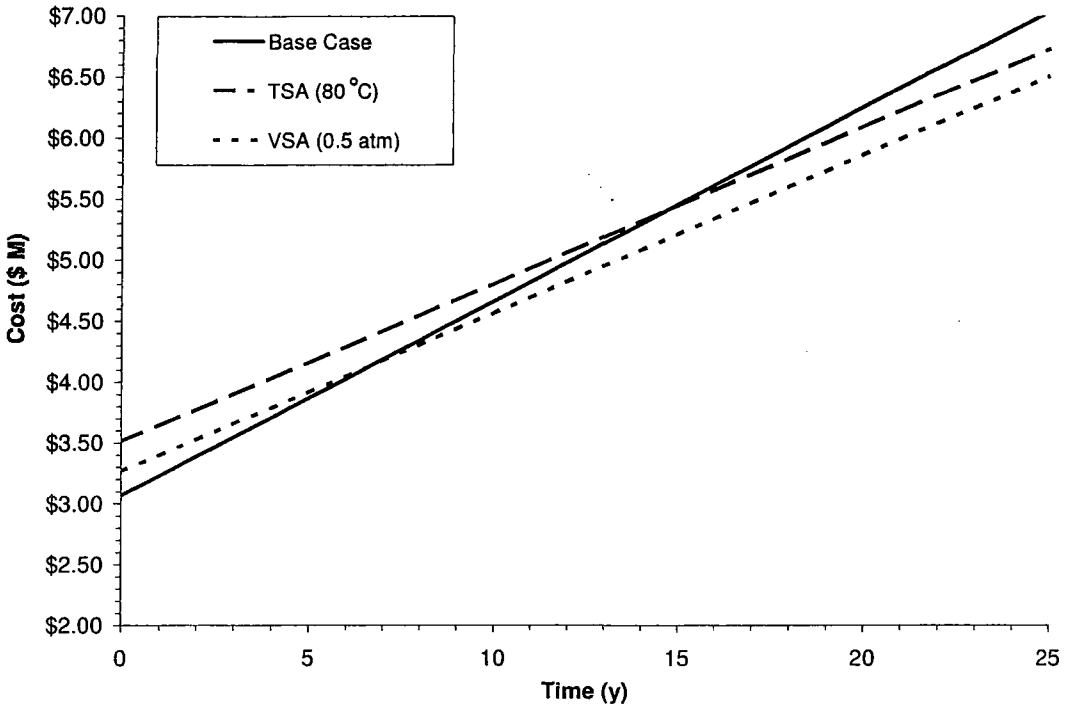

Figure IV.7 - Comparison of the cost as a function of time between a base case ethanol production model, a system with CO_2 stripping coupled with a TSA system at a purge gas temperature of 80°C and a VSA system at a desorption pressure of 0.5 atm.

When carbon dioxide stripping/adsorption is coupled to an ethanol production process, Figure IV.7 shows that the cumulative cost is smaller for the VSA after 7 years and smaller for TSA after 15 years of operation. For the TSA system, the operating cost increases marginally when the purge gas temperature is increased from 80°C to 120°C, suggesting the use of a lower temperature. For the VSA system, conducting desorption at a pressure of 0.5 atm is more economical than using pressures of 0.2 and 0.1 atm. Table IV.3 shows the percentage change in costs for the TSA/VSA processes using carbon dioxide stripping with respect to the base case fermentation model over 25 years. Table IV.3 shows the results for Alternatives 1 and 2 as well as the percentage change of the cumulative cost after 25 years compared with the base case.

Table IV.3 - Percentage change in costs over 25 years compared with TSA and VSA systems using carbon dioxide stripping compared with base case model.

System	Condition	Percent Change in Cost (%)			
(-)	(-)	Capital[1]	Operating[1]	Operating[2]	Cumulative[3]
TSA	80°C	14.4	-19.0	-16.3	-4.4
TSA	100°C	14.4	-18.7	-17.0	-4.2
TSA	120°C	14.4	-18.3	-16.7	-4.0
VSA	0.5 atm	6.4	-18.5	-15.8	-7.6
VSA	0.2 atm	13.2	-14.9	-12.2	-2.6
VSA	0.1 atm	19.5	-12.5	-9.8	1.5

1 - Capital and operating cost change comparing the three cases as brand new built facilities (Alternative 1)
2 - Capital cost is kept fixed with the operating cost varying (Alternative 2)
3 - Cumulative cost after 25 years including capital and operating costs compared to the base case

When analyzing the six scenarios presented in Table IV.3 for both alternatives, it appears that the most promising technology would be a carbon dioxide stripping process incorporating a VSA system with an adsorption and desorption pressure of 1 atm and 0.5 atm, respectively. Nevertheless, all scenarios incorporating the carbon dioxide stripping and adsorption technology showed improvements compared to the base case ethanol production process except for a VSA process with an adsorption and desorption pressure of 1 and 0.1 atm, respectively.

Conclusions

Using a combination of Aspen HYSYS and packed adsorber mathematical modeling, a base case ethanol production plant was simulated and compared with ethanol plants that incorporated carbon dioxide stripping and adsorption. Carbon dioxide stripping was introduced to increase ethanol productivity while adsorption was used to capture the ethanol entrained in the vapour phase. Two adsorption processes, a TSA and VSA system, were modeled in order to determine the economic feasibility for each alternative.

A preliminary economic analysis was completed comparing the three models. Along with the base case ethanol production model, three VSA systems with desorption

pressures of 0.5, 0.2 and 0.1 atm, and three TSA systems with desorption purge gas temperatures of 80, 100 and 120°C were analyzed. When comparing each process from a grass roots cost perspective assuming a brand new facility for each process (Alternative 1) built, all plants utilizing the carbon dioxide stripping and adsorption technology produced a lower cost compared to the base case after a number of years of operation except for a VSA process with an adsorption and desorption pressure of 1 and 0.1 atm, respectively. The orders in terms of performance are as follows: VSA (0.5 atm), TSA (80°C), TSA (100°C), TSA (120°C), VSA (0.2 atm), the base case and VSA (0.1 atm). Another means of comparison analyzes the change in operating cost when introducing the carbon dioxide stripping and adsorption technology to already existing ethanol production plants. All scenarios produced lower operating costs compared with the base case model with the orders in terms of performance are as follows: TSA (100°C), TSA (120°C), TSA (80°C), VSA (0.5 atm), VSA (0.2 atm), VSA (0.1 atm), followed by the base case model.

The preliminary results suggest benefits with using the aforementioned technology when looking at building new facilities or introducing the technology to already existing ethanol production plants. More research needs to be undertaken as well as a more comprehensive economic analysis to provide more accurate savings predictions. The current study does show that there is promise with this technology and is worth further analysis at this stage.

References

Aspen Technology, "HYSYS® 2004.2 Tutorials & Applications," Aspen Technology Inc., Copyright © 1981 - 2005

Bai, F.W., Anderson, W.A., Moo-Young, M., "Ethanol fermentation technologies from sugar and starch feedstocks," Biotechnology Advances, 26, 89-105, 2008

Capiro, N.L., Stafford, B.P., Rixey, W.G., Bedient, P.B., Alvarez, P.J.J., "Fuel-grade ethanol transport and impacts to groundwater in a pilot-scale aquifer tank," Water Research, 41, 656 - 664, 2007

Carmo, M. J., Gubulin, J. C., "Ethanol-water separation in the PSA process," Adsorption, 8, 235-248, 2002

Chang, H., Yuan, X-G., Tian, H., Zeng, A-W., "Experiment and prediction of breakthrough curved for packed bed adsorption of water vapour on cornmeal," Chemical Engineering and Processing, 45, 747-754, 2006

Guan, J., Hu, X., "Simulation and analysis of pressure swing adsorption: ethanol drying process by the electrical analogue," Separation and Purification Technology, 31, 31-35, 2003.

Hashi, M., Tezel, F.H., Thibault, J., "Ethanol recovery from carbon dioxide stripped ethanol-water vapour mixture using adsorption," University of Ottawa, Master's Thesis 2010

Kunkee, R.E., Ough, C.S., "Multiplication and fermentation of *Saccharomyces cerevisiae* under carbon dioxide pressure in wine," Applied Microbiology, 14 (4), 643 - 648, 1966

Kwiatkowski, J.R., McAloon, A.J., Taylor, F., Johnston, D.B., "Modeling the process and costs of fuel ethanol production by the corn dry-grind process," Industrial Crops and Products, 23, 288-296, 2006

L'Italien, Y., Thibault, J., LeDuy, A., "Improvement of ethanol fermentation under hyperbaric conditions," Biotechnology and Bioengineering, 33, 471 - 476, 1989

Lalik, E., Mirek, R., Rakoczy, J., Groszek, A., "Microcalorimetric study of sorption of water and ethanol in zeolites 3A and 5A," Catalysis Today, 114, 242-247, 2006

Liu, S., Skinner-Nemec, K.A., Leathers, T.D., "*Lactobacillus buchneri* strain NRRL B-30929 converts a concentrated mixture of xylose and glucose into ethanol and other products," Journal of Industrial Microbiology and Biotechnology, 35, 75 - 81, 2008

Lu, L., Shao, Q., Huang, L., Lu, X., "Simulation of adsorption and separation of ethanol-water mixture with zeolite and carbon nanotube," Fluid Phase Equilibria, 261, 191-198, 2007

Martini, S., Ricci, M., Bartolini, F., Bonechi, C., Braconi, D., Milucci, L., Santucci, A., Rossi, C., "Metabolic response to exogenous ethanol in yeast: An in vivo NMR and mathematical modeling approach," Biophysical Chemistry, 120 (2), 135-142, 2006

Perkis, D., Tyner, W., Dale, R., "Economic analysis of a modified dry grind ethanol process with recycle of pretreated and enzymatically hydrolyzed distillers' grains," Bioresource Technology, 99 (12), 5243-5249, 2008

Taylor, F., Kurantz, M.J., Goldberg, N., Craig Jr., J.C., "Control of packed column fouling in the continuous fermentation and stripping of ethanol," Biotechnology and Bioengineering, 51, 33-39, 1996

Taylor, F., Kurantz, M.J., Goldberg, N., Craig Jr., J.C., "Effects of ethanol concentration and stripping temperature on continuous fermentation rate," Applied Microbiology and Biotechnology, 48, 311-316, 1997

Taylor F., Kurantz, M. J., Goldberg, N., McAloon, A. J., Craig Jr., J. C., "Dry-grind process for fuel ethanol by continuous fermentation and stripping," Biotechnology Progress, 16, 541-547, 2000

Thibault, J., LeDuy, A., Cote, F., "Production of ethanol by *Saccharomyces cerevisiae* under high-pressure conditions," Biotechnology and Bioengineering, 30, 74 - 80, 1987

Watanabe, M., Tamura, K., Magbanua, J.P., Takano, K., Kitamoto, K., Kitagaki, H., Akao, T., Shimoi, H., "Elevated expression of genes under the control of stress response element (STRE) and Msn2p in an ethanol-tolerance sake yeast Kyokai No. 11," Journal of Bioscience and Bioengineering, 104, 163 - 170, 2007

Chapter V: Conclusions and Recommendations

Conclusions

An analysis of the feasibility of using carbon dioxide stripping and adsorption technology to increase the efficiency of an ethanol production process has been conducted. Some of the conclusions made are listed below.

1. An adsorption screening analysis comprised of six different adsorbents (four activated carbons and two ZSM-5 zeolites) showed that activated carbon WV-B 1500 had the highest ethanol adsorption capacity and second highest selectivity between ethanol and water.
2. A linear relationship was observed between the BET surface area of the activated carbons tested and the ethanol adsorption capacities with a correlation coefficient in excess of 0.95.
3. All activated carbons provided higher ethanol adsorption capacities compared to the zeolites tested.
4. Adsorption isotherms for ethanol in the presence of carbon dioxide, water in the presence of carbon dioxide and pure carbon dioxide were completed to characterize the adsorption behaviour for activated carbon WV-B 1500.
5. Using the adsorption isotherms, a mathematical model was developed to predict adsorption breakthroughs. The model was validated successfully using experimental data.
6. The experimental adsorption isotherms showed that ethanol adsorption capacities were almost an order of magnitude higher than water and carbon dioxide adsorption capacities.
7. The preliminary economic analysis, comparing a base case ethanol production model with three VSA systems (0.5, 0.2, and 0.1 atm) and three TSA systems (80, 100 and 120°C), showed that there are economic benefits using gas stripping and adsorption.
8. The orders in terms of most cost effective processes were as follows: VSA (0.5 atm), TSA (80°C), TSA (100°C), TSA (120°C), VSA (0.2 atm), VSA (0.1 atm), and the base case.

Recommendations

The preliminary results show that there are benefits using carbon dioxide stripping and adsorption to increase the efficiency for an ethanol production plant. The experiments conducted were done to characterize the adsorption behaviour but no research was done by incorporating fermentation within this thesis. In future experiments, it would be beneficial to run a carbon dioxide stripping experiment through an actual fermentation reactor as opposed to through pure ethanol and water flasks. As well, adsorption experiments downstream of the fermentation reactor should be performed to test the actual performance of this system. In addition, the modeling conducted in this investigation was restricted to the adsorption breakthrough predictions; in future modeling the fermentation process as along with the adsorption system would provide a total predictive tool that would be extremely beneficial for industrial purposes.

Chapter VI

Appendix 1 – Supplementary Information for Chapter II

Ethanol recovery from fermentation broth via carbon dioxide stripping and adsorption

Experimental Methodology

The main focus of Paper 1 entitled "Ethanol recovery from fermentation broth via CO_2 stripping and adsorption" was to determine the applicability of using adsorption to recover ethanol from the carbon dioxide stripped vapour mixture. Using carbon dioxide to strip ethanol lowers the product inhibition and increases ethanol productivity. An effective means to recover stripped ethanol is required for this carbon dioxide stripping technology to be technically viable. The experimental methodology was divided into two subsections: adsorbent screening and characterization.

Calculations

Adsorption Capacity

The most important performance parameter is the adsorption capacity. It measures the amount of adsorbate that can be captured. In this study, the adsorption capacity of adsorbents was determined using the breakthrough curve. Figure A1.1 shows an example of a breakthrough curve for an ethanol-carbon dioxide vapour mixture and Table A1.1 gives the associated experimental conditions.

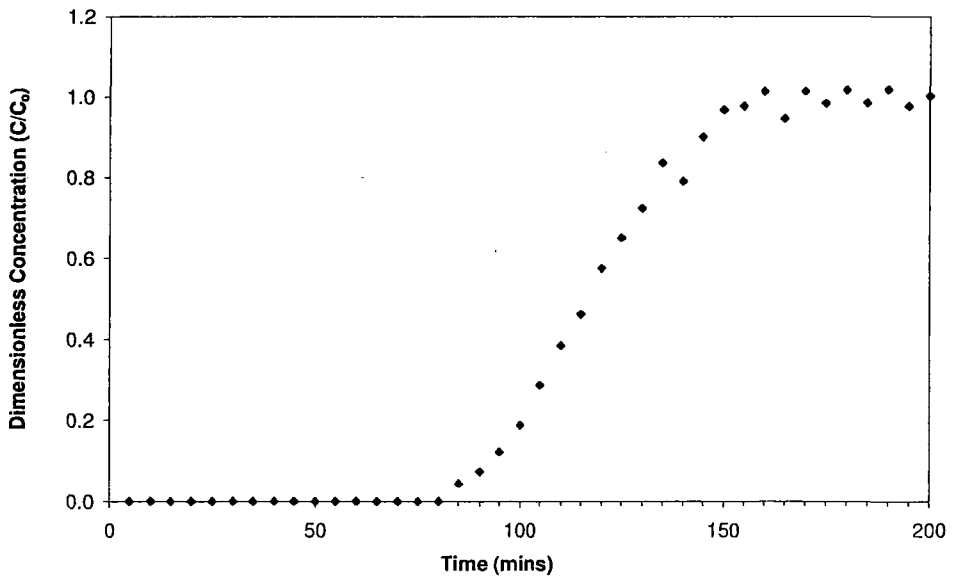

Figure A1.1 - Breakthrough curve of an ethanol-carbon dioxide vapour mixture, under atmospheric total pressure, at an ethanol partial pressure of 0.95 kPa and 24°C.

Table A1.1 - Characteristics of adsorption process and adsorbent.

Inlet ethanol concentration	0.94	mol%
Total volume flow rate	0.874	l/min
Mass of adsorbent	5.5	g
Ethanol mass flow rate	0.0156	g/min
Total time for breakthrough	200	min

The adsorption capacity is proportional to the area above the breakthrough curve and can be calculated using Equation (1). In Equation (1), AC_i, $m_{flow,i}$, and $m_{adsorbent}$ represent the adsorption capacity for component i (g/g adsorbent), the mass flow rate for component i (g/s), and the mass of the adsorbent (g), respectively.

$$AC_i = \frac{t_i \cdot m_{flow,i}}{m_{adsorbent}} \tag{1}$$

The variable t_i, defined in Equation (2), corresponds to the calculation of the area above the normalized breakthrough curve in units of time. c_i, and c_{io} represent the outlet and inlet concentrations for component i (g/l), respectively.

$$t_i = \int_0^\infty \left(1 - \frac{c_i}{c_{io}}\right) dt \tag{2}$$

The value of t_i was calculated using the Simpsons Rule. Using Simpsons Rule for the experimental results presented in Figure 1, the area above the curve is determined to be 118 min. The adsorption capacity for ethanol can therefore be calculated:

$$AC_i = \frac{t_i \cdot m_{flow,i}}{m_{adsorbent}}$$

$$AC_i = \frac{(117.95 \text{ min})(0.0156 \ g/\text{min})}{5.5 \ g \ adsorbent}$$

$$AC_i = 0.3342 \ g/g \ adsorbent$$

TOTH Isotherm

The ethanol adsorption capacity represents one point on the isotherm. The above procedure was repeated at different inlet concentrations of ethanol in the presence of carbon dioxide, inlet water concentrations in the presence of carbon dioxide, inlet carbon dioxide concentrations in the presence of nitrogen and finally varying inlet ethanol and water concentrations in the presence of carbon dioxide. The isotherms were fitted using

the TOTH isotherm and six fitting parameters. The fitting parameters were obtained using Excel Solver.

Separation Factors

The other set of calculations examined ternary experiments and their corresponding separation factors. The separation factors indicate the degree of separation between two adsorbing components based on the concentration in the fluid and on the adsorbed phase. Equation (3) can be used to determine the separation factor of a ternary system.

$$\lambda = \frac{X_w / X_e}{Y_w / Y_e} \tag{3}$$

Equation (3) gives the definition of the separation factor. X_w and X_e represent the mass fraction of water and ethanol in the adsorbed phase whereas Y_w and Y_e represent the mass fraction of water and ethanol in the vapour phase. Figure A1.2 shows the breakthrough curve for ethanol and water as a function of time.

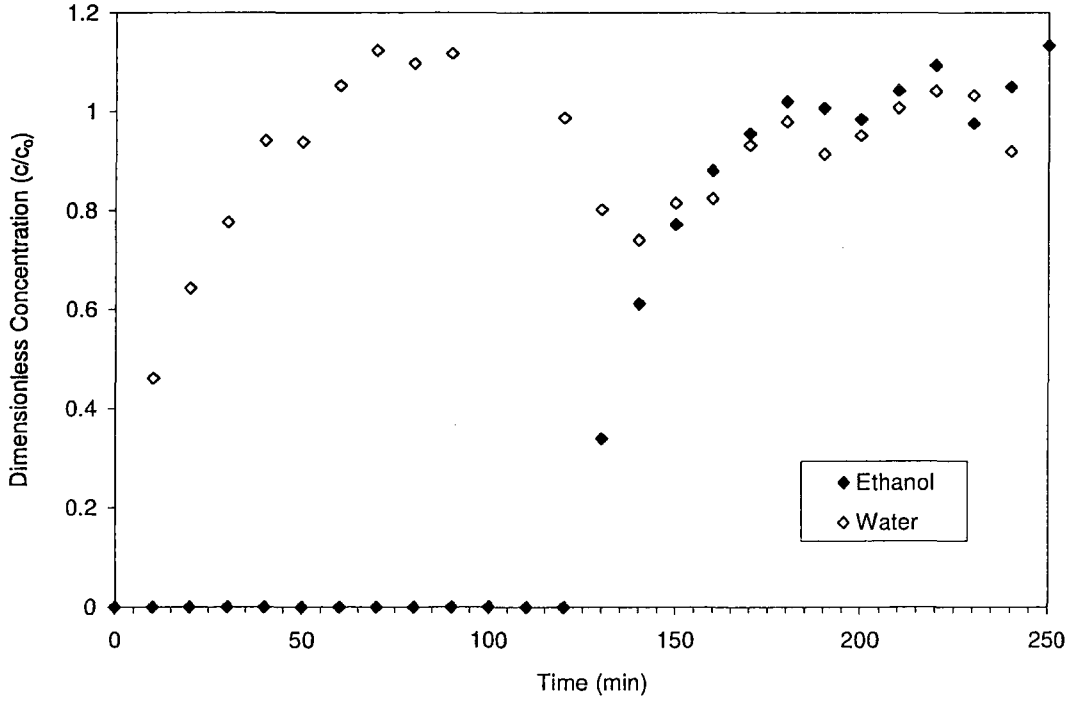

Figure A1.2 - Ternary breakthrough curves for ethanol (0.95 kPa) and water (1.93 kPa) in the presence of carbon dioxide at 24°C and atmospheric total pressure.

The ethanol and water mole fractions were converted into mass fractions in the fluid phase. With these the separation factor was calculated as follows.

$$\lambda = \frac{X_w / X_e}{Y_w / Y_e}$$

$$\lambda = \frac{73.17\ wt\% / 13.05\ wt\%}{0.99\ wt\% / 0.79\ wt\%}$$

$$\lambda = 4.43$$

Carbon Dioxide Adsorption Isotherms

Weighting Method

Ethanol and water isotherms were determined in the presence of carbon dioxide as the stripping gas. For the carbon dioxide adsorption isotherms, helium was used as the carrier gas. It was assumed that helium does not adsorb onto activated carbon, WV-B 1500. The proposed method to determine the carbon dioxide isotherms is as follows:

1. Regenerate the activated carbon WV-B 1500 overnight using air as a purge gas and a temperature of 250°C.

2. Next day, fill adsorption column with known amount of adsorbent as well as weighing of empty adsorption column.

3. Flow a known amount of carbon dioxide and helium through the adsorption column and wait at least one hour to ensure equilibrium has been reached. This was verified when analyzing the temperature profile for carbon dioxide adsorption with the temperature profile reaching steady state within 20 minutes.

4. Weight adsorption column with saturated adsorbent and the difference in weight is attributed to carbon dioxide adsorption.

A validation experiment was conducted with ethanol and carbon dioxide. Under atmospheric conditions, room temperature, flow rate of 0.59 l/min and an inlet ethanol concentration of 4.88 mol%, the breakthrough curve of Figure A.3 was obtained.

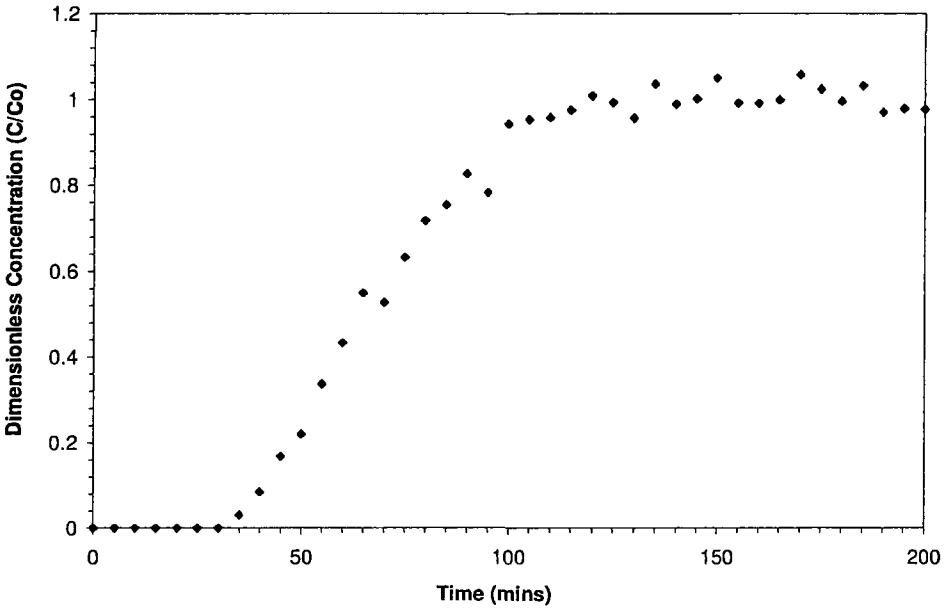

Figure A1.3 - Breakthrough curve for an ethanol-carbon dioxide vapour mixture at an ethanol molar concentration of 4.88 mol% under atmospheric conditions and 24°C.

From the breakthrough curve, the ethanol adsorption capacity was determined to be 0.607 g/g adsorbent. The difference in the weight the column after the experiment due to adsorption was 4 grams (156.8 g – 152.8 g). Given the amount of adsorbent in the column of 6.1 g, an adsorption capacity of 0.655 g/g adsorbent is estimated. This adsorption capacity takes into account ethanol and carbon dioxide adsorption. Another experiment was conducted to determine the amount for carbon dioxide adsorption. Using the same procedure except that pure carbon dioxide was used, a difference of weight of 0.405 g was obtained. For 6.6 g of adsorbent, a carbon dioxide adsorption capacity of 0.06 g/g adsorbent was estimated. For the previous experiment with an ethanol-carbon dioxide vapour mixture, assuming similar magnitude of carbon dioxide adsorption, the ethanol adsorption capacity was estimated to be 0.594 g/g adsorbent which is close to the 0.607 g/g adsorbent adsorption capacity calculated from the breakthrough curve. Even though this method is not the most accurate procedure to obtain an isotherm, the error associated using this procedure is small enough to provide a reasonable representation of the adsorbent performance.

Volumetric Method

To validate the results, another method was used to obtain carbon dioxide isotherms: the volumetric system. The volumetric system determines the adsorption capacity by measuring the change in pressure due to adsorption. Experiments were conducted at 50°C to compare with one isotherm obtained using the previous technique also done at 50°C. Figure A.4 presents the final results.

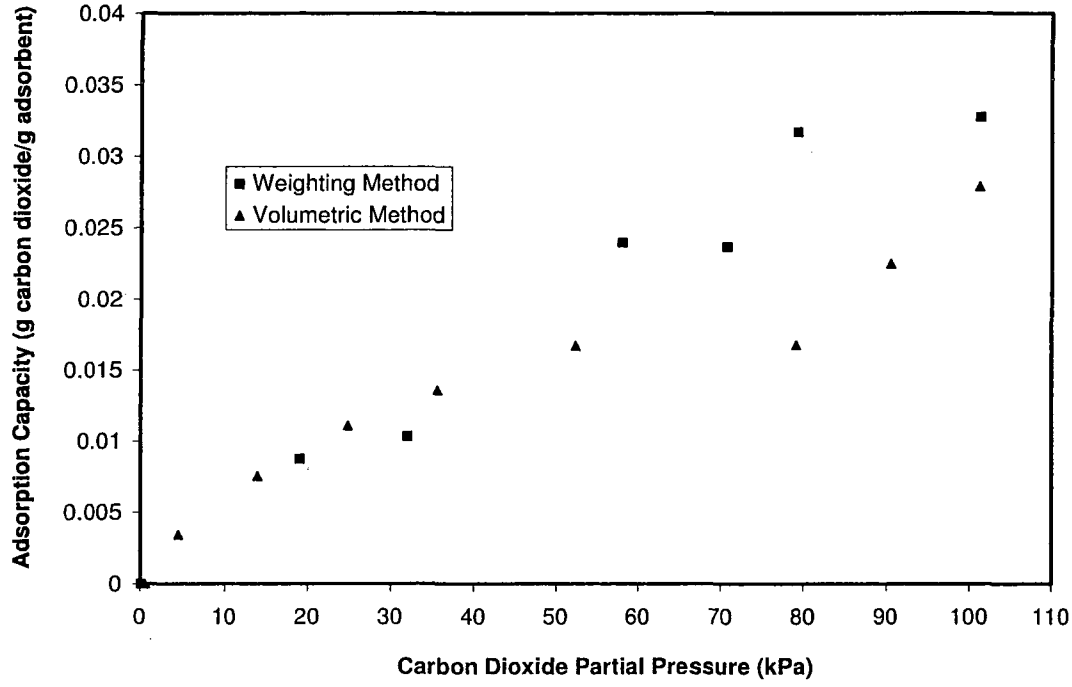

Figure A1.4 - Carbon dioxide adsorption isotherms at 50°C under atmospheric conditions comparing the weighting method with the volumetric method.

Both isotherms show similar results and with the accuracy of both measurements and the low amount of carbon dioxide adsorption, it was concluded that both procedures provide similar results.

Chapter VII

Appendix 2 – Supplementary Information for Chapter III

Recovery of ethanol from carbon dioxide stripped vapour mixture: Adsorption prediction and modelling

Modeling

Mathematical modeling of adsorption experiments was conducted in order to predict the performance of an industrial adsorption process for ethanol purification. The experiments were conducted under normal operating conditions: 24°C and 101 325 Pa. The experimental adsorption column, 36 cm long and 0.8 cm in diameter, was designed to include three thermocouples (see Figure A2.1) to generate a temperature profile during adsorption.

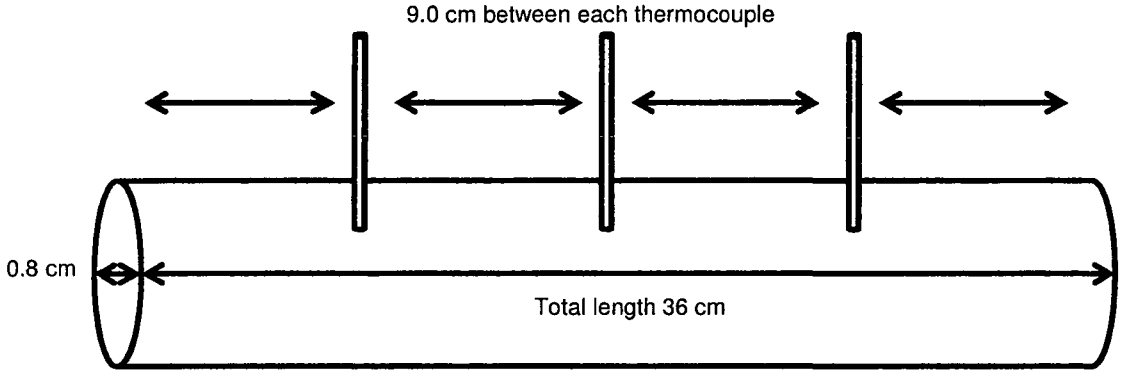

Figure A2.1 – Schematic diagram of the experimental adsorption column.

Mixtures with varying concentrations of ethanol, water and carbon dioxide were used to determine breakthrough curves and temperature profiles which were then used to validate the adsorption column model.

Assumptions made to simplify the solution include: constant void fraction throughout the column, instantaneous equilibrium between the fluid phase and the solid adsorbent surface, negligible radial mass and energy diffusion, perfectly spherical adsorbent particles, ideal gas law, and physical characteristics of bulk gas are close to those for pure carbon dioxide since a minimum of 95% of the vapour mixture composed of carbon dioxide.

Mass and energy balances are used to model the adsorption and desorption breakthrough curves. Mass balances account for species transport occurring in the bulk phase and within the adsorbent pellets. Energy balances examine energy transfer in the bulk phase, within the pellet and through the adsorption column wall.

Bulk Phase Mass Transfer

The mass balance for the bulk phase is given by Equation (1).

$$\varepsilon_c D_Z \frac{\partial^2 c_g}{\partial z^2} - \varepsilon_c v_g \frac{\partial c_g}{\partial z} - \varepsilon_c c_g \frac{\partial v_g}{\partial z} - k_f \frac{3}{r_p}\left(c_g - c_P\Big|^*\right) = \varepsilon_c \frac{\partial c_g}{\partial t} \qquad (1)$$

Equation (1) represents the material balance for one component. Therefore, this equation will be used for each species of the gas mixture: carbon dioxide, ethanol and water. The assumed or known values are the void fraction (ε_c = 0.35), pellet radius (r_p = 0.7 mm) and superficial velocity (v_g = 0.189 m/s). The superficial velocity corresponds to a volumetric flow rate of 0.534 L/min. The axial dispersion (D_Z) and the mass transfer coefficient (k_f) need to be estimated. The axial dispersion can be estimated using the molecular diffusivity, the Reynolds number and the Schmidt number (Brokaw, 1969). For a binary mixture, the molecular diffusivity can be calculated using Equation (2).

$$D_M = \frac{0.001858 T^{1.5}\left(\frac{1}{M_A} + \frac{1}{M_B}\right)^{0.5}}{P\sigma_{AB}^2 \Omega_D} \qquad (2)$$

Molecular diffusivity can be estimated using the Lennard-Jones parameters (collision integral Ω_D and the collision diameter σ_{AB}) (Brokaw, 1969).

$$\Omega_D = \left(44.54 T^{o-4.909} + 1.911 T^{o-1.575}\right)^{0.10} \qquad (3)$$

$$T^o = kT / \varepsilon_{AB} \qquad (4)$$

$$\varepsilon / k = 0.75 T_c \qquad (5)$$

$$\sigma = 0.841 V_c^{1/3} \qquad (6)$$

$$\sigma_{AB} = \left(\sigma_A \cdot \sigma_B\right)^{1/2} \qquad (7)$$

The axial dispersion and mass transfer coefficients are correlated with the Reynolds number, Schmidt number, and molecular diffusivity. The Reynolds and Schmidt numbers are defined using Equations (8) and (9), respectively.

$$\mathrm{Re} = \frac{\rho_g v_g D_p}{\mu_g} \qquad (8)$$

$$Sc = \frac{\mu_g}{\rho_g D_M} \qquad (9)$$

The axial dispersion and mass transfer coefficients can then be determined using Equations (10) and (11), respectively (Wakao and Funazkri, 1978).

$$D_Z = \frac{D_M}{\varepsilon_c}[20 + 0.5(\mathrm{Re})(Sc)] \tag{10}$$

$$k_f = \frac{D_M}{D_p}\left[2.0 + 1.1(\mathrm{Re})^{0.6}(Sc)^{0.33}\right] \tag{11}$$

Bulk Phase Energy Balance

Equation (12) accounts for the temperature variation of the bulk gas flowing through the column. T_g represents the combined temperature of the bulk gas and the solid particles.

$$\eta\frac{\partial T_g}{\partial t} = k_g\frac{\partial^2 T_g}{\partial z^2} - v_g\rho_g C_{Pg}\varepsilon_c\frac{\partial T_g}{\partial z} - \rho_b\Delta H_{ads}k_f\frac{3(1-\varepsilon_c)}{\varepsilon_c r_p}\{c_A^* - \bar{c}_A\} - h_{fD}\frac{2}{r_c}(T_g - T_w) \tag{12}$$

η, defined in Equation (13), is the heat thermal capacity of the bulk gas/solid system within the column. It accounts for the respective density of the gas and solids as well as the column void fraction porosity and the porosity of the adsorbent pellets.

$$\eta = \rho_g C_{Pg}(\varepsilon_c + (1-\varepsilon_c)\varepsilon_P) + (1-\varepsilon_c)(1-\varepsilon_P)\rho_s C_{Ps} \tag{13}$$

The heat transfer coefficients are calculated using the Prandtl and Reynolds numbers and are calculated using Equations (14) through (19).

$$\mathrm{Re}_D = \frac{\rho v_g D_c}{\mu} \tag{14}$$

$$\mathrm{Pr} = \frac{\nu}{\alpha} \tag{15}$$

$$\nu = \frac{\mu}{\rho} \tag{16}$$

$$\alpha = \frac{k}{\rho c_p} \tag{17}$$

$$h_{fD} = \frac{k \cdot Nu_D}{D_c} \tag{18}$$

$$h_{fP} = \frac{k \cdot Nu_D}{D_P} \tag{19}$$

Heat losses through Column Wall

Heat loss across the column wall to the environment is calculated through the calculation of the wall temperature using Equation (20).

$$\left[r_o^2 - r_c^2\right]\rho_w C_{Pw}\frac{\partial T_w}{\partial t} = 2r_c h_{fD}\left(T_g - T_w\right) - 2r_o h_o\left(T_w - T_{atm}\right) \tag{20}$$

Conduction through the column wall was considered negligible and therefore only convection within the adsorption column, convection to the surrounding environment and accumulation are considered. The overall heat transfer coefficient within the adsorption wall is already calculated using Equation (18) with Equations (21) – (23) used to determine the overall heat transfer coefficient in the surroundings (Churchill and Chu, 1975; Incropera at al., 2007).

$$Ra = \frac{\beta \Delta T g L^3 \,\mathrm{Pr}}{\nu^2} \tag{21}$$

$$Nu_D = \left\{0.60 + \frac{0.387 Ra_D^{1/6}}{\left[1 + \left(0.559/\mathrm{Pr}\right)^{9/16}\right]^{8/27}}\right\} \tag{22}$$

$$h_o = \frac{k \cdot Nu}{D} \tag{23}$$

Derivations of Mass and Energy Balance for a differential element

This section presents the derivations of the mass and energy balances for a differential element of the column. These same equations will be used to solve numerically the heat and mass transfer balances using finite differences. Three governing equations are considered: a material balance for the bulk phase, an energy balance for the bulk phase and an energy balance within column wall to account for heat losses. The material balance in the bulk phase is specific to a component and therefore a ternary system including ethanol, water and carbon dioxide would require a separate balance. The energy balance takes into account all components but the heat of adsorption of each component must be considered. Finite differences equations could be obtained by discretizing Equations (1), (12), and (20) or by deriving them from first principles.

Structure for Derivations

The column id discretized into NK cylindrical disk as shown in Figure A2.2.

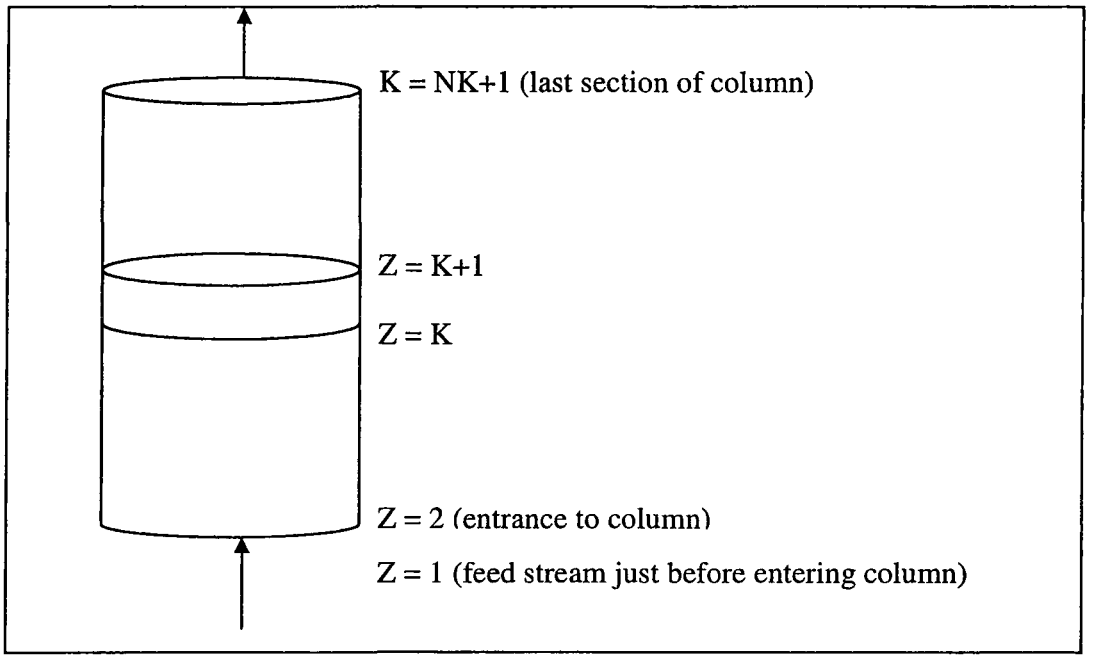

Figure A2.2 - Notation used within the material and energy balances along the adsorption column in the column phase.

If the concentration and temperature profiles are required within the pellet, the notation of Figure A2.3 is used.

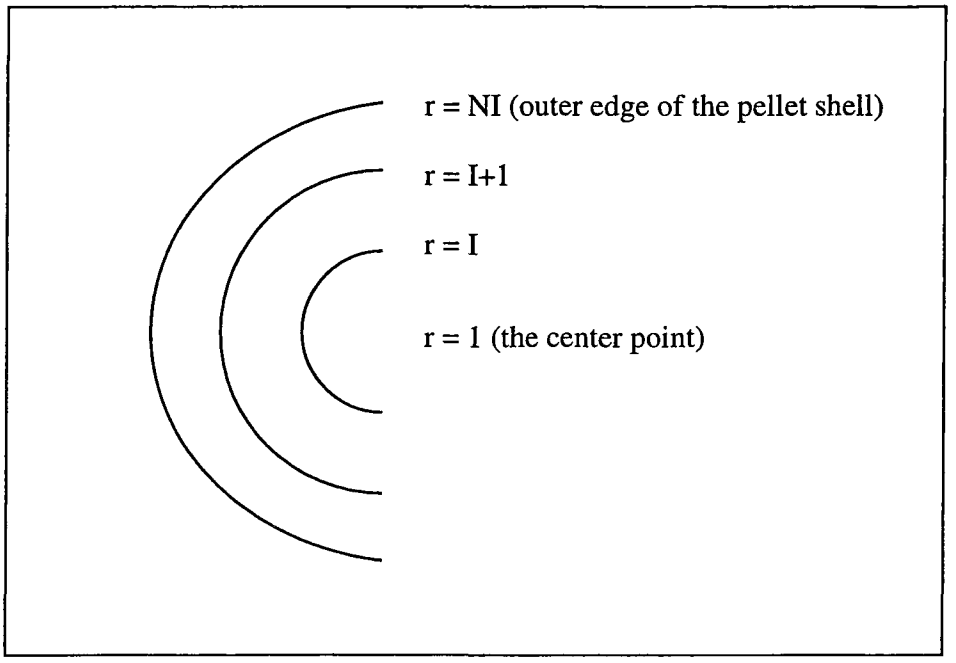

Figure A2.3 - Notation used within the material and energy balances along the adsorption column in the pellet phase

Bulk Phase Mass Transfer Derivation

The component material balance for one component is shown as follows.

In - out + generation - disappearance = accumulation

$$N_A^{i-1}\varepsilon_c A - N_A^i \varepsilon_c A - k_f \frac{3}{r_p}\left(c_g - c_P\big|^*\right) = \varepsilon_c A \Delta z \frac{\partial c_g}{\partial t}$$

$$\left[-D_Z \frac{\partial c_g^{i-1}}{\partial z} + c_g^{i-1} v_g\right]\varepsilon_c A - \left[-D_Z \frac{\partial c_g^{i}}{\partial z} + c_g^{i} v_g\right]\varepsilon_c A - k_f \frac{3}{r_p}\left(c_g - c_P\big|^*\right) A\Delta z = \varepsilon_c A \Delta z \frac{\partial c_g}{\partial t}$$

$$\frac{\left[-D_Z \frac{\partial c_g^{i-1}}{\partial z} + c_g^{i-1} v_g\right]\varepsilon_c A - \left[-D_Z \frac{\partial c_g^{i}}{\partial z} + c_g^{i} v_g\right]\varepsilon_c A}{A\Delta z} - k_f \frac{3}{r_p}\left(c_g - c_P\big|^*\right) = \varepsilon_c \frac{\partial c_g}{\partial t}$$

$$\varepsilon_c \frac{\partial}{\partial z}\left(D_Z \frac{\partial c_g}{\partial z}\right) - \varepsilon_c \frac{\partial v_g c_g}{\partial z} - k_f \frac{3}{r_p}\left(c_g - c_P\big|^*\right) = \varepsilon_c \frac{\partial c_g}{\partial t}$$

$$\varepsilon_c D_Z \frac{\partial^2 c_g}{\partial z^2} - \varepsilon_c v_g \frac{\partial c_g}{\partial z} - \varepsilon_c c_g \frac{\partial v_g}{\partial z} - k_f \frac{3}{r_p}\left(c_g - c_P\big|^*\right) = \varepsilon_c \frac{\partial c_g}{\partial t} \; [=] \frac{mol}{s\, m_c^3}$$

$$\frac{m_l^3}{m_c^3}\frac{m_c}{s}\frac{mol}{m_l^3 m_c} - \frac{m_l^3}{m_c^3}\frac{m_c}{s}\frac{mol}{m_l^3 m_c} - \frac{m_l^3}{m_c^3}\frac{m_c}{s}\frac{mol}{m_l^3 m_c} - \frac{m_l}{s}\frac{m_l^2}{m_c^3}\frac{mol}{m_l^3} = \frac{m_l^3}{m_c^3}\frac{mol}{s\, m_l^3}$$

Bulk Phase Mass Transfer Boundary Conditions

The boundary conditions at the two ends of the column must be incorporated such that the discretized equation becomes:

When z = 2,

$$c_g\Big|_{z-1}^{t} = c_g\Big|_{z}^{t}$$

$$c_g\Big|_{z}^{t+\Delta t} = c_g\Big|_{z}^{t} + \frac{D_Z \Delta t}{\Delta z^2}\left[2c_g\Big|_{z+1}^{t} - 2c_g\Big|_{z}^{t}\right] - \frac{3\Delta t k_f}{\varepsilon_c r_P}\left[c_g\Big|_{z}^{t} - c_P\Big|^{*}\right] - \frac{c_g \Delta t}{\Delta z}\left[v_g\Big|_{z}^{t} - v_g\Big|_{z-1}^{t}\right]$$

When z = 1 to NK

$$c_g\Big|_{z}^{t+\Delta t} = c_g\Big|_{z}^{t} + \frac{D_Z \Delta t}{\Delta z^2}\left[c_g\Big|_{z-1}^{t} - 2c_g\Big|_{z}^{t} + c_g\Big|_{z+1}^{t}\right] - \frac{3\Delta t k_f}{\varepsilon_c r_P}\left[c_g\Big|_{z}^{t} - c_P\Big|^{*}\right] - \frac{v_g \Delta t}{\Delta z}\left[c_P\Big|_{z}^{t} - c_g\Big|_{z-1}^{t}\right]$$

$$- \frac{c_g \Delta t}{\Delta z}\left[v_g\Big|_{z}^{t} - v_g\Big|_{z-1}^{t}\right]$$

When z = NK+1

$$\frac{\partial c_g}{\partial z} = 0 \text{ or } c_g\Big|_{z}^{t} = c_g\Big|_{z-1}^{t}$$

$$c_g\Big|_{z}^{t+\Delta t} = c_g\Big|_{z}^{t} + \frac{D_Z \Delta t}{\Delta z^2}\left[2c_g\Big|_{z-1}^{t} - 2c_g\Big|_{z}^{t}\right] - \frac{3\Delta t k_f}{\varepsilon_c r_P}\left[c_g\Big|_{z}^{t} - c_P\Big|^{*}\right] - \frac{c_g \Delta t}{\Delta z}\left[v_g\Big|_{z}^{t} - v_g\Big|_{z-1}^{t}\right]$$

Pellet Phase Mass Transfer Derivation

When taking into account the pellet phase, the bulk phase mass balance equation changes slightly. Term $c_P\Big|^{*}$, which represents the pellet with the assumption that once the adsorbate comes into contact with the adsorbent it is adsorbed, is replaced with $c_P\Big|_{r=R_P}$. The component material balance for one component is shown as follows.

In - out + generation - disappearance = accumulation

$$N_{A,r}\varepsilon_P 4\pi r^2 - N_{A,r+\Delta r}\varepsilon_P 4\pi (r+\Delta r)^2 - k_{ads}a_P\left(c_P - c_P^*\right)4\pi r^2\Delta r = \varepsilon_P 4\pi r^2\Delta r\frac{\partial c_P}{\partial t}$$

$$-D_e\frac{\partial c_P{}^{r}}{\partial r}\varepsilon_P 4\pi r^2 - \left(-D_e\frac{\partial c_P{}^{r+\Delta r}}{\partial r}\right)\varepsilon_P 4\pi (r+\Delta r)^2 - k_{ads}a_P\left(c_P - c_P^*\right)4\pi r^2\Delta r = \varepsilon_P 4\pi r^2\Delta r\frac{\partial c_P}{\partial t}$$

$$\frac{D_e\varepsilon_P\frac{1}{r^2}\left((r+\Delta r)^2\frac{\partial c_P{}^{r+\Delta r}}{\partial r} - r^2\frac{\partial c_P{}^{r+\Delta r}}{\partial r}\right)}{\Delta r} - k_{ads}a_P\left(c_P - c_P^*\right) = \varepsilon_P\frac{\partial c_P}{\partial t}$$

$$D_e\varepsilon_P\left[\frac{1}{r^2}\frac{\partial}{\partial r}\left(r^2\frac{\partial c_P}{\partial r}\right)\right] - k_{ads}a_P\left(c_P - c_P^*\right) = \varepsilon_P\frac{\partial c_P}{\partial t}$$

$$D_e\varepsilon_P\left[\frac{2}{r}\frac{\partial c_P}{\partial r} + \frac{\partial^2 c_P}{\partial r^2}\right] - k_{ads}a_P\left(c_P - c_P^*\right) = \varepsilon_P\frac{\partial c_P}{\partial t}$$

$$D_e\varepsilon_P\left[\frac{2}{r}\frac{\partial c_P}{\partial r} + \frac{\partial^2 c_P}{\partial r^2}\right] = \left[\varepsilon_P + (1-\varepsilon_P)\rho_S\frac{\partial c_A}{\partial c_P}\right]\frac{\partial c_P}{\partial t}$$

$$\frac{m_P^2}{s}\frac{m_l^3}{m_P^3}\left[\frac{1}{m_P}\frac{mol}{m_l^3 m_P} + \frac{mol}{m_l^3 m_P^2}\right] = \left[\frac{m_l^3}{m_P^3} + \frac{m_s^3}{m_P^3}\frac{kg}{m_s^3}\frac{mol/kg}{mol/m_l^3}\right]\frac{mol}{m_l^3 s}$$

Pellet Phase Mass Transfer Boundary Conditions

The following discretization equations show how the boundary conditions were incorporated into the equations. An implicit finite differences scheme is used within the pellets.

$$\alpha = \frac{D_e}{\varepsilon_P + (1-\varepsilon_P)\rho_S\left[\partial c_A \big/ \partial c_P\right]}$$

When r = 1,

$$\frac{\partial c_P}{\partial z} = 0$$

$$c_P\Big|_r^{t+\Delta t} = c_P\Big|_r^t + 3\alpha\Delta t\left[\frac{2c_P\Big|_{r+1}^{t+\Delta t} - 2c_P\Big|_r^{t+\Delta t}}{\Delta r^2}\right]$$

$$c_P\Big|_r^t = \left[1 + \frac{6\alpha\Delta t}{\Delta r^2}\right]c_P\Big|_r^{t+\Delta t} - \frac{6\alpha\Delta t}{\Delta r^2}c_P\Big|_{r+1}^{t+\Delta t}$$

When r = 1+NI-1,

$$c_P\Big|_r^{t+\Delta t} = c_P\Big|_r^{t} + \alpha\Delta t\left[\frac{c_P\Big|_{r-1}^{t+\Delta t} - 2c_P\Big|_r^{t+\Delta t} + c_P\Big|_{r+1}^{t+\Delta t}}{\Delta r^2} + \frac{c_P\Big|_{r+1}^{t+\Delta t} - c_P\Big|_{r-1}^{t+\Delta t}}{(i-1)\Delta r^2}\right]$$

$$c_P\Big|_r^{t} = \left[1 + \frac{2\alpha\Delta t}{\Delta r^2}\right]c_P\Big|_r^{t+\Delta t} + \left[\frac{1}{i-1} - 1\right]\frac{\alpha\Delta t}{\Delta r^2}c_P\Big|_{r-1}^{t+\Delta t} - \left[\frac{1}{i-1} + 1\right]\frac{\alpha\Delta t}{\Delta r^2}c_P\Big|_{r+1}^{t+\Delta t}$$

When r = NI,

$$-D_e\frac{\partial c_P}{\partial r} = k_f\left(c_g\Big|_z^t - c_P\Big|_{r=R_P}^t\right)$$

$$c_P\Big|_r^{t+\Delta t} = c_P\Big|_r^{t} + \alpha\Delta t\left[\frac{2c_P\Big|_{r-1}^{t+\Delta t} - 2c_P\Big|_r^{t+\Delta t} - \dfrac{2k_f\Delta r\left(c_g\Big|_z^t - c_P\Big|_{r=R_P}^t\right)}{D_e}}{\Delta r^2} - \frac{2k_f\Delta r\left(c_g\Big|_z^t - c_P\Big|_{r=R_P}^t\right)}{(i-1)\Delta r^2 D_e}\right]$$

$$c_P\Big|_r^{t} = \left[1 + \frac{2\alpha\Delta t}{\Delta r^2}\right]c_P\Big|_r^{t+\Delta t} - \frac{2\alpha\Delta t}{\Delta r^2}c_P\Big|_{r-1}^{t+\Delta t} - \left[\frac{1}{i-1} + 1\right]\frac{2k_f\alpha\Delta t}{D_e\Delta r^2}\left(c_g\Big|_z^t - c_P\Big|_{r=R_P}^t\right)$$

Bulk Phase Heat Transfer Derivation

The component material balance for one component is shown as follows.

In - out + generation - disappearance = accumulation

$$\eta = \rho_g C_{Pg}(\varepsilon_c + (1-\varepsilon_c)\varepsilon_P) + (1-\varepsilon_c)(1-\varepsilon_P)\rho_s C_{Ps}$$

$$\left(-k_g\frac{\partial T_g^{\,z-1}}{\partial z}+v_g\rho_g C_{Pg}\varepsilon_c T_g^{z-1}\right)A-\left(-k_g\frac{\partial T_g^{\,z}}{\partial z}+v_g\rho_g C_{Pg}\varepsilon_c T_g^{z}\right)A-\rho_b\Delta H_{ads}A\Delta z\frac{\partial c_A}{\partial t}$$

$$-h_{fD}\frac{2}{r_c}A\Delta z\left(T_g-T_w\right)=\eta A\Delta z\frac{\partial T_g}{\partial t}$$

$$\frac{\left(-k_g\frac{\partial T_g^{\,z-1}}{\partial z}+v_g\rho_g C_{Pg}\varepsilon_c T_g^{z-1}\right)A-\left(-k_g\frac{\partial T_g^{\,z}}{\partial z}+v_g\rho_g C_{Pg}\varepsilon_c T_g^{z}\right)A}{\Delta z}-\rho_b\Delta H_{ads}\frac{\partial c_A}{\partial t}$$

$$-h_{fD}\frac{2}{r_c}\left(T_g-T_w\right)=\eta\frac{\partial T_g}{\partial t}$$

$$k_g\frac{\partial^2 T_g}{\partial z^2}-v_g\rho_g C_{Pg}\varepsilon_c\frac{\partial T_g}{\partial z}-\rho_b\Delta H_{ads}k_f\frac{3(1-\varepsilon_c)}{\varepsilon_c r_p}\left\{c_A^*-\bar{c}_A\right\}-h_{fD}\frac{2}{r_c}\left(T_g-T_w\right)=\eta\frac{\partial T_g}{\partial t}\ [=]\ \frac{W}{m_c^3}$$

$$\frac{W}{m_c K}\frac{K}{m_c^2}-\frac{m_c}{s}\frac{kg}{m_l^3}\frac{J}{kg\,K}\frac{m_l^3}{m_c^3}\frac{K}{m_c}-\frac{W}{m_P^2 K}\frac{1}{m_p}\frac{m_P^3}{m_c^3}K-\frac{kg}{m_P^3}\frac{J}{mol}\frac{m_l}{s}\frac{m_l^2}{m_c^3}\frac{m_P^3}{m_c^3}\frac{m_c^3}{m_l^3}\frac{mol}{kg}=\frac{kg}{m_l^3}\frac{J}{kg\,K}\frac{m_l^3}{m_c^3}\frac{K}{s}$$

Bulk Phase Energy Transfer Boundary Conditions

The following discretization shows how the boundary conditions were incorporated into the equations.

When z = 0,

$$\frac{\partial T_g}{\partial z}=0$$

$$T_g\Big|_z^{t+\Delta t}=T_g\Big|_z^t+\frac{k_g\Delta t}{\Delta z^2\eta}\left[2T_g\Big|_{z+1}^t-2T_g\Big|_z^t\right]+\frac{\Delta H_{ads}\rho_b\Delta t}{\eta}\left(k_f\frac{3(1-\varepsilon_c)}{\varepsilon_c r_p}\left\{c_A^*-\bar{c}_A\right\}\right)-\frac{v_g\rho_g C_{Pg}\varepsilon_c\Delta t}{\eta\Delta z}\left[T_g\Big|_z^t-T_g\Big|_{z-1}^t\right]$$

$$-h_{fD}\frac{2\Delta t}{\eta r_c}\left(T_g-T_w\right)$$

When z = 1 to N-1

$$T_g\Big|_z^{t+\Delta t}=T_g\Big|_z^t+\frac{k_g\Delta t}{\Delta z^2\eta}\left[T_g\Big|_{z-1}^t-2T_g\Big|_z^t+T_g\Big|_{z+1}^t\right]+\frac{\Delta H_{ads}\rho_b\Delta t}{\eta}\left(k_f\frac{3(1-\varepsilon_c)}{\varepsilon_c r_p}\left\{c_A^*-\bar{c}_A\right\}\right)-\frac{v_g\rho_g C_{Pg}\varepsilon_c\Delta t}{\eta\Delta z}\left[T_g\Big|_z^t-T_g\Big|_{z-1}^t\right]$$

$$-h_{fD}\frac{2\Delta t}{\eta r_c}\left(T_g-T_w\right)$$

When z = N

$$\frac{\partial T_g}{\partial z}=0\qquad T_g\Big|_z^{t+\Delta t}=T_g\Big|_z^t+\frac{k_g\Delta t}{\Delta z^2\eta}\left[2T_g\Big|_{z-1}^t-2T_g\Big|_z^t\right]+\frac{\Delta H_{ads}\rho_b\Delta t}{\eta}\left(k_f\frac{3(1-\varepsilon_c)}{\varepsilon_c r_p}\left\{c_A^*-\bar{c}_A\right\}\right)-h_{fD}\frac{2\Delta t}{\eta r_c}\left(T_g-T_w\right)$$

Pellet Phase Energy Transfer Derivation

The pellet phase energy balance within the adsorption column is shown as follows.

In – out +generation – disappearance = accumulation

$$-k_{GS}\frac{\partial T_P}{\partial r}^{r} 4\pi r^2 - \left(-k_{GS}\frac{\partial T_P}{\partial r}^{r+\Delta r} 4\pi(r+\Delta r)^2\right) + \Delta H_{ads}\rho_P \frac{\partial c_a}{\partial c_p}\frac{\partial c_p}{\partial t} 4\pi r^2 \Delta r$$

$$= \left[(\varepsilon_P)\rho_g C_{Pg} + (1-\varepsilon_P)\rho_s C_{PS}\right]\frac{\partial T_P}{\partial t} 4\pi r^2 \Delta r$$

$$\frac{-k_{GS}\frac{\partial T_P}{\partial r}^{r} r^2 - \left(-k_{GS}\frac{\partial T_P}{\partial r}^{r+\Delta r}(r+\Delta r)^2\right)}{r^2\Delta r} + \Delta H_{ads}\rho_P \frac{\partial c_a}{\partial c_p}\frac{\partial c_p}{\partial t} = \left[(\varepsilon_P)\rho_g C_{Pg} + (1-\varepsilon_P)\rho_s C_{PS}\right]\frac{\partial T_P}{\partial t}$$

$$k_{GS}\left[\frac{1}{r^2}\frac{\partial}{\partial r}\left(r^2\frac{\partial T_P}{\partial r}\right)\right] + \Delta H_{ads}\rho_P \frac{\partial c_a}{\partial c_p}\frac{\partial c_p}{\partial t} = \left[(\varepsilon_P)\rho_g C_{Pg} + (1-\varepsilon_P)\rho_s C_{PS}\right]\frac{\partial T_P}{\partial t}$$

$$k_{GS}\left[\frac{2}{r}\frac{\partial T_P}{\partial r} + \frac{\partial^2 T_P}{\partial r^2}\right] + (\Delta H_{ads})\rho_P \frac{\partial c_a}{\partial c_p}\frac{\partial c_p}{\partial t} = \left[(\varepsilon_P)\rho_g C_{Pg} + (1-\varepsilon_P)\rho_S C_{PS}\right]\frac{\partial T_P}{\partial t} \quad [=] \frac{W}{m_P^3}$$

$$\frac{W}{m_P K}\left[\frac{1}{m_P}\frac{K}{m_P} + \frac{K}{m_P^2}\right] + \frac{J}{mol}\frac{kg}{m_P^3}\frac{mol/kg}{mol/m_l^3}\frac{mol}{m_l^3 s} = \left[\frac{m_l^3}{m_P^3}\frac{kg}{m_l^3}\frac{J}{kg_g\ K} + \frac{m_s^3}{m_P^3}\frac{kg}{m_s^3}\frac{J}{kg_S\ K}\right]\frac{K}{s}$$

$$\beta = \frac{k_{gs}}{\varepsilon_P\rho_P C_{Pg} + (1-\varepsilon_P)\rho_S C_{PS}}$$

$$\lambda = \frac{\Delta H_{ads}\rho_P \frac{\partial c_A}{\partial c_P}\frac{\partial c_P}{\partial t}}{\varepsilon_P\rho_P C_{Pg} + (1-\varepsilon_P)\rho_S C_{PS}}$$

$$\beta\left[\frac{2}{r}\frac{\partial T_P}{\partial r} + \frac{\partial^2 T_P}{\partial r^2}\right] + \lambda = \frac{\partial T_P}{\partial t}$$

Pellet Phase Energy Transfer Derivation

The pellet phase energy balance within the adsorption column is shown as follows.

In – out +generation – disappearance = accumulation

$$k_{GS}\left[\frac{1}{r^2}\frac{\partial}{\partial r}\left(r^2\frac{\partial T_P}{\partial r}\right)\right] + (\Delta H_{ads})\rho_{bed}\frac{\partial c_a}{\partial c_p}\frac{\partial c_p}{\partial t} = \left[(\varepsilon_P)\rho_g C_{Pg} + (1-\varepsilon_P)\rho_S C_{PS}\right]\frac{\partial T_P}{\partial t}$$

$$\beta = \frac{k_{gs}}{\varepsilon_P \rho_P C_{Pg} + (1-\varepsilon_P)\rho_S C_{PS}}$$

$$\lambda = \frac{\Delta H_{ads} \rho_{bed} \frac{\partial c_A}{\partial c_P} \frac{\partial c_P}{\partial t}}{\varepsilon_P \rho_P C_{Pg} + (1-\varepsilon_P)\rho_S C_{PS}}$$

Pellet Phase Energy Transfer Boundary Conditions

The following discretization, using an implicit scheme, shows how the boundary conditions were incorporated into the equations.

When r = 0,

$$\frac{\partial T_P}{\partial z} = 0$$

$$T_P\Big|_r^{t+\Delta t} = T_P\Big|_r^t + 3\beta\Delta t\left[\frac{2T_P\Big|_{r+1}^{t+\Delta t} - 2T_P\Big|_r^{t+\Delta t}}{\Delta r^2}\right] + \lambda\Delta t$$

$$T_P\Big|_r^t + \lambda\Delta t = \left[1 + \frac{6\beta\Delta t}{\Delta r^2}\right] T_P\Big|_r^{t+\Delta t} - \frac{6\beta\Delta t}{\Delta r^2} T_P\Big|_{r+1}^{t+\Delta t}$$

When r = 1 to M-1,

$$T_P\Big|_r^{t+\Delta t} = T_P\Big|_r^t + \beta\Delta t\left[\frac{T_P\Big|_{r-1}^{t+\Delta t} - 2T_P\Big|_r^{t+\Delta t} + T_P\Big|_{r+1}^{t+\Delta t}}{\Delta r^2} + \frac{T_P\Big|_{r+1}^{t+\Delta t} - T_P\Big|_{r-1}^{t+\Delta t}}{(i-1)\Delta r^2}\right] + \lambda\Delta t$$

$$T_P\Big|_r^t + \lambda\Delta t = \left[1 + \frac{2\beta\Delta t}{\Delta r^2}\right] T_P\Big|_r^{t+\Delta t} + \left[\frac{1}{i-1} - 1\right]\frac{\beta\Delta t}{\Delta r^2} T_P\Big|_{r-1}^{t+\Delta t} - \left[\frac{1}{i-1} + 1\right]\frac{\beta\Delta t}{\Delta r^2} T_P\Big|_{r+1}^{t+\Delta t}$$

When r = M,

$$-k_{gs}\frac{\partial T_P}{\partial z} = h_{fP}\left(T_g\Big|_z^t - T_P\Big|_{r=R_P}^t\right)$$

$$T_P\Big|_r^{t+\Delta t} = T_P\Big|_r^t + \beta\Delta t\left[\frac{2T_P\Big|_{r-1}^t - 2T_P\Big|_r^t - \frac{h_{fP}2\Delta r\left(T_g\Big|_z^t - T_P\Big|_{r=R_P}^t\right)}{k_{gs}}}{\Delta r^2} - \frac{\frac{h_{fP}2\Delta r\left(T_g\Big|_z^t - T_P\Big|_{r=R_P}^t\right)}{k_{gs}}}{(i-1)k_{gs}\Delta r^2}\right] + \lambda\Delta t$$

$$T_P\Big|_r^t + \lambda\Delta t = \left[1+\frac{2\beta\Delta t}{\Delta r^2}\right]T_P\Big|_r^{t+\Delta t} - \frac{2\beta\Delta t}{\Delta r^2}T_P\Big|_{r-1}^{t+\Delta t} - \left[1+\frac{1}{i-1}\right]\frac{2h_{fP}\beta\Delta t}{k_{gs}\Delta r}\left(T_g\Big|_z^t - T_P\Big|_{r=R_P}^t\right)$$

Heat Losses through the Column Wall

The bulk phase energy balance within the adsorption column is shown as follows.

In - out + generation - disappearance = accumulation

$$h_f\left(T_g - T_w\right)2\pi r_c L - h_o\left(T_w - T_{atm}\right)2\pi r_o L = \pi\left[r_o^2 - r_c^2\right]L\rho_w C_{Pw}\frac{\partial T_w}{\partial t}$$

$$2r_c h_f\left(T_g - T_w\right) - 2r_o h_o\left(T_w - T_{atm}\right) = \left[r_o^2 - r_c^2\right]\rho_w C_{Pw}\frac{\partial T_w}{\partial t}$$

$$m_c\frac{W}{m_c^2 K}K - m_c\frac{W}{m_c^2 K}K = m_c^2\frac{kg}{m_c^3}\frac{J}{kg\,K}\frac{K}{s}$$

Heat Losses through the Column Wall Boundary Conditions

The following discretization shows how the boundary conditions were incorporated into the equation.

$$T_w\Big|_z^{t+\Delta t} = T_w\Big|_z^t + \frac{2h_f r_c\left(T_g - T_w\Big|_z^t\right)\Delta t}{\left[r_o^2 - r_c^2\right]\rho_w C_{Pw}} - \frac{2h_o r_o\left(T_w\Big|_z^t - T_{atm}\right)\Delta t}{\left[r_o^2 - r_c^2\right]\rho_w C_{Pw}}$$

Sample Calculations

The following sample calculations are performed for the experiment completed on May 30, 2009 with Table A2.1 showing the experimental conditions.

Table A2.1 – Experimental Conditions

Ethanol concentration	2.62	mol%
Water concentration	0	mol%
Carbon dioxide concentration	97.38	mol%
Total volumetric flow rate	0.534	l/min
Mass of adsorbent	4.8	g
Final adsorption capacity	0.5818	g/g adsorbent

In the FORTRAN source code, the concentration profile was converted to mol/m^3. Figure A2.4 shows the breakthrough curve and Figure A2.5 shows the adsorption capacity as a function of time.

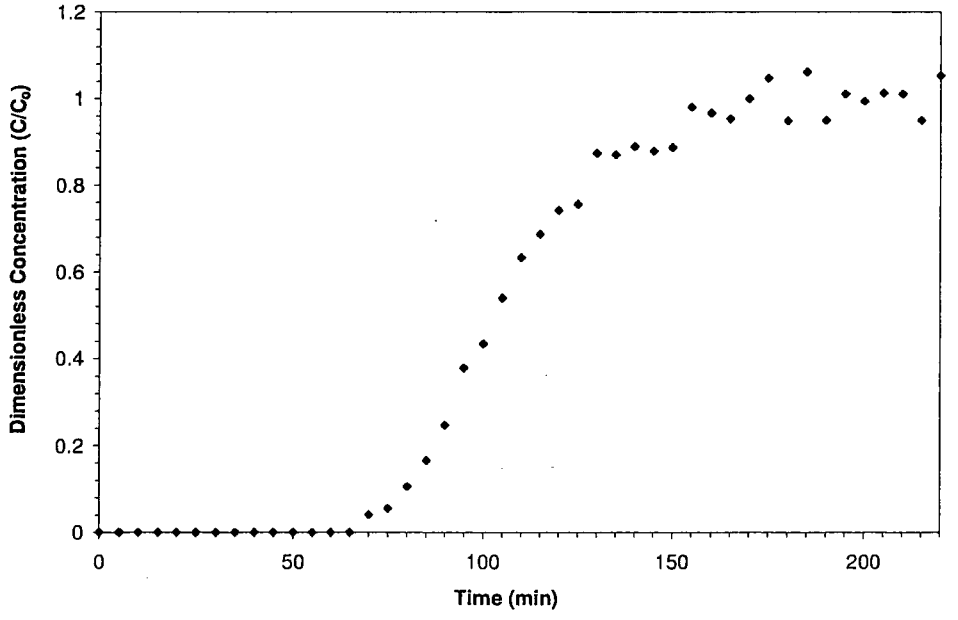

Figure A2.4 – Breakthrough curve for ethanol from May 30, 2009 experiment.

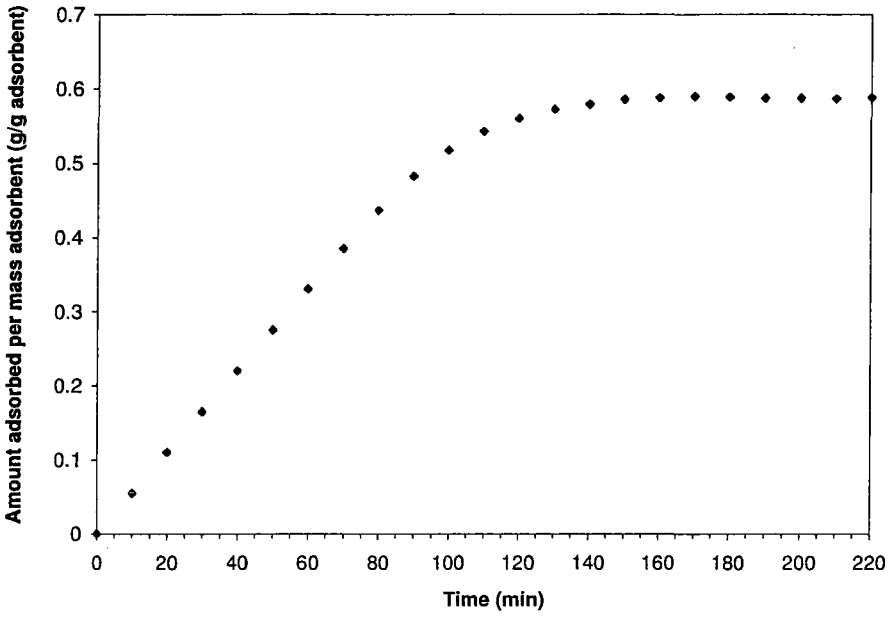

Figure A2.5 – Adsorption capacity as a function of time for May 30, 2009 experiment.

Mass Transfer in Bulk Phase

The calculations associated with the mass transfer in the bulk phase are, with the conditions listed Tables A2.2 and A2.3, are shown below.

Table A2.2 - Column and gas parameters

Column Void fraction	0.35	-
Molar Mass of Ethanol	46.07	g/mol
Molar Mass of Water	18.02	g/mol
Molar Mass of Carbon Dioxide	44.01	g/mol
Average Molar Mass of Mixture	44.09	g/mol
Solid Density	2300	kg/m^3
Bed Density	320	kg/m^3
Tortuosity	4	-
Pore Radius (WV-B 1500)	$1.75x10^{-09}$	m

Table A2.3 - Parameters to determine molecular diffusivity (Brokaw, 1969)

Carbon dioxide molar volume	94	cm^3/mol
Ethanol molar volume	168	cm^3/mol
Carbon dioxide critical temperature	304.4	K
Ethanol critical temperature	513.9	K

Parameters are needed to be calculated before the material balances for the bulk and pellet phases described earlier can be used. The material balances are identical for all species within the vapour mixture, in this case ethanol and carbon dioxide. The axial dispersion coefficient is directly proportional to the molecular diffusivity. The molecular diffusivity was calculated using Equation (2). The calculation step to determine parameters Ω_D and σ_{AB}, with A as carbon dioxide and B as ethanol, are:

$$\sigma_A = 0.841 V_c^{1/3}$$
$$\sigma_A = 0.841 (94\ cm^3/mol)^{1/3}$$
$$\sigma_A = 3.824$$

$$\sigma_B = 0.841 V_c^{1/3}$$
$$\sigma_B = 0.841 (168\ cm^3/mol)^{1/3}$$
$$\sigma_B = 4.6405$$

$$\sigma_{AB} = 0.5 \cdot (\sigma_A + \sigma_B)$$
$$\sigma_{AB} = 0.5 \cdot (3.824 + 4.6405)$$
$$\sigma_{AB} = 4.232$$

$$\varepsilon / k_A = 0.75 T_c$$
$$\varepsilon / k_A = 0.75 (304.4\ K)$$
$$\varepsilon / k_A = 228.3$$

$$\varepsilon / k_B = 0.75 T_c$$
$$\varepsilon / k_B = 0.75 (513.9\ K)$$
$$\varepsilon / k_B = 385.425$$

$$\varepsilon / k_{AB} = [(\varepsilon / k_A)(\varepsilon / k_B)]^{1/2}$$
$$\varepsilon / k_{AB} = [(228.3)(385.425)]^{1/2}$$
$$\varepsilon / k_{AB} = 296.635$$

$$T_o = kT / \varepsilon_{AB}$$
$$T_o = (297.15\ K)(296.635\ K)^{-1}$$
$$T_o = 1.002$$

$$\Omega_D = \left(44.54 T_o^{-4.909} + 1.911 T_o^{-1.575}\right)^{0.10}$$
$$\Omega_D = \left(44.54(1.002)^{-4.909} + 1.911(1.002)^{-1.575}\right)^{0.10}$$
$$\Omega_D = 1.467$$

The molecular diffusivity can then be estimated:

$$D_M = \frac{0.001858 T^{1.5}\left[\frac{1}{M_{AB}}\right]^{0.5}}{P\sigma_{AB}^2 \Omega_D}$$

$$D_M = \frac{0.001858(297.15\ K)^{1.5}\left(\frac{1}{44.068\ g/mol}\right)^{0.5}}{(1\ atm)(4.232)^2(1.467)}$$

$$D_M = 0.055\ cm^2/s$$
$$D_M = 5.51\ x10^{-6}\ m^2/s$$

For the pellet phase, the effective diffusivity is needed to determine the pellet phase concentration profiles. The Knudsen diffusion coefficient and effective diffusivity calculations are explained in details in Wakao and Funazkri (1978).

$$D_K = 9700 r_p \sqrt{T / MW_{AB}}$$
$$D_K = 9700(1.75 x10^{-9}\ m)\sqrt{297.15\ K / 44.088\ g/mol}$$
$$D_K = 4.407 x10^{-5}\ m^2/s$$

$$D_e = \frac{\left[\frac{1}{D_M} + \frac{1}{D_K}\right]^{-1}}{\tau}$$

$$D_e = \frac{\left[\frac{1}{0.0000055\ m^2/s} + \frac{1}{0.0000441\ m^2/s}\right]^{-1}}{4}$$

$$D_e = 1.222\ x10^{-6}\ m^2/s$$

The axial dispersion coefficient is now estimated.

Table A2.4 - Parameters to determine the Reynolds number

Carbon dioxide density	1.805	kg/m^3
Carbon dioxide viscosity	$1.5x10^{-5}$	kg/m s
Superficial velocity	0.189	m/s
Particle diameter	1.354	mm

$$\mathrm{Re}_P = \frac{\rho_g v_g D_p}{\mu_g}$$

$$\mathrm{Re}_P = \frac{(1.807\ kg/m^3)(0.189\ m/s)(0.00135\ m)}{1.5x10^{-5}\ kg/ms}$$

$$\mathrm{Re}_P = 30.77$$

$$\mathrm{Re}_D = \frac{\rho_g v_g D_c}{\mu_g}$$

$$\mathrm{Re}_D = \frac{(1.807\ kg/m^3)(0.189\ m/s)(0.00775\ m)}{1.5x10^{-5}\ kg/ms}$$

$$\mathrm{Re}_D = 176.12$$

$$Sc = \frac{\mu_g}{\rho_g D_M}$$

$$Sc = \frac{1.5x10^{-5}\ kg/ms}{(1.807\ kg/m^3)(5.5\ x10^{-6}\ m^2/s)}$$

$$Sc = 1.509$$

$$D_Z = \frac{D_M}{\varepsilon_c}[20 + 0.5(\mathrm{Re}_P)(Sc)]$$

$$D_Z = \frac{5.5x10^{-6}\ m^2/s}{0.35}[20 + 0.5(30.77)(1.509)]$$

$$D_Z = 0.00068\ m^2/s$$

The mass transfer coefficient is now estimated (Wakao and Funazkri, 1978).

$$k_f = \frac{D_M}{D_p}\left[2.0 + 1.1(\mathrm{Re}_P)^{0.6}(Sc)^{0.33}\right]$$

$$k_f = \frac{5.5x10^{-6}\ m^2/s}{0.00135\ m}\left[2.0 + 1.1(30.77)^{0.6}(1.509)^{0.33}\right]$$

$$k_f = 0.04826\ m/s$$

Energy Transfer in Bulk Phase

The bulk and pellet phase energy balance equations requires the overall heat transfer coefficient in order for the solution to be completed. The gas Reynolds number is:

$$\mathrm{Re}_D = \frac{\rho_g v_g D_p}{\mu_g}$$

$$\mathrm{Re}_D = \frac{(1.807\ kg/m^3)(0.189\ m/s)(0.00775\ m)}{1.5x10^{-5}\ kg/ms}$$

$$\mathrm{Re}_D = 176.12$$

$$\nu = \frac{\mu}{\rho}$$

$$\nu = \frac{1.5x10^{-5}\ kg/ms}{1.8072\ kg/m^3}$$

$$\nu = 8.304x10^{-6}\ m^2/s$$

$$\alpha = \frac{k}{\rho c_p}$$

$$\alpha = \frac{0.0146\ W/mK}{(1.8072\ kg/m^3)(887.6\ J/kg\ K)}$$

$$\alpha = 9.1022x10^{-6}\ m^2/s$$

$$\mathrm{Pr} = \frac{\nu}{\alpha}$$

$$\mathrm{Pr} = \frac{8.304x10^{-6}\ m^2/s}{9.1022x10^{-6}\ m^2/s}$$

$$\mathrm{Pr} = 0.9123$$

Under the experimental conditions, the Nusselt number is 4.36. The overall heat transfer coefficient can be calculated (Incropera, at al., 2007).

$$h_{fD} = \frac{k \cdot Nu_D}{D_c}$$

$$h_{fD} = \frac{\left(0.0146\ \frac{W}{mK}\right)\cdot(4.36)}{0.00775\ m}$$

$$h_{fD} = 8.217\ \frac{W}{m^2 K}$$

Heat Losses through the Column Wall

An energy balance across the wall was performed, assuming negligible heat conduction through the wall due to a thin wall thickness. The energy balance was derived earlier as in Equation (20). Using the Rayleigh number, the external Nusselt number and outside heat transfer coefficient can be calculated as follow (Churchill and Chu, 1975; Incropera et al., 2007).

$$Ra_D = \frac{\beta \Delta T g D^3 \Pr}{\nu^2}$$

$$Ra_D = \frac{\left(\frac{1}{298.15}\right)(298.15\,K - 297.15)\left(9.81\frac{m}{s^2}\right)(0.00775\,m)^3(0.9123)}{\nu^2}$$

$$Ra_D = 202.4$$

$$Nu_D = \left\{0.60 + \frac{0.387 Ra_D^{1/6}}{\left[1 + (0.559/\Pr)^{9/16}\right]^{8/27}}\right\}^2$$

$$Nu_D = \left\{0.60 + \frac{0.387(202.4)^{1/6}}{\left[1 + (0.559/(0.9123))^{9/16}\right]^{8/27}}\right\}^2$$

$$Nu_D = 1.401$$

$$h_o = \frac{k \cdot Nu}{D}$$

$$h_o = \frac{\left(0.0146\ \frac{W}{mK}\right) \cdot (1.401)}{(0.00775 + 0.0009)\ m}$$

$$h_o = 2.365 \frac{W}{m^2 K}$$

References

Brokaw, R.S., "Predicting transport properties of dilute gases," Industrial & Engineering Chemistry Process Design and Development, 8 (2), 240 - 253, 1969

Churchill, S. W., Chu, H.H.S., "Correlating equations for laminar and turbulent free convection from a horizontal cylinder," International Journal of Heat and Mass Transfer, 18, 1049, 1975

Incropera, F.P., DeWitt, D.P., Bergman, T.L., Lavine, A.S., "Fundamentals of Heat and Mass Transfer - 6th Edition," John Wiley and Sons, Inc. 2007

Wakao, N., Funazkri, T., "Effect of fluid dispersion coefficients on particle-to-fluid mass transfer coefficients in packed beds: Correlation of Sherwood numbers," Chemical Engineering Science, 33 (10), 1375 – 1384, 1978

Chapter VIII

Appendix 3 – Supplementary Information for Chapter IV

Economic analysis of an ethanol production plant coupled with carbon dioxide stripping and adsorption

Process Description

The separation processes for an ethanol fermentation plant has been modeled using Aspen HYSYS. The base case fermenter model contains six major pieces of equipment; a flash tank, three absorbers, a stripping column and an adsorption unit. The simulation analyzes the separation processes downstream of the fermenter with only a simple simulation of the fermentation process to determine the final concentration of ethanol in the broth. The feed stream for the HYSYS simulation represents the batch fermentation product divided by the time of fermentation. The main components of the feed stream are ethanol, water and carbon dioxide with trace amounts of methanol, 1-propanol, 2-propanol, 1-butanol, 2-methyl-1-butanol, 2-pentanol, and acetic acid. Figure A3.1 shows the process flow sheet for the base case ethanol production plant.

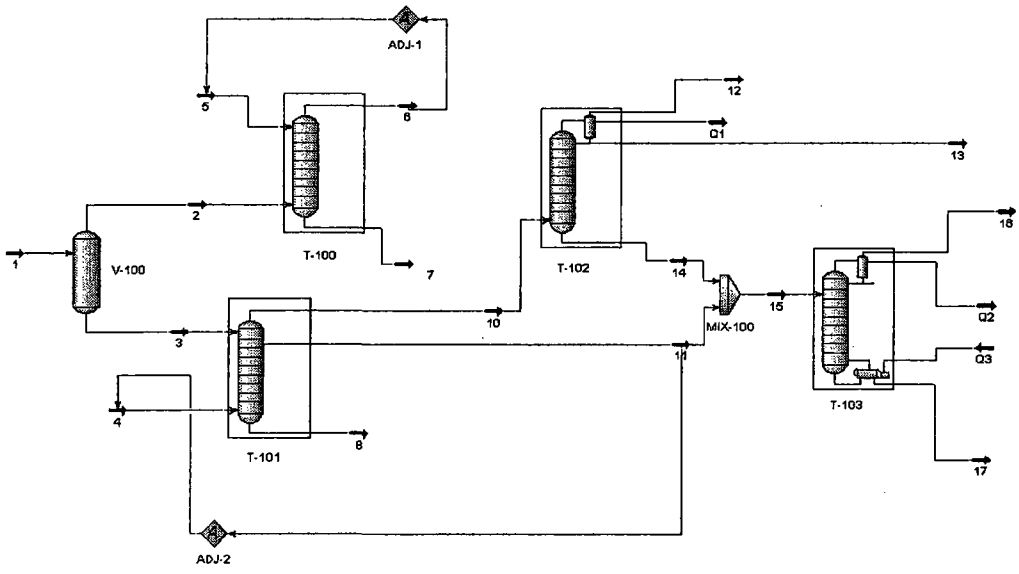

Figure A3.1 – Base Case Ethanol Plant PFD

The base case fermenter model simulates an ethanol fermenter with a final concentration of approximately 4.34% by weight ethanol (46 g/l). There is no gas stripping and therefore any carbon dioxide present was produced from the fermentation. Due to the limitation of HYSYS, the simulation was performed under steady-state which for batch fermentation is not straightforward. Therefore, the productivity of the fermentation broth was determined to be 1.84 g l^{-1} h^{-1} which corresponded to typical

literature values of 2 g l^{-1} h^{-1} (Taylor et al., 1997). A total fermentation time of 25 hours was assumed based on literature showing similar behaviour (Martini et al., 2006).

The base case fermentation model using HYSYS simulates the separation systems needed to convert the fermentation broth product to fuel grade ethanol (Aspen Technology, 2005). Stream 1 represents the fermentation broth final concentration of 4.34% ethanol by weight (46 g/l). Table A3.1 shows the key parameters associated with Stream 1.

Table A3.1 - Stream conditions for Stream 1

Steam Number	1	-
Vapour Fraction	0.0184	-
Temperature	30.0	°C
Pressure	101.3	kPa
Molar Flow rate	541	kmole/h
Mass Flow rate	10 280	kg/h
Composition		
Ethanol	1.79×10^{-2}	mole fraction
Water	9.64×10^{-1}	mole fraction
Carbon Dioxide	1.80×10^{-2}	mole fraction
Methanol	2.69×10^{-5}	mole fraction
Acetic Acid	3.33×10^{-6}	mole fraction
1-Propanol	9.08×10^{-6}	mole fraction
2-Propanol	9.1×10^{-6}	mole fraction
1-Butanol	6.58×10^{-6}	mole fraction
2-Methyl-1-Butanol	2.15×10^{-5}	mole fraction
2-Pentanol	5.25×10^{-6}	mole fraction
Glycerol	6.64×10^{-6}	mole fraction

Stream 1 is a two-phase fluid and is flashed using a two-phase separator (V-100) producing a vapour (Stream 2) and liquid (Stream 3) stream.

Stream 2 contains ethanol in the vapour phase mostly comprised of carbon dioxide and needs to be recovered. A water scrubber has been modeled using an

absorption unit (T-100) with Stream 5 representing the process water needed to absorb the ethanol vapour. The amount of water needed was adjusted within HYSYS to an amount that would ensure no more than 0.5 kg/h of ethanol was lost in the vapour phase which represents a 95% recovery in the absorption unit. The scrubbed ethanol stream, represented by Stream 7, is recycled back as fermentation broth product, i.e. added to stream 1. The column was assumed to operate under atmospheric conditions with 10 theoretical trays. All four stream inlet and outlet conditions are shown in Table A3.2.

Table A3.2 - Stream conditions for unit T-100

Steam Number (-)	5	2	6	7
Vapour Fraction (-)	0	1	1	0
Temperature (°C)	25.0	30.0	30.8	30.8
Pressure (kPa)	101.3	101.3	101.3	101.3
Molar Flow rate (kgmole/h)	7.80	9.95	9.86	7.89
Mass Flow rate (kg/h)	140.5	427.5	422.6	145.3
Composition (mol fraction)				
Ethanol	0.00	1.20×10^{-2}	1.1×10^{-3}	1.38×10^{-2}
Water	1.00	4.12×10^{-2}	4.37×10^{-2}	9.86×10^{-1}
Carbon Dioxide	0.00	9.43×10^{-1}	9.55×10^{-1}	4.78×10^{-4}
Methanol	0.00	1.27×10^{-5}	6.64×10^{-9}	9.85×10^{-6}
Acetic Acid	0.00	2.10×10^{-7}	0.00	1.63×10^{-7}
1-Propanol	0.00	9.49×10^{-6}	2.91×10^{-6}	5.16×10^{-6}
2-Propanol	0.00	8.90×10^{-6}	1.53×10^{-6}	5.75×10^{-6}
1-Butanol	0.00	5.76×10^{-6}	2.19×10^{-6}	2.81×10^{-6}
2-Methyl-1-Butanol	0.00	8.14×10^{-6}	1.24×10^{-7}	6.24×10^{-6}
2-Pentanol	0.00	6.05×10^{-6}	2.72×10^{-6}	2.62×10^{-6}
Glycerol	0.00	0.00	0.00	0.00

Stream 3 exits the phase separator (V-100) and enters the beer column (T-101) where steam (Stream 6) is is used to further purify the product. The beer column is represented by a stripping column that contains two draws represented by Streams 10 and 11. Stream 10 exits to a reflux absorber while Stream 11 enters directly the distillation

column. The liquid phase draw of the beer column mainly contains heavy hydrocarbons and water. The column was assumed to operate under atmospheric conditions with 10 theoretical trays. All five stream inlet and outlet conditions are shown in the Table A3.3.

Table A3.3 - Stream conditions for unit T-101

Steam Number (-)	3	4	10	11	8
Vapour Fraction (-)	0	1	1	1	0
Temperature (°C)	30.0	140.0	86.2	94.8	100.3
Pressure (kPa)	101.3	101.3	101.3	101.6	102.3
Molar Flow rate (kgmole/h)	531.4	114.8	1.8	47.75	596.7
Mass Flow rate (kg/h)	9 852	2 068	52.5	1 117	10 750
Composition (mol fraction)					
Ethanol	0.02	0.00	2.69×10^{-1}	1.90×10^{-1}	0.00
Water	0.98	1.00	5.73×10^{-1}	8.09×10^{-1}	1.00
Carbon Dioxide	0.00	0.00	1.55×10^{-1}	0.00	0.00
Methanol	0.00	0.00	1.61×10^{-4}	2.06×10^{-4}	0.00
Acetic Acid	0.00	0.00	1.97×10^{-6}	3.28×10^{-6}	0.00
1-Propanol	0.00	0.00	3.21×10^{-4}	5.99×10^{-5}	0.00
2-Propanol	0.00	0.00	3.12×10^{-4}	6.06×10^{-5}	0.00
1-Butanol	0.00	0.00	1.50×10^{-4}	4.62×10^{-5}	0.00
2-Methyl-1-Butanol	0.00	0.00	1.26×10^{-4}	1.64×10^{-4}	0.00
2-Pentanol	0.00	0.00	2.51×10^{-4}	3.22×10^{-5}	0.00
Glycerol	0.00	0.00	0.00	0.00	0.00

Stream 10 contains ethanol among light hydrocarbons. The reflux absorber removes the light hydrocarbons as a vapour (Stream 11) with a liquid and vapour side draw. The side draw (Stream 13) and liquid stream (Stream 14) contains the desired ethanol product with Stream 14 entering the distillation column for further purification. The column was assumed to operate under atmospheric conditions with 10 theoretical trays. The absorber contains a reflux condenser and therefore additional operating parameters are required for convergence. The two specifications were a draw rate of 0.7 kmole/h and an ethanol mass fraction of 0.88 in the liquid phase. These specifications

were set in accordance to a HYSYS ethanol production plant model used as a basis from literature provided by Aspen. All four stream inlet and outlet conditions are shown in Table A3.4.

Table A3.4 - Stream conditions for unit T-102

Steam Number (-)	10	12	13	14
Vapour Fraction (-)	1	1	0	0
Temperature (°C)	86.2	51.9	51.9	80.3
Pressure (kPa)	101.3	101.3	101.3	101.3
Molar Flow rate (kgmole/h)	1.8	0.4	0.3	1.1
Mass Flow rate (kg/h)	52.5	17.1	12.0	23.4
Composition (mol fraction)				
Ethanol	2.69×10^{-1}	2.48×10^{-1}	7.48×10^{-1}	1.39×10^{-1}
Water	5.73×10^{-1}	6.69×10^{-2}	2.48×10^{-1}	8.58×10^{-1}
Carbon Dioxide	1.55×10^{-1}	6.85×10^{-1}	7.66×10^{-4}	4.27×10^{-5}
Methanol	0.00	1.33×10^{-4}	3.53×10^{-4}	7.80×10^{-5}
Acetic Acid	0.00	0.00	1.93×10^{-8}	3.44×10^{-6}
1-Propanol	6.00×10^{-4}	6.09×10^{-5}	5.88×10^{-4}	2.66×10^{-4}
2-Propanol	5.09×10^{-4}	1.55×10^{-4}	8.12×10^{-4}	1.17×10^{-4}
1-Butanol	4.02×10^{-4}	5.95×10^{-7}	1.71×10^{-5}	2.54×10^{-4}
2-Methyl-1-Butanol	2.13×10^{-4}	6.78×10^{-9}	4.54×10^{-7}	2.21×10^{-4}
2-Pentanol	6.25×10^{-4}	2.29×10^{-6}	6.33×10^{-5}	4.08×10^{-4}
Glycerol	0.00	0.00	0.00	0.00

Streams 11 and 14 enter the distillation column where it is desired to increase the ethanol concentration from 39 to approximately 85 wt%. A mass fraction of 0.85 was selected as the ethanol final concentration because of the significant increase in energy load as the azeotrope is approached. The azeotrope occurs at an ethanol mass fraction 0.956. To resolve the two degrees of freedom associated with the distillation column, a reflux ratio of 5 and a distillate ethanol purity of 85 wt% were used. The inlet and outlet conditions of the three stream are presented in Table A3.5.

Table A3.5 - Stream conditions for unit T-103

Steam Number (-)	15	16	17
Vapour Fraction (-)	0.978	1	0
Temperature (°C)	94.6	79.6	100.0
Pressure (kPa)	101.3	101.3	101.3
Molar Flow rate (kgmole/h)	48.8	13.6	35.2
Mass Flow rate (kg/h)	1 140	506	634
Composition (mol fraction)			
Ethanol	1.89×10^{-1}	6.77×10^{-1}	0.00
Water	8.10×10^{-1}	3.20×10^{-1}	1.00
Carbon Dioxide	0.00	2.79×10^{-6}	0.00
Methanol	3.06×10^{-4}	7.05×10^{-4}	0.00
Acetic Acid	3.28×10^{-6}	2.78×10^{-7}	0.00
1-Propanol	5.99×10^{-5}	2.21×10^{-4}	0.00
2-Propanol	6.06×10^{-5}	2.14×10^{-4}	0.00
1-Butanol	4.62×10^{-5}	1.74×10^{-4}	0.00
2-Methyl-1-Butanol	1.64×10^{-4}	5.74×10^{-4}	0.00
2-Pentanol	3.22×10^{-5}	1.36×10^{-4}	0.00
Glycerol	0.00	0.00	0.00

Equipment Sizing

The base case fermentation model contains five major units: three absorption units, a distillation column and a phase separator. This section presents the design equations and assumptions as well as the sample calculations showing the calculation steps taken throughout the analysis.

V-100

The fermentation tanks were modeled using an Excel macro. For the base case fermentation model, a volume of 9.755 m^3 was determined. Using an L/D ratio of three, the diameter for the fermentation tank can be determined.

$$\frac{L}{D} = 3$$

$$V = \pi r^2 L$$

$$V = \frac{\pi D^2 (3D)}{4}$$

$$D = \left[\frac{4V}{3\pi}\right]^{1/3}$$

$$D = \left[\frac{4(9.755\ m^3)}{3\pi}\right]^{1/3}$$

$$D = 1.70\ m$$

The height of the vessel is then determined:

$$L = 3D$$

$$L = 3(1.70\ m)$$

$$L = 5.10\ m$$

T-100

The next equipment unit is the water scrubber. The vapour outlet from the phase separator V-100 (Stream 2) contains mainly carbon dioxide with some ethanol and water due to equilibrium with the liquid phase. It is desired to lose as little ethanol as possible such that an absorber (T-100) was used to recover the entrained ethanol within the vapour mixture. Water was used as the stripping fluid. It was assumed that the absorber is packed using 51-mm Ceramic Intalox saddles with physical characteristics shown in Table A3.6. Some of the benefits of using this type of packing are for stability and low cost due to the simple geometry of the packing (ISA 9001, 2000).

Table A3.6 - Absorber packing physical characteristics

Packing Type	Ceramic Intalox saddles	51 mm
Packing Density	609	kg/m^3
Specific area	108	m^2/m^3
F_p	130	1/m

With the type of packing being known, Figure A3.2 can be used to determine the diameter of the column using the flow characteristics of the stripping fluid and vapour stream.

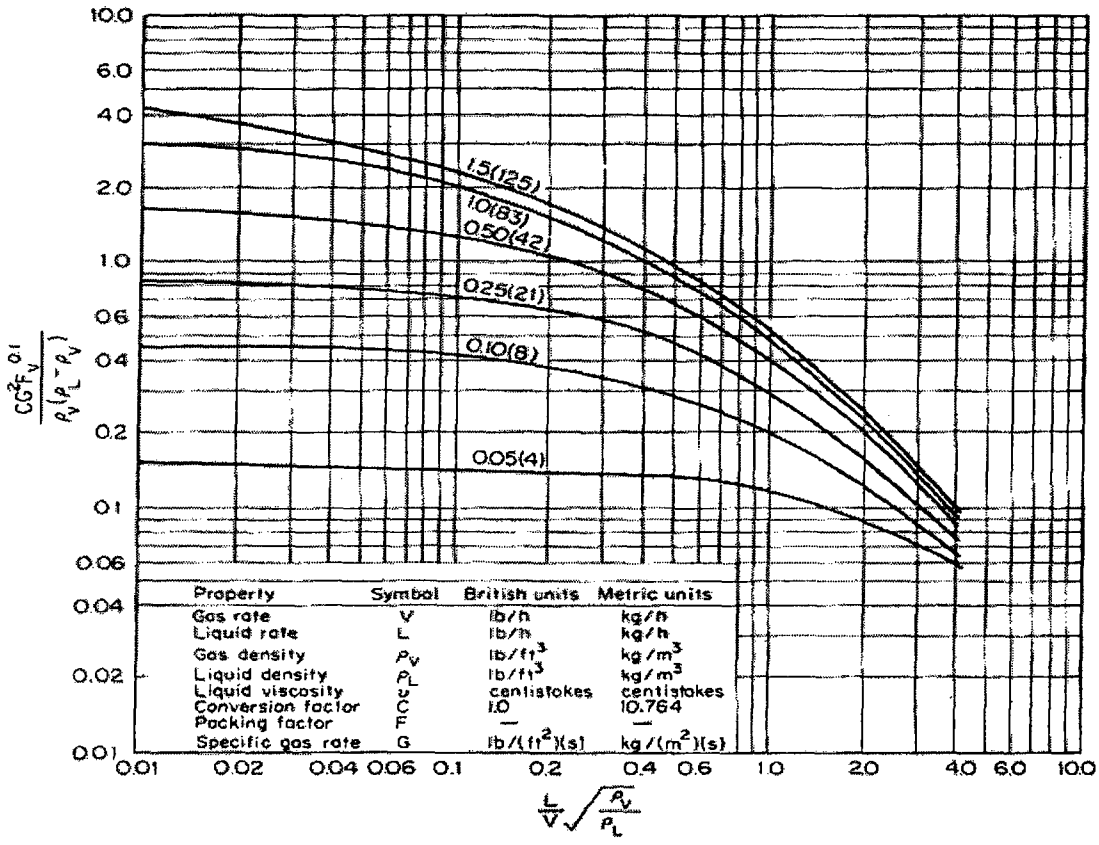

Figure A3.2 – Gas rate correlation graph derived from the Sherwood equation (Cheresource, 2008)

The following equations can be used to determine the specific gas flow rate where the following equations represent the x-axis and y-axis from Figure A3.2, respectively. Note that the value for K_4 was obtained from Figure A3.2.

$$F_{LV} = \left[\frac{L}{V}\right]\sqrt{\frac{\rho_V}{\rho_L}}$$

$$F_{LV} = \left[\frac{140.5\ kg/h}{427.5\ kg/h}\right]\sqrt{\frac{1.727\ kg/m^3}{1007\ kg/m^3}}$$

$$F_{LV} = 0.014$$

$$K_4 = \frac{10.764 G^2 F_P \mu_L{}^{0.1}}{\rho_V(\rho_L - \rho_V)}$$

$$K_4 = 1.6\ (from\ Figure\ 2)$$

$$G = \frac{K_4 \rho_V(\rho_L - \rho_V)}{10.764 F_P \mu_L{}^{0.1}}$$

$$G = \frac{(1.6)(1.727\ kg/m^3)(1007\ kg/m^3 - 1.727\ kg/m^3)}{10.764\left(130\frac{1}{m}\right)(0.884\ cSt)^{0.1}}$$

$$G = 1.417\ \frac{kg}{m^2 s}$$

$$A = \frac{V}{G}$$

$$A = \frac{427.5\ \frac{kg}{h} \cdot \frac{1\ h}{3600\ s}}{1.417\ \frac{kg}{m^2 s}}$$

$$A = 0.084\ m^2$$

$$A = \frac{\pi D^2}{4}$$

$$D = \left(\frac{4A}{\pi}\right)^{1/2}$$

$$D = \left(\frac{4(0.083\ m^2)}{\pi}\right)^{1/2}$$

$$D = 0.327\ m$$

$$SH = 0.5D^{0.3}$$

$$SH = 0.5(0.327\ m)^{0.3}$$

$$SH = 0.357\ m/stage$$

$$H = 3.57\ m$$

T-101

The purification tower T-101 removes most of the methanol from the fermentation broth and is modeled as a stripping column with a side vapour draw. This column acts as the beer column used to further purify the ethanol product.

T-102

A purification tower T-102 is downstream of both T-100 and T-101 absorbers and is modeled as a refluxed absorber with a condenser unit. The main purpose is to recover any ethanol vapour before entering the distillation column, T-103. The design calculations to size absorbers T-101 and T-102 follow the same steps as for T-100.

T-103

A rectifier was used within the ethanol plant simulation to purify the final product to 85 wt%. The rectifier, T-103, was modeled as a simple bubble-cap distillation column with a condenser and a reboiler.

The following calculations were done to estimate the diameter and height of the column needed to perform the desired separation. Figure A3.3 shows the relation between parameters C_{sb} and F_{LV}.

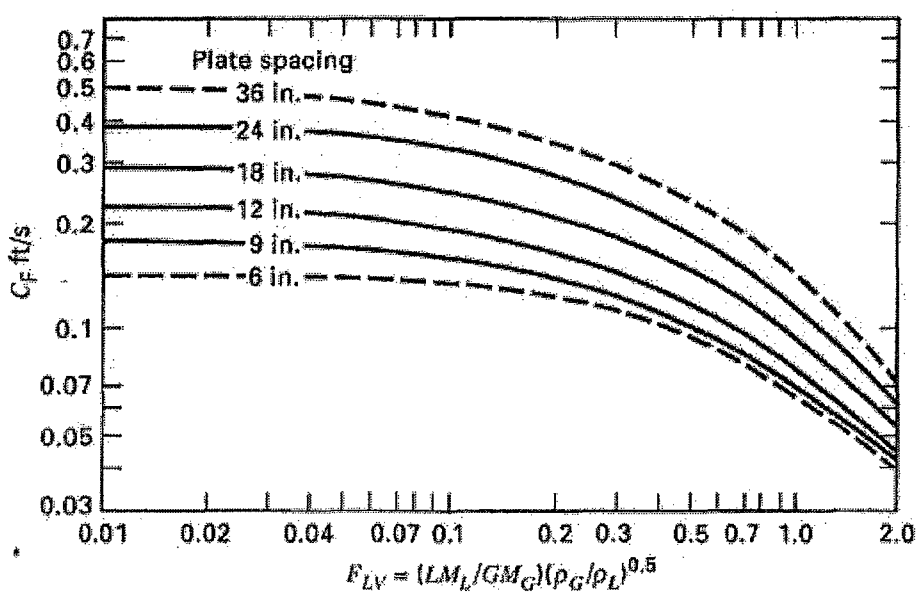

Figure A3.3 – C_F versus F_{LV} graph assuming a spacing of 24 inches (Tremaine and Stewart, 2005).

The value of factor F_{LV} is determined using the liquid and vapour flow rates through the reboiler. Figure A3.3 is used to determine C_F using F_{LV} and the plate spacing. In this simulation, the plate spacing was assumed to be 61 cm (24 inches).

Assuming there is some foaming in the process, a foaming factor of 0.9 was assumed. Since bubble-cap trays are used, the hole-area factor (F_{HA}) is equal to 1. The surface tension factor is calculated using the following equation.

$$F_{ST} = \left(\frac{\sigma_L}{20}\right)^{0.2}$$

$$F_{ST} = \left(\frac{58.61\ dynes/cm}{20}\right)^{0.2}$$

$$F_{ST} = 1.24$$

With the surface tension factor, and a few assumptions, including assuming 5 man-ways (α) each 0.3 m (β) in height and a friction factor of 0.8, the diameter and height of the rectifier column can be determined. Note that the equation used to calculate the height of the rectifier tower can be used only when the diameter is greater than 0.5 m, which is valid for the current rectifier tower.

$$\frac{A_d}{A_T} = 0.1 \quad when \quad F_{LV} \leq 0.1$$

$$F_{HA} = 1 \ for\ bubble\ trays$$

$$U_f = C_{sb} F_{ST} F_F F_{HA} \sqrt{\frac{\rho_L - \rho_G}{\rho_G}}$$

$$U_f = (0.1188\ m/s)(1.24)(0.8)(1)\sqrt{\frac{948\ kg/m^3 - 0.588\ kg/m^3}{0.588\ kg/m^3}}$$

$$U_f = 0.591\ m/s$$

$$D_T = \sqrt{\frac{4G}{(fU_f)\pi(1-\frac{A_d}{A_T})\rho_G}}$$

$$D_T = \sqrt{\frac{4(590\ kg/h)\cdot\frac{1\ h}{3600\ s}}{(0.8\cdot 0.591\ m/s)\pi(1-0.1)(0.588\ kg/m^3)}}$$

$$D_T = 0.913\ m$$

$$H_P = 0.5D^{0.3}\cdot(\#\ stages)$$

$$H_P = 0.5(2.388\ m)^{0.3}\cdot 29\ stages$$

$$H_P = 18.826\ m$$

$$H_C = H_P + (\alpha\beta)$$

$$H_C = 18.826m + (5\cdot 0.3m)$$

$$H_C = 20.326\ m$$

General Heat Exchanger Calculations

Within the ethanol plant, there are three heat exchangers: condenser for T-102, condenser for T-103 and reboiler for T-103. HYSYS provides an estimate of the overall heat transfer coefficient multiplied with the area. From literature, the corresponding overall heat transfer coefficients can be estimated depending on the nature of the fluid on the tube and shell sides. Then, the area of the heat exchangers can be calculated. Using the heat exchanger from the distillation column (the reboiler), the calculations are shown below:

$$A = \frac{UA}{U}$$

$$A = \frac{41300\ \frac{kJ}{^oC\,h}\cdot\frac{1000\ J}{1\ kJ}\cdot\frac{1\ h}{3600\ s}}{1140\ \frac{J}{m^2\ s\ ^oC}}$$

$$A = 10.06\ m^2$$

Fermenter Model using Carbon Dioxide Stripping

Carbon dioxide gas stripping has two main benefits: carbon dioxide is a by-product of fermentation and ethanol stripped lessens the effect of ethanol inhibition. In

1996, Taylor et al. incorporated carbon dioxide stripping within a pilot scale fermentation process and obtained an ethanol productivity of 15.8 g l^{-1} h^{-1} at a certain carbon dioxide flow rate while typical fermenter plants have productivities in the vicinity of 2.0 g l^{-1} h^{-1}. Table A3.7 lists the main pieces of equipment for the base case fermentation model and the alternative processes.

Table A3.7 - Equipment summary for three ethanol production plant cases

Simulation	Identification	Unit Name	Description
Base Case	V-100	Phase separator	Flash the carbon dioxide from fermentation broth
	T-100	Absorption Scrubber	Capture the vapour phase ethanol using water to scrub from vapour mixture
	T-101	Beer Column	Addition of steam to further purify fermentation outlet
	T-102	Lights Column	Remove light hydrocarbons from ethanol stream
	T-103	Distillation Column	Ethanol dehydration to remove water up to 85 wt% ethanol levels
	T-104	Adsorption Column	Ethanol dehydration unit to produce fuel grade ethanol
Alternatives using CO_2 stripping and adsorption	V-101	Adsorption Column	Replaces absorption scrubber with an adsorption unit
	E-101	TSA Heat Exchanger	Used to increase temperature of purge gas to desired conditions

Since Aspen HYSYS was used as the simulation software, there are some limitations. HYSYS is predominantly a steady-state simulator such that the following assumptions were made to compare the different scenarios.

Assumptions for Fermenter Models

1. Fermenters operate in batch mode. To adapt the fermentation data for a separation train that operates under steady-state, an average flow rate of liquid broth was calculated to represent one batch of ethanol production. The volume of the fermentation broth for the base cases was 9 755 L whereas it was 7 504 L the ethanol process with gas stripping and adsorption.
2. Each ethanol production plant consists of 3 fermenters and ordered in a way that for every 25 hour interval: a fermenter is being cleaned and prepared for

new batch, a fermenter having sugars converted into ethanol and a fermenter having the liquid ethanol concentration of 4.32 wt% leaving the fermentation tank and towards the separation units downstream of the fermenter. Having this system produces a continuous process for ethanol production.

3. A fermentation total time of 25 h with gas stripping starting after 4 h until the fermentation is completed. The carbon dioxide flow rate was varied once 46 g/l of ethanol was reached.
4. Initial carbon dioxide stripping flow rate of 450 m^3/h (vvm = 1.0 L $min^{-1}L^{-1}$) was utilized. As glucose depletes, less ethanol is produced and the amount of carbon dioxide decreased accordingly.
5. An Excel Macro was used to determine the outlet composition of the stripping gas and the resulting composition of the fermentation broth.

Comparison Study Structure

The addition of carbon dioxide stripping and adsorption to an ethanol production process can be compared with the base case to quantify the benefits of this new technology. Two cases incorporating gas stripping/adsorption units were analyzed: a new plant (Alternative 1) and incorporating the new technology to a pre-existing ethanol production plant (Alternative 2). For each alternative, a TSA and VSA process was simulated and compared on how well ethanol was recovered from the stripping gas.

Desorption Techniques

The proposed adsorption process needs an effective desorption system to efficiently recover the ethanol from the adsorbed phase. A technique that is economically feasible as well as resulting to high the ethanol purity. Two desorption techniques were analyzed within the study: temperature swing adsorption (TSA) and vacuum swing adsorption (VSA).

Economic Analysis

An economic analysis was performed to compare the performance of the TSA and the VSA adsorption system combined with carbon dioxide stripping with a base case ethanol production process assuming a plant life of 25 years and a yearly production rate of 1 000 000 litres of fuel-grade ethanol produced. All costs were corrected from 1996 cost values to 2009 values. The materials of construction for all scenarios were stainless steel due to the corrosive nature of ethanol. Carbon steel was used to calculate the bare module cost and therefore determine the grass roots cost.

Capital Cost

The analysis of the capital cost was broken up into three main categories: vessels, towers, and heat exchangers. Sample calculations for the capital cost of these pieces of equipment are shown below. All calculations were done for the base case model with the calculation steps given in Turton et al. (2006).

Vessel – V-100

A vessel was used to represent the fermentation tank. For the base case, the volume calculated was 9.755 m^3. The purchased cost of the phase separator (C_P) can be calculated using the following correlation. The K_1, K_2, and K_3 terms are specific to the type of equipment with the following parameters used for vessels.

$$\log_{10} C_P = K_1 + K_2 \log_{10} V + K_3 (\log_{10} V)^2$$

$$\log_{10} C_P = 3.4974 + 0.4485 \log_{10}(9.755\ m^3) + 0.1074 (\log_{10}(9.755\ m^3))^2$$

$$C_P = \$12\,398$$

The next step is to take into account effects of the operating pressure and the material of construction. The pressure factor (F_M) for a vessel is determined using the following correlation where operation under atmospheric conditions (0 barg) is assumed. If the pressure factor is below one, F_P is set to one.

$$F_P = \frac{\frac{(P+1)D}{2[850-0.6(P+1)]} + 0.00315}{0.0063}$$

$$F_P = \frac{\frac{(0\,barg+1)(1.7\,m)}{2[850-0.6(0\,barg+1)]} + 0.00315}{0.0063}$$

$$F_P = 0.6588 < 1$$

$$F_P = 1$$

There are two material factors (F_M) needed, for stainless steel and for carbon steel. Since ethanol is present throughout the process, stainless steel is used. The carbon steel material factor is used to calculate the grass roots total cost.

$$F_M = 1$$

$$F_M^0 = 3.1$$

The bare module costs using the two material factors are shown below with the first calculation using stainless steel followed by the carbon steel calculation. Again, the carbon steel calculations are only used to determine the bare module cost, the actual materials of construction is stainless steel.

$$C_{BM}^0 = C_P F_{BM}^0$$

$$C_{BM}^0 = C_P\left(B_1 + B_2 F_M^0 F_P\right)$$

$$C_{BM}^0 = \$12\ 398(2.25 + (1.82)(3.1)(1))$$

$$C_{BM}^0 = \$97\ 846$$

$$C_{BM} = C_P F_{BM}$$

$$C_{BM} = C_P\left(B_1 + B_2 F_M F_P\right)$$

$$C_{BM} = \$12\ 398(2.25 + (1.82)(1)(1))$$

$$C_{BM} = \$50\ 460$$

The total module cost represents the cost of making small-to-moderate expansions or alterations to an existing facility and can be calculated using the bare module cost using stainless steel shown below.

$$C_{TM} = 1.18 C_{BM}^0$$

$$C_{TM} = 1.18(\$97\ 846)$$

$$C_{TM} = \$115\ 458$$

The grass roots cost represents a completely new facility in which construction is done essentially on undeveloped land and can be calculated using the bare module cost using carbon steel and the total module cost shown below.

$$C_{GR} = C_{TM} + 0.5(C_{BM})$$
$$C_{GR} = \$115\ 458 + 0.5(\$50\ 460)$$
$$C_{GR} = \$140\ 688$$

Correcting the 1996 (CEPCI = 382) values for 2009 (CEPCI = 539.6) values, the grass roots cost grows to $198 731.

Towers – T-101

Towers were used as absorption and distillation columns. The calculations, although similar to the calculations steps to cost a vessel, have some differences. The sample calculations were done for the base case tower T-101. Similar to the vessel calculations, the cost depends on the volume of the tower.

$$V = \pi \frac{D^2}{4} L$$
$$V = \pi \frac{(0.327\ m)^2}{4} (5.07\ m)$$
$$V = 0.425\ m^3$$

The purchased cost of the tower (C_P), with appropriate values of K_1, K_2, and K_3, is calculated as follows.

$$\log_{10} C_P = K_1 + K_2 \log_{10} V + K_3 (\log_{10} V)^2$$
$$\log_{10} C_P = 3.4974 + 0.4485 \log_{10}(0.425\ m^3) + 0.1074(\log_{10}(0.425\ m^3))^2$$
$$C_P = \$2216$$

The next step is to take into account effects of pressure and material of construction. The pressure factor (F_M) for a vessel is determined using the following correlation where atmospheric conditions (0 barg) were assumed. For a tower, a pressure factor of one prevails for pressures below 5 barg.

The material factors (F_M) for stainless steel and for carbon steel are shown as follows.

$$F_P = 1$$
$$F_{BM} = 1$$
$$F_{BM}^0 = 1.8$$

For towers, the numbers of trays must be taken into account in the cost calculation. Factor F_q takes into account the number of trays.

$$\log_{10} F_q = 0.4771 + 0.08516 \log_{10} N - 0.3473 (\log_{10} N)^2$$
$$\log_{10} F_q = 0.4771 + 0.08516 \log_{10}(10\ stages) - 0.3473 (\log_{10}(10\ stages))^2$$
$$\log_{10} F_q = 0.215$$
$$F_q = 1.64$$

The equation for the bare module cost for a tower is shown below. The bare module cost using the two material factors are shown below for stainless steel and carbon steel, respectively.

$$C_{BM}^0 = C_P N F_{BM}^0 F_q$$
$$C_{BM}^0 = \$2\ 216(10\ stages)(1.8)(1.64)$$
$$C_{BM}^0 = \$65\ 435$$

$$C_{BM} = C_P N F_{BM} F_q$$
$$C_{BM} = \$2\ 216(10\ stages)(1)(1.14)$$
$$C_{BM} = \$36\ 353$$

The total module cost represents the cost of making small-to-moderate expansions or alterations to an existing facility and can be calculated using the bare module cost using stainless steel shown below.

$$C_{TM} = 1.18 C_{BM}^0$$
$$C_{TM} = 1.18(\$65\ 435)$$
$$C_{TM} = \$77\ 213$$

The grass roots cost represents a completely new facility in which construction is done essentially on undeveloped land and can be calculated using the bare module cost using carbon steel and the total module cost shown below.

$$C_{GR} = C_{TM} + 0.5(C_{BM})$$
$$C_{GR} = \$77\ 213 + 0.5(\$36\ 353)$$
$$C_{GR} = \$95\ 390$$

Correcting the 1996 (CEPCI = 382) values for 2009 (CEPCI = 539.6) values, the grass roots cost grows to $134 744.

Heat Exchangers - Reboiler

The third main piece of equipment to be costed is the heat exchanger. The following analysis was done using the design conditions from the base case reboiler used in the distillation column T-103.

The heat transfer area is needed to cost the heat exchanger. Based on the design calculations, the base case distillation column reboiler area is equal to 10.06 m^2.

The purchased cost of the heat exchanger (C_P), with appropriate values of K_1, K_2, and K_3, is:

$$\log_{10} C_P = K_1 + K_2 \log_{10} A + K_3 (\log_{10} A)^2$$
$$\log_{10} C_P = 4.8306 - 0.8509 \log_{10}(10.06\ m^2) + 0.3187(\log_{10}(10.06\ m^2))^2$$
$$C_P = \$19\,853$$

The next step is to take into account effects of pressure and material of construction. The pressure factor (F_M) is unity since pressures below 5 barg are used. Material factors (F_M) for stainless steel and for carbon steel are required.

$$F_P = 1$$
$$F_M = 1$$
$$F_M^0 = 3$$

The bare module cost for the two material factors for stainless steel and carbon steel are:

$$C_{BM}^0 = C_P F_{BM}^0$$
$$C_{BM}^0 = C_P (B_1 + B_2 F_M^0 F_P)$$
$$C_{BM}^0 = \$19\,853(1.63 + (1.66)(3)(1))$$
$$C_{BM}^0 = \$131\ 232$$

$$C_{BM} = C_P F_{BM}$$
$$C_{BM} = C_P (B_1 + B_2 F_M F_P)$$
$$C_{BM} = \$19\,853(1.63 + (1.66)(1)(1))$$
$$C_{BM} = \$65\,318$$

The total module cost represents the cost of making small-to-moderate expansions or alterations to an existing facility and can be calculated using the bare module cost using stainless steel shown below.

$$C_{TM} = 1.18 C_{BM}^{0}$$
$$C_{TM} = 1.18(\$131\,232)$$
$$C_{TM} = \$154\,854$$

The grass roots cost represents a completely new facility in which construction is done essentially on undeveloped land and can be calculated using the bare module cost using carbon steel and the total module cost shown below.

$$C_{GR} = C_{TM} + 0.5(C_{BM})$$
$$C_{GR} = \$154\,85 + 0.5(\$65\,318)$$
$$C_{GR} = \$187\,513$$

Correcting the 1996 (CEPCI = 382) values for 2009 (CEPCI = 539.6) values, the grass roots cost grows to $264 875.

Compressor – VSA Blower

The VSA process requires a blower to introduce a vacuum for the desorption process. The following analysis was done using the design conditions from the VSA blower used during the adsorption process.

The power requirement (in kW) is needed to cost the blower. Based on the design calculations, running a vacuum for the VSA process from 1 atmosphere to 0.5 atmospheres requires 28 kW.

The purchased cost of the blower (C_P), with appropriate values of K_1, K_2, and K_3, is:

$$\log_{10} C_P = K_1 + K_2 \log_{10} A + K_3 (\log_{10} A)^2$$
$$\log_{10} C_P = 5.0355 - 1.8002 \log_{10}(28\ kW) + 0.8253(\log_{10}(28\ kW))^2$$
$$C_P = \$14\,412$$

The next step is to take into account effects of pressure and material of construction. The pressure factor (F_M) is unity since pressures below 5 barg are used. Material factors (F_M) for stainless steel and for carbon steel are required for the blower.

$$F_P = 1$$
$$F_M = 3.4$$
$$F_M^0 = 7$$

The bare module cost for the two material factors for stainless steel and carbon steel are:

$$C_{BM}^0 = C_P F_M^0$$
$$C_{BM}^0 = \$14\ 412(7)$$
$$C_{BM}^0 = \$100\ 884$$

$$C_{BM} = C_P F_M$$
$$C_{BM} = \$14\ 412(3.4)$$
$$C_{BM} = \$49\ 001$$

The total module cost represents the cost of making small-to-moderate expansions or alterations to an existing facility and can be calculated using the bare module cost using stainless steel shown below.

$$C_{TM} = 1.18 C_{BM}^0$$
$$C_{TM} = 1.18(\$100\ 884)$$
$$C_{TM} = \$119\ 043$$

The grass roots cost represents a completely new facility in which construction is done essentially on undeveloped land and can be calculated using the bare module cost using carbon steel and the total module cost shown below.

$$C_{GR} = C_{TM} + 0.5(C_{BM})$$
$$C_{GR} = \$119\ 043 + 0.5(\$49\ 001)$$
$$C_{GR} = \$143\ 544$$

Correcting the 1996 (CEPCI = 382) values for 2009 (CEPCI = 539.6) values, the grass roots cost grows to $202 765.

Operating Costs

The operating costs were taken from HYSYS in the form of utility loads. The main loads came from steam, process water and electricity needed for the PSA alternative fermentation model. For the process water and steam, the cost was based on a dollar per kilogram basis at 0.0000148 $/kg and 0.01622 $/kg, respectively.

Comparison Study Results

Along with a base case fermentation ethanol production plant model, two alternatives were analyzed. The first alternative introduces carbon dioxide as a stripping gas to remove ethanol and a TSA system used to capture the ethanol from the vapour phase. The second alternative is similar to the first except that a VSA system is used to capture the ethanol vapour as opposed to a TSA operation. Using the capital cost and operating costs determined earlier and a predicted plant lifetime of 25 years for comparisons, Figure A3.4 compares the base case with a TSA system with purge gas temperatures of 80, 100, and 120°C while Figure A3.5 compares the base case with a VSA system with desorption pressures of 0.5, 0.2, and 0.1 atm.

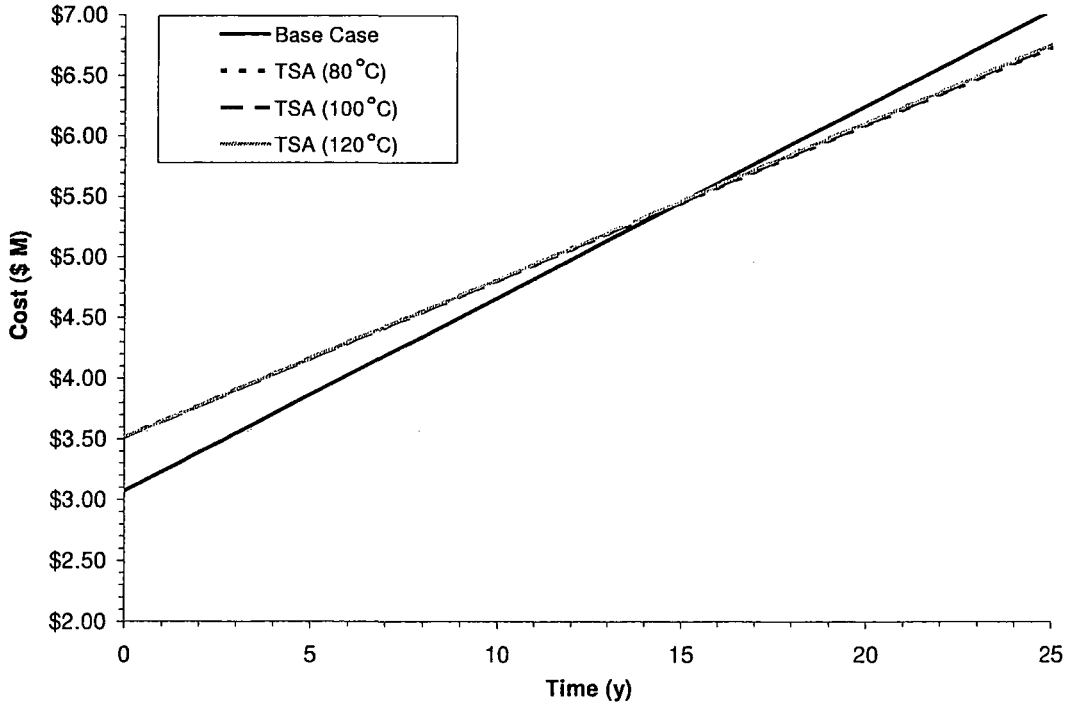

Figure A3.4 - Cost as a function of time comparison between a base case fermentation model with a model introducing CO_2 stripping and a TSA system at 80, 100, and 120°C

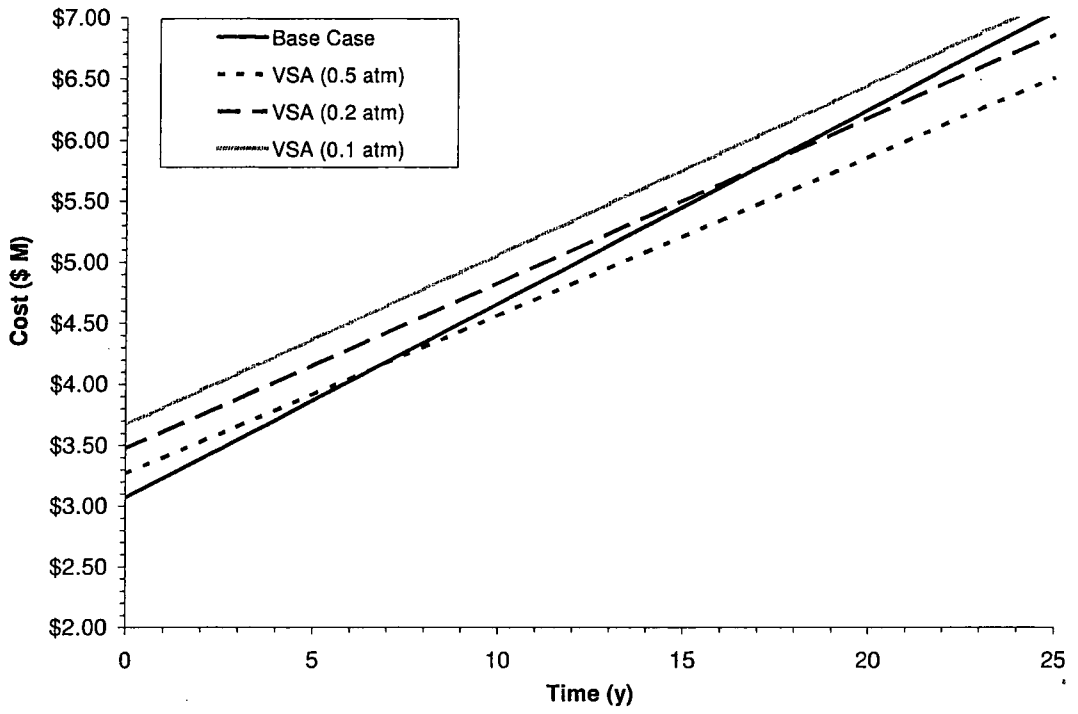

Figure A3.5 - Cost as a function of time comparison between a base case fermentation model with a model introducing CO_2 stripping and a VSA system operating at 0.5, 0.2, and 0.1 atm.

Table A3.8 shows the tabulated values for the base case and the varying TSA and VSA scenarios.

Table A3.8 - Base case costs over 25 years compared with TSA and VSA systems using carbon dioxide stripping assuming building brand new facilities

Time (years)	Base Case ($M)	TSA (80 °C) ($M)	TSA (100 °C) ($M)	TSA (120 °C) ($M)	VSA (0.5 atm) ($M)	VSA (0.2 atm) ($M)	VSA (0.1 atm) ($M)
0	$3.07	$3.52	$3.52	$3.52	$3.27	$3.48	$3.67
1	$3.23	$3.65	$3.65	$3.65	$3.40	$3.61	$3.81
2	$3.39	$3.77	$3.78	$3.78	$3.53	$3.75	$3.95
3	$3.55	$3.90	$3.90	$3.91	$3.66	$3.88	$4.09
4	$3.71	$4.03	$4.03	$4.04	$3.79	$4.02	$4.23
5	$3.87	$4.16	$4.16	$4.17	$3.92	$4.15	$4.37
6	$4.03	$4.29	$4.29	$4.30	$4.05	$4.29	$4.51
7	$4.18	$4.42	$4.42	$4.42	$4.18	$4.42	$4.64
8	$4.34	$4.55	$4.55	$4.55	$4.31	$4.56	$4.78
9	$4.50	$4.67	$4.68	$4.68	$4.44	$4.69	$4.92
10	$4.66	$4.80	$4.81	$4.81	$4.56	$4.83	$5.06
11	$4.82	$4.93	$4.94	$4.94	$4.69	$4.96	$5.20
12	$4.98	$5.06	$5.07	$5.07	$4.82	$5.10	$5.34
13	$5.14	$5.19	$5.20	$5.20	$4.95	$5.23	$5.48
14	$5.30	$5.32	$5.32	$5.33	$5.08	$5.37	$5.62
15	$5.45	$5.45	$5.45	$5.46	$5.21	$5.50	$5.76
16	$5.61	$5.57	$5.58	$5.59	$5.34	$5.64	$5.90
17	$5.77	$5.70	$5.71	$5.72	$5.47	$5.77	$6.03
18	$5.93	$5.83	$5.84	$5.85	$5.60	$5.91	$6.17
19	$6.09	$5.96	$5.97	$5.98	$5.73	$6.05	$6.31
20	$6.25	$6.09	$6.10	$6.11	$5.86	$6.18	$6.45
21	$6.41	$6.22	$6.23	$6.24	$5.99	$6.32	$6.59
22	$6.57	$6.35	$6.36	$6.37	$6.12	$6.45	$6.73
23	$6.72	$6.47	$6.49	$6.50	$6.25	$6.59	$6.87
24	$6.88	$6.60	$6.62	$6.63	$6.38	$6.72	$7.01
25	$7.04	$6.73	$6.74	$6.76	$6.51	$6.86	$7.15

Both Figures A3.4 and A3.5 clearly show that carbon dioxide stripping followed by an adsorption process has lower operating costs even though the capital cost may be greater. For the TSA systems, Figure A3.4 shows the change in desorption purge gas temperature does not change the feasibility of the TSA process with the process being more economical compared to the base case after 5 years.. For the VSA system Figure A3.5 shows the higher the vacuum, the longer it takes before the process becomes economically beneficial compared to the base case. Table A3.9 shows the percentage change in costs for the TSA/VSA processes using carbon dioxide stripping in relation to the base case fermentation model over 25 years.

Table A3.9 - Percentage change in costs over 25 years compared with TSA and VSA systems using carbon dioxide stripping compared with base case model

System	Condition	Percent Change in Cost (%)			
(-)	(-)	Capital[1]	Operating[1]	Operating[2]	Cumulative[3]
TSA	80°C	14.4	-19.0	-16.3	-4.4
TSA	100°C	14.4	-18.7	-17.0	-4.2
TSA	120°C	14.4	-18.3	-16.7	-4.0
VSA	0.5 atm	6.4	-18.5	-15.8	-7.6
VSA	0.2 atm	13.2	-14.9	-12.2	-2.6
VSA	0.1 atm	19.5	-12.5	-9.8	1.5

1 - Capital and operating cost change comparing the three cases as brand new built facilities (Alternative 1)
2 - Capital cost is kept fixed with the operating cost varying (Alternative 2)
3 - Cumulative cost after 25 years including capital and operating costs compared to the base case

This analysis suggests that the most promising technology would be a carbon dioxide stripping process incorporating a VSA system with an adsorption and desorption pressure of 1 atm and 0.5 atm respectively.

References

Aspen Technology, "HYSYS® 2004.2 Tutorials & Applications," Aspen Technology Inc., Copyright © 1981 - 2005

Cheresource, "Packed Column," The Chemical Engineers' Resource Page, Midlothian, VA, http://www.cheresources.com/packcolzz.shtml (Retrieved May, 23, 2009)

ISA 9001:2000 Registered Manufacturer, "Ceramic Saddles Ring," ChemPack Tower Packing Co. Ltd., www.tower-packing.com/ceramic/ceramic_saddles_ring_chemical_packing.htm (Received November 3, 2009)

Martini, S., Ricci, M., Bartolini, F., Bonechi, C., Braconi, D., Milucci, L., Santucci, A., Rossi, C., "Metabolic response to exogenous ethanol in yeast: An in vivo NMR and mathematical modeling approach," Biophysical Chemistry, 120 (2), 135-142, 2006

Taylor, F., Kurantz, M.J., Goldberg, N., Craig Jr., J.C., "Control of packed column fouling in the continuous fermentation and stripping of ethanol," Biotechnology and Bioengineering, 51, 33-39, 1996

Taylor, F., Kurantz, M.J., Goldberg, N., Craig Jr., J.C., "Effects of ethanol concentration and stripping temperature on continuous fermentation rate," Applied Microbiology and Biotechnology, 48, 311-316, 1997

Tremaine, D., Stewart, L., "McCabe-Thiele Graphical Method for the Design of a Column for the Distillation of Ethanol in Water Using Origin™ and HYSYS™," Separation Process Principles, Chemical Engineering, 340, 2005

Turton, R.., Baillie, R. C., Whiting, W. B., Shaeiwitz, J. A., "Analysis, Synthesis, and Design of Chemical Processes - Second Edition," Prentice Hall 2003

Chapter IX

Appendix 4 - Adsorption Fundamentals

Adsorption Fundamentals

Adsorption is a surface phenomenon where one or more species of a fluid selectively adsorbs onto the surface of the adsorbent. This type of separation takes advantage of the adsorbents attractive nature towards some fluid components. Adsorption separation processes have a wide range of applicability and many industrial applications. The type of adsorbent and operating conditions can make adsorption a very selective purification process and, in many cases, a more cost-effective separation process compared to other systems such as a distillation column. Table A4.1 list some important different commercial applications for adsorption.

Table A4.1 - Commercial adsorption separations (Keller et al., 1987)

Separation	Adsorbent
Gas bulk separations	
Normal paraffins, isoparaffins, aromatics	zeolite
N_2/O_2	zeolite
O_2/N_2	carbon molecular sieve
CO, CH_4, CO_2, N_2, Ar, NH_3/H_2	zeolite, activated carbon
Acetone/vent streams	activated carbon
C_2H_4/vent streams	activated carbon
H_2O/ethanol	zeolite
Gas purifications	
H_2O/olefin-containing cracked gas, natural, air, Synthesis gas etc.,	silica, alumina, zeolite
CO_2/C_2H_4, natural gas, etc.	zeolite
Organics/vent streams	activated carbon, others
Sulfur compounds/natural gas, hydrogen, liquefied Petroleum gas (LPG), etc.	zeolite
Solvents/air	activated carbon
Odours/air	activated carbon
NO_x/N_2	zeolite
SO_2/vent streams	zeolite
Hg/chlor-alkali cell gas effluent	zeolite

There are two types of adsorption: chemical and physical adsorption. In physical adsorption the forces are relatively weak, and mainly involve van der Waals interactions. Chemical adsorption is stronger since a chemical reaction and therefore a chemical bond between the adsorbent and adsorbate is formed. Table A4.2 outlines some of the main differences between physical and chemical adsorption.

Table A4.2 - Parameters of Physical and Chemical Adsorption (Ruthven, 2000)

Parameter	Physical Adsorption	Chemical Adsorption
Heat of adsorption	low, < 1.5 or 2 times latent heat of evaporation	high, > 2 or 3 times latent heat of evaporation
Specificity	nonspecific	highly specific
Nature of adsorbed phase	monolayer or multilayer, no dissociation of adsorbed species	monolayer may involve dissociation
Temperature range	only significant at relative low temperatures	possible over a wide range of temperature
Forces of adsorption	no electron transfer, although polarization of sorbate may occur	electron transfer leading to bond formation between sorbate and surface
Reversibility	rapid, non-activated, reversible	activated, may be slow and irreversible

The research conducted dealt with physical adsorption using either activated carbon or zeolites. Some of the main adsorption characteristics important for physical adsorption are the pore sizes of the adsorbent, hydrophobicity, and surface area. The pore sizes of the adsorbent determine whether the molecules attach to the surface of the adsorbent or pass through. For example, zeolite 3A is a molecular sieve used for ethanol dehydration. The pore size for zeolite 3A is 3Å while the molecular diameters for water and ethanol are 2.8 and 4.4 Å, respectively. Therefore the water molecules being smaller than the pores within the zeolite 3A become trapped while the bigger ethanol molecules pass through. For a fluid mixture containing two components that have different polarities, the hydrophobicity of the adsorbent becomes important. While activated carbons are hydrophobic, zeolites can have a wide range of hydrophobicity depending on the SiO_2/Al_2O_3 ratio. A higher SiO_2/Al_2O_3 ratio suggests a more hydrophobic surface and therefore can attract more non-polar molecules. The surface area of the adsorbent indicates the number of adsorption sites that are potentially available for adsorption. A higher number of available adsorption sites typically lead to a higher adsorption capacity (maximum ability the adsorbent has to adsorb a specific compound per unit mass of adsorbent).

References

Keller II, G.E., Anderson, R.A., Yon, C.M., in Rousseau, R.W., "Handbook of Separation Process Technology," John Wiley & Sons, Inc., New York, 644 - 696, 1987

Ruthven, D.M., "Adsorption," Kirk-Othmer Encyclopaedia of Chemical Technology, John Wiley & Sons, In., New York, 582 - 617, 2000